MODIFIED NEWTONIAN DYNAMICS AT ALL ASTROPHYSICAL SCALES

Garry William Angus

A Thesis Submitted for the Degree of PhD
at the
University of St. Andrews

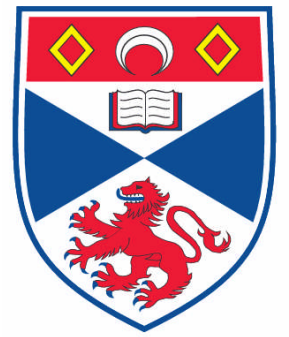

2008

THE UNIVERSITY OF ST. ANDREWS

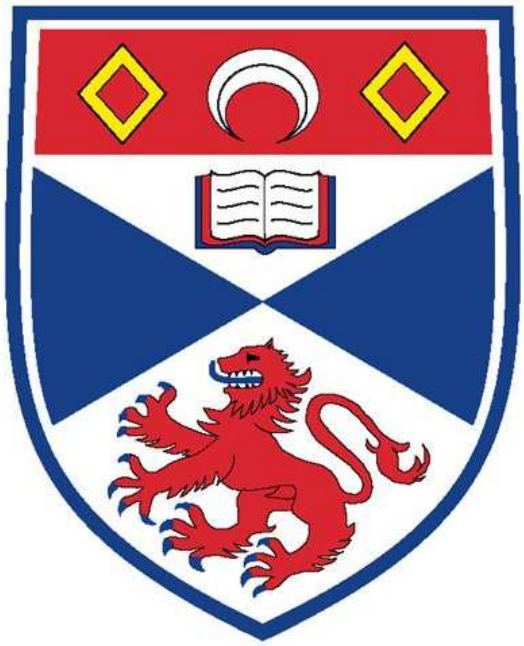

Modified Newtonian Dynamics at all astrophysical scales

Garry William Angus

Submitted for the degree of Ph.D

2008

Abstract

In this thesis I test the modified Newtonain dynamics as an alternative to the cold dark matter hypothesis. In the Milky Way, I show that the dynamics of the dwarf galaxies are well described by the paradigm and I confirm its distant low suface brightness globular clusters provide a strong test, for which I make predictions. Through analysis of a sample of 26 X-ray bright galaxy groups and clusters I demonstrate that the three active neutrinos and their anti-particles are insufficient to reconcile modified Newtonian dynamics with the observed temperatures of the X-ray emitting gas, nor with weak-lensing measurements, in particular for the bullet cluster. To this end, I propose an 11eV sterile neutrino to serendipitously resolve the residual mass problem in X-ray bright groups and clusters, as well as matching the angular power spectrum of the Cosmic Microwave Background. With this in mind, I show that the large collision velocity of the bullet cluster and the high number of colliding clusters is more naturally reproduced in MOND than in standard dynamics.

Kites rise highest against the wind, not with it . . .

Winston Churchill

Contents

List of Figures

List of Tables

Acknowledgments

Three people deserve enormous credit for encouragement through myriad email exchanges and listening to my half-baked ideas: Benoit Famaey, Stacy McGaugh and Tom Zlosnik without whom astrophysics would be a much less entertaining occupation. Other people who were of incalculable help are Françoise Combes, Moti Milgrom, Carlo Nipoti, Bob Sanders and Steve Vine.

I owe a huge debt to my parents and family for getting me near the goal posts in the first place and to my girlfriend Liselotte for supporting me through everything.

I'm now going to list the friends who have either been of some scientific help or have been victims of countless practical jokes that would've left Feynman in stitches: Alexis, Noé, Ewan, Chris, David, Martin, Ben, Tim, John, Rowan, Tom, Katharine, Ettore, Leslie, Ed, Greg and some good, non-astronomical friends Ruairi, Paul-Jonathan, Barry, Solomon and Mike.

Finally, I thank my supervisor HongSheng Zhao, our systems administrator Ian and other members of staff at St. Andrews University especially Ian Bonnell, Simon Driver and Keith Horne.

This thesis is based on all the first author papers listed below.

Angus G.W., Famaey B. & Zhao H.S., 2006, MNRAS, 371, 138

Angus G.W. & Zhao H.S., 2007 MNRAS, 375, 1146

Angus G.W., Shan H.Y., Zhao H.S. & Famaey B., 2007, ApJ, 654, L13 (§2.1)

Angus G.W. & McGaugh S.S., 2008, MNRAS, 383, 417 (§2.2)

Angus G.W., Famaey B., Tiret O., Combes F. & Zhao H.S., 2008, MNRAS, 383, L1 (§2.4)

Angus G.W., Famaey B. & Buote D.A., 2008, MNRAS, (§2.3)

Angus G.W., 2008, MNRAS, (§3.2)

Angus G.W., 2008, arXiv:0805.4014, submitted to MNRAS, (§2.5)

Angus G.W. & McGaugh S.S., 2008, submitted to A & A, (§3.4)

I, Garry William Angus, hereby certify that this thesis, which is approximately 30,000 words in length, has been written by me, that it is the record of work carried out by me and that it has not been submitted in any previous application for a higher degree.

I was admitted as a research student in October 2005 and as a candidate for the degree of PhD in October 2006; the higher study for which this is a record was carried out in the University of St Andrews between 2005 and 2008.

Date: August 15, 2008 Signature of Candidate:

I hereby certify that the candidate has fulfilled the conditions of the Resolution and Regulations appropriate for the degree of PhD in the University of St Andrews and that the candidate is qualified to submit this thesis in application for that degree.

Date: August 15, 2008 Signature of Supervisor:

The following is an agreed request by candidate and supervisor regarding the electronic publication of this thesis:

Access to printed copy and electronic publication of thesis through the University of St Andrews.

Date: August 15, 2008 Signature of Candidate:

Date: August 15, 2008 Signature of Supervisor:

Chapter 1

Introduction

1.1 ΛCDM

Anthropic and inflationary arguments as well as considerable observational evidence has led cosmologists to the understanding that the Universe has the critical density and therefore a flat geometry ($\Omega = \frac{\rho}{\rho_c} = 1$); now, in the past and in the future. This critical density, $\rho_c = \frac{3H_o^2}{8\pi G}$ is attained by the construction of the three pillars of cosmology: Einstein's general relativity, cold dark matter (CDM) and Einstein's cosmological constant Λ.

This so called ΛCDM model of concordance cosmology is publicised as the final chapter in cosmology. Proponents claim that joining dark energy (Peebles & Ratra 2003) in the form of Einstein's cosmological constant, Λ, with cold dark matter (Bond & Efstathiou 1984), which means extremely weakly interacting massive (>100GeV) particles from supersymmetry theory, is in total agreement with all astrophysical data (Spergel et al. 2007; Tegmark et al. 2004; Colless et al. 2001; Primack 2007). This is actually far from the truth.

The lines of evidence that led to ΛCDM are many. Dark matter (DM), not necessarily cold, was originally proposed by Fritz Zwicky in the 30s to explain why the galaxies in the Coma cluster had such high random speeds which required a total mass for the cluster, several hundred times the luminous mass in the galaxies. He made the assumption of virial equilibrium i.e. that the gravitational potential energy ($W = -\frac{1}{2}\Sigma_{i\neq j}\frac{Gm_im_j}{r_{ij}}$) was equal to twice the kinetic energy ($K = \frac{1}{2}\Sigma_i m_i v_i^2$) of the galaxies. This can be re-arranged to give the total necessary mass for virial equilibrium

$$(M/L)L_g \approx \frac{3R_G\sigma_r^2}{G}, \tag{1.1}$$

where L_g is the summed luminosity of all the cluster galaxies in some bandpass, R_G is the gravitational radius (related to typical size of the cluster) and σ_r^2 is the radial velocity dispersion found from deprojecting the line of sight (measured) velocity dispersion.

If no DM was present, the mass-to-light ratio (M/L) should be of order unity. Since M/L is several hundred, there must be DM or the galaxies cannot stay bound in the cluster – they would have escape speed and the cluster would evaporate. It subsequently turned out that hot ionised gas made up a considerable fraction of the DM, observable only at X-ray wavelengths, but still the M/L remained about four or five.

As will be explained in more detail in §1.3 the rotation speeds of spiral galaxies gave additional strong evidence for DM. By measuring the rotation speeds at intervals of radius from the H-I neutral hydrogen gas, which should be forced onto circular orbits, it is possible to reconstruct the mass at a given radius from $M(r) = \frac{rV_c^2}{G}$. Again because the spirals rotate so fast, given the luminous matter distribution, that they should fly apart unless bound together with additional DM providing extra gravity. Dwarf galaxies that are satellites of the Milky Way also have such large internal mean squared velocities that they require huge M/L, for instance the Draco dwarf spheroidal has a M/L reaching one thousand.

The theory of the creation of the light elements (Big Bang Nucleosynthesis, BBN) in the first three minutes (Weinberg 1993) after the Big Bang gives strict limits on the amount of ordinary matter in the Universe. Only about 5% of the critical density, ρ_c can come from baryons. Therefore, if we want a flat Universe where $\Omega = 1$ which prefered by inflation theories i.e. that if the Universe was ever anything but completely flat, it decays from that value so quickly, that it would be a ridiculous coincidence to have 5% of the critical value now. So the remaining 95% was assumed to be some weakly-interacting massive particle (WIMP), but this model was shown to be incongruent with the observations of the anisotropies in the cosmic microwave background (§2.5) and the ratio of dark matter to baryons in clusters of galaxies measured by weak-lensing and X-ray studies which all prefer an $\Omega_{DM} \approx 0.22$. This left an embarrassing 70% of the critical density to explain. Luckily, this was met with evidence for something

called "dark energy" which causes the Universes expansion to accelerate at low redshifts, that can complete the energy budget. The evidence came from experiments using supernovae of type 1A (Schmidt et al. 1998; Perlmutter et al. 1999) which can be used as standard candles and because they are dimmer than expected (if the Universe wasn't accelerating) we assume the Universe is accelerating causing them to be further away. Other evidence for dark energy comes from the relative speeds of galaxies in the local group (Chernin et al. 2007) which shows there is a radius at which galaxies have escape velocity from the local group and beyond that radius increase in velocity with distance. This cannot be the Hubble expansion because these galaxies have decoupled from the Hubble flow. Finally, the Sachs-Wolf effect (Granett et al. 2008) which shows cosmic microwave photons passing through potentials of galaxy clusters and gaining energy because the potential has been stretched at the near end (to us, the observer) by the dark energy making the potential non-symmetric along the line of sight.

Putting this all together: the baryons from BBN, the dark matter needed in clusters of galaxies and the dark energy is in good agreement with observations of the large scale structure of the Universe (Tegmark et al. 2004), the acoustic peaks of the cosmic microwave background (Spergel et al. 2007) and the angular sizes of objects as modified by the cosmological expansion. However, the theory has some issues.

First of all, we know of no physics that can produce the negative pressure effect of dark energy (Diaferio 2008) that causes the Universes expansion to accelerate at late times. The vacuum expectation energy is 120 orders of magnitude (Carroll 2006) above the value of the dark energy density (cosmological constant). Secondly, we have no good candidates for the CDM particle and the parameter space of spin-independent cross section against mass is being probed with dedicated underground detector experiments (see Baer et al. 2008; CDMS Collaboration 2008) and surprisingly nothing is being found. Thirdly, Einstein's general relativity (GR) is only accurately tested in very strong gravity like in the Solar System.

We have no guarantee that GR will hold at accelerations 10^{11} times smaller than experienced in everyday life. At sizes 10^{11} times smaller than in everyday life, quantum mechanics are necessary to accurately describe observations and speeds 10^{11} times higher cannot even be achieved. Near the speed of light, new

physics is required also.

Of course, these are only cosmetic issues which may or may not be resolved. More pressing is the fact that there are many other incongruities with the observables. For instance, cosmological simulations accounting for the growth of structures (Springel 2005) predicts that one or two orders of magnitude more dwarf galaxies should exist in orbit around galaxies like the Milky Way (Klypin et al. 1999; Moore et al. 1999a). Observations show that only ∼10-20 dwarfs exist near the Milky Way (<300kpc distant) and recent measurements of the proper motions of the Magellanic clouds (Kallivayalil et al. 2006b,a) show the Magellanic clouds are not bound to the Milky Way, so the observed number of nearby small galaxies overestimates the number of satellites. A common explanation is that feedback processes such as supernovae extinguish the star formation of such small galaxies. However, observations of the ultra low luminosity dwarf galaxy Leo T (Ryan-Weber et al. 2008) show star formation in a very weakly bound dwarf galaxy can continue for extended periods of time, so this idea is very weakly motivated. This is discussed in more detail at the beginning of §3.

Another major problem for the ΛCDM model is the fine tuning of dark matter (DM) halos in fits to rotation curves of spiral galaxies. As will be shown in §1.3 there is an absolute 1:1 correlation between the observed baryon distribution and that of the DM in galaxies which does not follow in any sense from the expectations of the ΛCDM model. Additionally, Gilmore et al. (2007) have shown that the DM density profiles in dwarf galaxies are cored (constant) at the centre, in contrast to the CDM predictions of DM density rising to the centre (cusped). This is expected because CDM particles are so massive (>100GeV) that they are "cold" meaning their mean free path is very short so they cannot diffuse, or free stream out of small overdensities as easily as, for instance, a hot DM candidate like the neutrino can. This is also seen in the rotation curves of spiral galaxies (McGaugh & de Blok 1998; Gentile et al. 2004) where the observed DM density does not increase towards the centre. AGN feedback and supernovae winds have been unsuccessfully postulated as effects that can reduce the DM density in the centres of galaxies (Gnedin & Zhao 2002).

Although, the ΛCDM model has failed extraordinarily well at the scale of large galaxies (Milgrom & Sanders 2003) and all the way down to dwarf galaxies, it has, until now, fared well in passing cosmological tests. However, just like the

type 1A supernovae are standard candles, the angular scale of the peaks (in particular the first peak) of the cosmic microwave background are standard rulers. Another standard ruler which has a well-known physical size are baryonic acoustic oscillations. Baryonic acoustic oscillations are related to the acoustic peaks in the cosmic microwave background in that perturbations in the photon-baryon fluid propogated with some sound speed dependent on the well known temperature of the microwave background photons. Before the temperature decayed to a low enough temperature to allow recombination of the electrons with the protons (at which time the sound wave halts), there was a well fixed time for a sound wave to travel through the coupled photon-baryon fluid which creates an overdensity in the baryons present at the scales this wave travelled ($\sim$150Mpc). This was predicted to be a small bump on the matter power spectrum which is obviously dominated by dark matter and was measured by Eisenstein et al. (2005). The history of the cosmological expansion, determind by the values of the dark energy, dark matter and baryon abundances encode the measured size of this standard ruler (as if we look through a metre stick with a strange lens). Measurements predict a distance-redshift relation that is 2.4σ from the ΛCDM prediction (Percival et al. 2007). What this means is that the distance redshift relation is not well matched by the dark matter and energy densities measured from the CMB, or the dark energy and dark matter don't behave as expected in the simplest models.

1.2 Modified Newtonian Dynamics

The Modified Newtonian Dynamics (MOND) paradigm proposed by Milgrom (1983c) remains the only worthwhile competitor to the ΛCDM model of concordance cosmology. It is not obvious why MOND has not been accepted in the wider astronomy community except that it has been difficult to test cosmologically excluding it from participating in tests in the era of "precision cosmology". The confirmed predictions of MOND at the galaxy scale are astounding and I will try to highlight these in the following sections.

In the late 1970's, work by Rubin et al. (1978) and others showed that there was an acceleration discrepancy in spiral galaxies because the rotation velocities become constant (instead of falling) at large radii, in addition to the well known

problem in clusters of galaxies (Zwicky 1933). Simply, there is not enough gravity to support the motions of the stars in a galaxy, or galaxies in a cluster of galaxies. Something is missing.

The Poisson equation is defined as

$$\nabla^2\Phi(r) = 4\pi G\rho(r), \tag{1.2}$$

where Φ is the gravitational potential from which gravity is defined (as $g = -\nabla\Phi$) and ρ is the matter density. To increase the gravity, we have to either add another source term to the right hand side, or we can change the way gravity is related to potential.

Another way of looking at it is from rotation curves. The centripetal motion of stars and gas on circular orbits of velocity V, at a radius, r, can be simply related to the mass interior to the orbit, M(r) such that

$$\frac{V(r)^2}{r} = g_n = \frac{GM(r)}{r^2}. \tag{1.3}$$

Which means that in order for velocity to be constant with radius, either M(r) must increase linearly with distance in some DM halo or Newton's gravitational laws that work well in the Solar Sytem fail in weak gravity. Since the mass in stellar galactic disks is seen to rise much more slowly than $\propto r$ there must be DM whose mass increases $\propto r$. This was certainly the conventional wisdom at the time i.e. that these galaxies were formed in massive halos of DM which also grants the galaxies stability (White & Rees 1978).

However, Milgrom showed in his seminal papers of 1983 that the flat rotation curves of spiral galaxies could have a much simpler solution that requires no unobservable matter in what is an entirely free distribution. His theory was fully predictive of the gravitational field surrounding a mass distribution and by definition resulted in flat rotation curves for spiral galaxies as discussed below. It was called Modified Newtonian Dynamics or MOND for short.

The basis of MOND is that a new constant of physics with the dimensions of acceleration, a_o, is added to the list including Planck's constant, the speed of light, Boltzmann's constant etc. The value of the constant is experimentally deduced (as are the other constants) to be $a_o \sim 10^{-10} ms^{-2}$ (see e.g. Sanders & Verheijen 1998).

When accelerations, g, are much greater than a_o, we have standard Newtonian dynamics restored in pristine condition. Alternatively, when accelerations are considerably less than a_o, we have modified dynamics such that the gravity a test particle experiences is given by

$$g = \sqrt{g_n a_o}. \tag{1.4}$$

These two regimes, the Newtonian and MONDian, must be connected via an interpolating functions that smoothly moves between them. Sadly, the interpolation function, which is a function of the total gravity g, comes from no prescribed theory, unlike special relativity where $\gamma = (1 - \frac{v^2}{c^2})^{-1/2}$ relates proper time with inertial time.

In general, the MOND equation relating the expected Newtonian gravity and the physically imposed gravity felt by any test particle becomes

$$g\mu(x) = g_n, \tag{1.5}$$

where $x = g/a_o$. The search for an interpolating function (Milgrom 1983c; Famaey & Binney 2005; Famaey et al. 2007c) is a thesis in itself and a rather boring diversion, so here we settle on two interpolating functions.

$$\mu(x) = x/\sqrt{1 + x^2}, \tag{1.6}$$

Which is the most commonly used interpolating function and so is refered to as the *standard* function. The other is most famous for being used to fit the terminal velocity curve of the Milky Way in the work of Famaey & Binney (2005) and has the form

$$\mu(x) = x/(1 + x), \tag{1.7}$$

Owed to its simplicity, this function is cunningly called the *simple* function. The only serious constraint of the interpolating function is that it is x when x is small and unity when x is large.

The interpolating function is a crucial part of MOND because much of the interesting dynamics of galactic systems occurs in the transitional regime between Newtonian and MONDian dynamics. In the next year, it should be possible to well constrain the shape of the interpolating function for the high resolution

studies of H-I gas in spiral galaxies from the THINGS (The H-I Nearby Galaxy Survey) collaboration (Walter et al. 2005). This, coupled with K-band photometry of the galaxies, should have enough constraint on the mass profile and velocity curve to generate detailed information about the interpolating function's form.

Sadly, the above formulation of MOND only holds in high symmetry and in general we should use the version outlined in Bekenstein & Milgrom (1984) where a modified Poisson's Equation allows for the conservation laws to be respected

$$\nabla \cdot [\mu(|\nabla\Phi|/a_o)\nabla\Phi] = 4\pi G\rho. \tag{1.8}$$

As with the standard Poisson equation (Eq 1.2), Φ is the gravitational potential and ρ is the matter distribution (density). Angus et al. (2006) showed that the approximation Eq 1.5 makes is a good one in high symmetry. There are plenty of other, larger errors in astrophysical measurements that contribute to the systems studied in this thesis and therefore Eq 1.8 shan't worry us too much. The interested reader is directed to Ciotti et al. (2006) for a more detailed account and also Milgrom (1986); Brada & Milgrom (1995); Nipoti et al. (2007a); Tiret & Combes (2007a) for methods of solving the complicated, non linear Eq 1.8.

1.3 Rotation curves and the Tully-Fisher relation

As mentioned above, MOND predicts rotation curves should be asymptotically flat. For this there are myriad examples in the review of MOND by Sanders & McGaugh (2002) which I have reproduced courtesy of Stacy McGaugh in Fig 1.1.

There are certain complicating factors, but on the whole the fits are excellent and have virtually no free parameters. The mass-to-light of the stellar disk is constrained by population synthesis models which take into account the age of the stellar population and the band-pass in which the light is measured in. The a_o constant is fixed by these observations and cannot vary from system to system.

Not only does MOND predict that rotation curves should be asymptotically flat, but it was also an original prediction of Milgrom (1983c) that galaxies with a low surface brightness (LSB) such that the gravity was, at all radii, significantly lower than a_o should have a characteristic shape in contrast to galaxies with strong

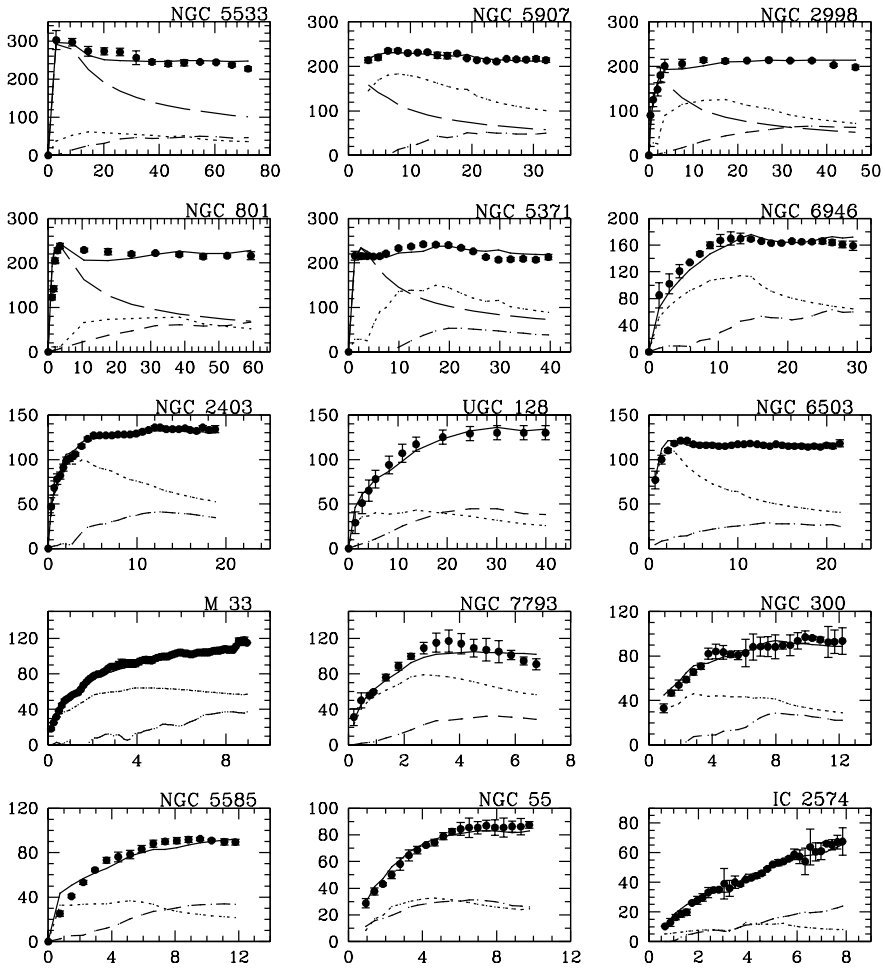

Figure 1.1: Example rotation curves: velocity in km/s against radius in kpc. Dots are observations, dashed lines are gas, dotted lines are stars and the solid lines are the MOND fits using the MOND formula. Reproduced courtesy of Stacy McGaugh.

internal gravities or high surface brightnesses (HSBs). It can be seen in Fig 1.2 that the LSB galaxy NGC 1560 rises monotonically with radius until it becomes asymptotically flat at large radii. On the other hand, the HSB galaxy NGC 2903 rises to a maximum and then decreases in a Keplerian fashion ($V \propto r^{-1/2}$) until becoming asymptotically flat.

The simple explanation of why the LSB galaxy rises is obvious. The dynamics are MONDian everywhere, thus $V^2(r)r^{-1} = \sqrt{a_o GM(r)r^{-2}}$, which gives

$$V = [GM(r)a_o]^{1/4}, \tag{1.9}$$

so the rotation speed rises with the quartic root of the mass. Alternatively, at small radii, the HSB galaxy is not within the MOND regime, but has dynamics entirely in the Newtonian regime because $g >> a_o$. This is why the rotation speed decreases after a maximum because $V^2(r)r^{-1} = GM(r)r^{-2}$, so

$$V = \sqrt{GM(r)r^{-1}}, \tag{1.10}$$

such that if dM(r)/dr<1 then the rotation speed can drop before the radius at which it enters the MOND regime and flattens.

At some radius all galaxies enter the MOND regime and when the mass stops rising significantly, Eq 1.9 is valid and there should, in MOND, be a direct relation between enclosed mass, M(r), and rotation speed at the edge of the galaxy. This gives us the MONDian form of the baryonic Tully-Fisher relation (McGaugh et al. 2000; McGaugh 2005b) which exactly states that

$$V^4 = GMa_o, \tag{1.11}$$

where M is the total enclosed mass of the galaxy and V is the flat value of the outer rotation curve.

The fact that MOND predicts the exact form of this relation is extremely powerful evidence especially since the Tully-Fisher relation now covers more than five orders of magnitude in mass.

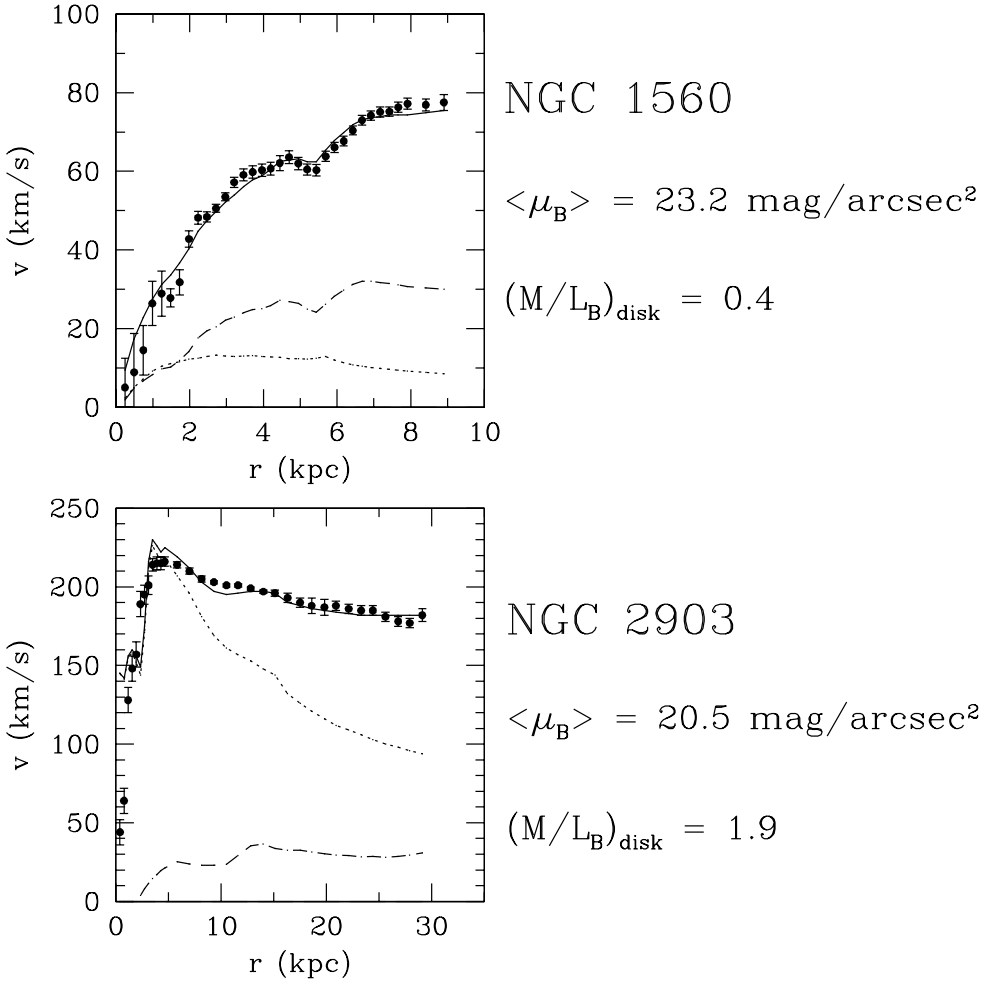

Figure 1.2: Shows the example of low surface brightness galaxies and high surface brightness galaxy rotation curve shapes. The LSB has the characterstic steady rise at all radii until flattening off. The HSB characteristically maxes out and falls before flattening. Reproduced courtesy of Stacy McGaugh.

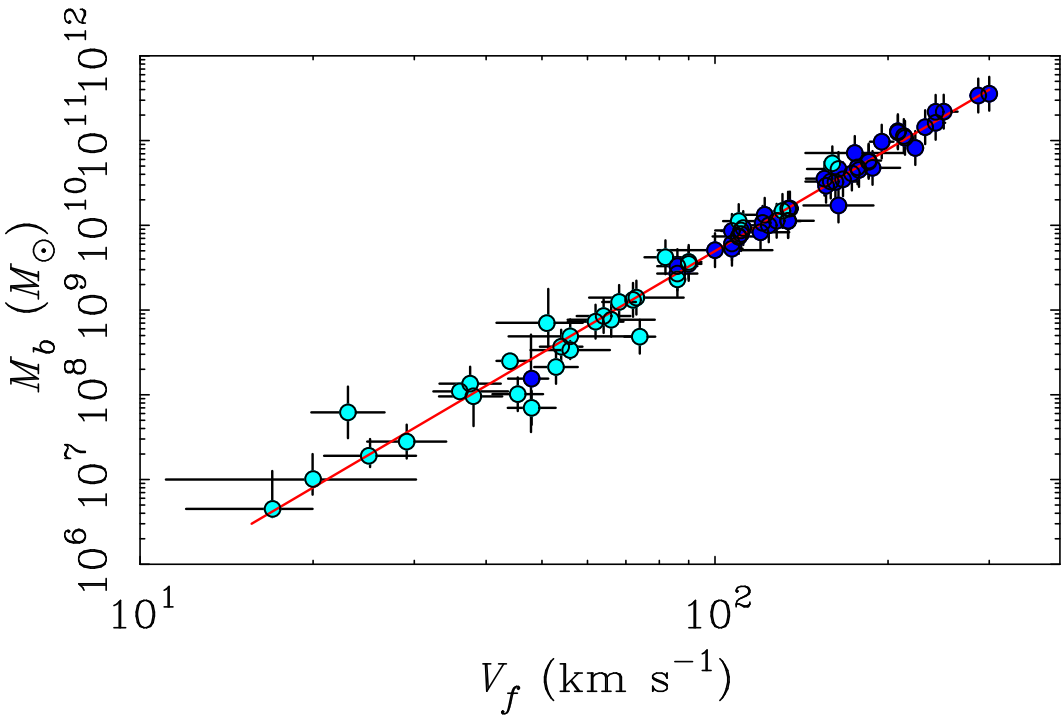

Figure 1.3: Shows the baryonic Tully-Fisher relation. The points are the measured flat outer rotation speed and total measured galaxy baryonic mass. The best fit line is the MOND prediction with slope of 4 and intercept of $log(Ga_o)$. Reproduced courtesy of Stacy McGaugh.

1.4 The external field effect

MOND effects are only observed in systems where the absolute value of the gravity both internal, g_i and external g_e (from a host galaxy) is less than a_o. If $g_e < g_i < a_o$ then we have standard MOND effects as described above. However, if the hierarchy goes as $g_i < g_e < a_o$ then we don't have MONDian behaviour, but rather we have Newtonian gravity with a renormalised gravitational constant of $G/\mu(g_e/a_o)$, where $\mu \leq 1$. The reason for this is quite obvious, if I take Eq 1.5 then the argument of the interpolating function is the total gravity $|g_i + g_e|$. If indeed $g_e > g_i$ then the equation for the internal gravity (Eq 1.5) is simply

$$g_i = g_n/\mu(g_e/a_o) = \frac{G}{\mu(g_e/a_o)} M r^{-2}. \tag{1.12}$$

This is an extremely important result for subsystems in galaxies, most crucially the dwarf spheroidals of the Milky Way where this has strong effects (see §3). You can immediately see that these systems will not lie on the Tully-Fisher relation because gravity (although boosted) still falls with the square of distance. A spiral galaxy, in such an external field, will not have the characteristic flat rotation curve, but would fall in a Keplerian fashion. A corollory of this might be that spirals in clusters of galaxies are harassed by the external field inducing an environmental - galaxy type relation.

1.5 Recent work on MOND unrelated to this thesis

There was a superb review of MOND by Sanders & McGaugh (2002) that covers all the important work between its inception and 2002. Since then, the field has grown fairly rapidly thanks to several factors. Possibly the two most important are the continual technological advances in astronomy, space missions etc that have basically opened up the entire electromagnetic spectrum. Another, unforeseen factor was the publishing of Bekenstein's 2004 work on the covariant formulation of MOND. This added interest to MOND, since it became possible to directly ask questions about cosmology and gravitational lensing. However, it is my personal opinion, backed up by calculations in §2.5, that MOND is not

important in the early universe and all other questions regarding MOND, can be asked in the classical sense, including gravitational lensing. The only place where I think MOND may offer something new to these kind of discussions, apart from galaxy formation, is in the late time expansion of the universe where dark energy begins to dominate. At these times the accelerations in the universe on large scales are weak and MOND may provide some insight since $a_o \sim cH_o \sim c\sqrt{\frac{\Lambda}{3}}$. Of course, it may be possible for a_o to vary with redshift (Bekenstein & Sagi 2008) but there is currently no evidence that supports this.

1.5.1 Tidal dwarf galaxies

A recent analysis of the rotation curves of several tidal dwarf galaxies formed from the debris of NGC5291 by Bournaud et al. (2007) had provided more solid evidence for MOND, but also has given strong evidence against the CDM paradigm. Since the dwarfs have condensed from debris cast out by an encounter between two galaxies, only a very limited amount of CDM could have condensed along with the gas. Nevertheless, the gas debris has gone on to form a stellar disk and has rotation that has been measured. Since very little CDM could have accompanied the gas due to its collisionless nature, the rotation velocities measured should be exactly that predicted by the enclosed mass at all radii (Eq 1.3). More to the point, the rotation curve should fall at large radii (Eq 1.10).

This is not at all what is observed and as it happens, the rotation curves are exactly matched by Milgrom's simple formula (Eq 1.5; see Milgrom 2007b and Gentile et al. 2007 for details). To reconcile this with the CDM paradigm, Bournaud et al. (2007) invoked a second species of dark matter in the form of a molecular gas disk that would've originally traced the HI disk of the progenitor galaxy. This dark disk would have to be several times more massive than the observed stellar and gaseous disks of ordinary galaxies in order to have condensed in such a large abundance. It is therefore puzzling that no dark disks are observed in other spiral galaxies. What is even more startling is that this galaxy also lies nicely on the Tully-Fisher relation, therefore, this empirical relation has no apparent relation to the CDM.

1.5.2 Numerical simulations

Galaxy Formation

The new vogue in astrophysical numerical simulations and theoretical endeavours is galaxy formation techniques trying to reproduce the observed redshift distribution of galaxies and the abundance of Hubble types. Although it may seem a bit ridiculous to be doing this without 100% knowledge of the correct cosmological model, as Binney (2004) pointed out, if we didn't accept the ΛCDM model, then the field of galaxy formation would have stagnated and no progress would have been made, whereas actually a lot of results can be incorporated into MOND.

The arena of galaxy formation seems to be the best and possibly only way to distinguish between modified gravity and cold dark matter. As things like rotation curves and velocity dispersion profiles as tracers of mass are snapshots of the dynamical state they are not as laced with information as the creating of the galaxies themselves which incodes myriad implications. To date, the over-abundance of satellite galaxies (Klypin et al. 1999; Moore et al. 1999a) predicted from ΛCDM numerical simulations and the creation of dark matter densities at the centres of galaxies much higher than observed (McGaugh & de Blok 1998; de Blok & McGaugh 1998; Gentile et al. 2004) have been virtually ignored because ad hoc predictions of stellar feedback have been suggested, but never fully tested as resolutions. Now the time is coming where the recipes (Kennicutt 1998; Cole et al. 1994; Somerville & Primack 1999) and understanding of star formation processes (Bonnell et al. 1998, 2001) as well as evolution and deaths of stars and their impact on the surrounding volume is reaching a level, where the cusps and satellites cannot hide any longer and eventually will have to be taken extremely seriously as a cancer on the theory.

With recent advances in techniques that rapidly solve the modified Poisson equation of MOND (Eq 1.8), for example several papers by Nipoti et al. and Tiret & Combes) the idea of testing theories of galaxy formation is slowly becoming a possibility in MOND.

Sanders (2008) made an interesting step towards identifying the epoch of galaxy formation in MOND. It suffers from the lack of a strong cosmological model for MOND, like the one mooted in §2.5 of this thesis. It uses a baryons only model (therefore a large dark energy component) and the idea of perturbations

decoupling from the Hubble flow and collapsing under their self gravity and using the MOND equation to calculate the time taken for the perturbations to virialise. It shows that actually under less than favourable conditions, MOND can form structures like the massive, red elliptical galaxies seen at high redshift.

Dynamical Friction

Dynamical friction is when a satellite galaxy is orbiting a host galaxy and moving through the halo of that galaxy (whether dark or stellar). Depending on the mass and velocity of the satellite, stars and dark matter particles are scattered by the satellite and owed to the relative motion of the satellite, it feels a drag or frictional force that evaporates its angular momentum causing it to spiral in towards the host. The important quantity to be gained is the timescale for dynamical friction i.e. a measure of how long it will take the satellite to spiral in and merge.

Tiret & Combes (2007a) looked at the dynamical friction timescale for a galactic bar to be significantly slowed by the other stellar and gaseous material of the galactic disk. They found that the longer range forces of MOND caused a slightly shorter dynamical friction time. This is fully expected for a bar, embedded in a galactic disk because the centres of galaxies differ very little in MOND and standard dynamics. To fit the rotation curves in the centres of galaxies that are massive enough to sustain a bar requires very little dark matter. This can do little to distinguish between MOND and standard dynamics, but it is comforting to know that the timescale isn't so short, that we should observe no galaxies with bars. This has been confirmed by Nipoti et al. (2008), but only in the situation where all mass distributions are identical and the enhanced gravity of MOND boosts the number and strength of interations at long distances.

However, a dynamical friction issue that has been cited as a big problem for MOND (Ciotti & Binney 2004; Sánchez-Salcedo et al. 2006; Nipoti et al. 2008) is the existence of 5 globulars clusters surrounding the Fornax dwarf spheroidal galaxy at projected radii 1.60, 1.05, 0.43, 0.24, 1.43kpc from the optical centre (the core radius of Fornax is 0.6kpc and the tidal radius is 2kpc) and weighing between 100-1000 times less than the dwarf itself. It was suggested by Sánchez-Salcedo et al. (2006) using analytical arguments that dynamical friction can occur on significantly shorter timescales in MOND than standard dynamics causing the globulars to spiral in and merge within at most 2 Gyrs.

It is generally a dangerous game to extrapolate special case results in MOND to other scales or systems. The inherent non-linearity of the theory opposes such endeavours. Fornax has very low surface brightness and so is external field dominated everywhere. This means the gravity can be simply modeled by renormalizing Newton's constant to be $G\frac{g_{ex}}{a_o}$. The formula for the deceleration due to dynamical friction has a G^2 term and so has also been renormalised to give the dynamical friction in MOND. However, there is a flaw here because the scattering of the stars occurs near to the globular cluster and the globular clusters, being very high surface brightness and compact, are the only places in the Fornax system that have high accelerations and therefore scatter stars in a Newtonian way. All this means is that the dynamical friction of the globular cluster system in Fornax is vastly more sophisticated than can be modeled analyically. It is therefore of the utmost importance to run high resolution N-body simulations in MOND with realistic initial conditions to check if this is actually a real problem or an artifact of inadequate modelling.

Galaxy Merging

The merging of galaxies is a well known mechanism to build larger galaxies known from observations of mid-stage mergers at many redshifts and theory. Nipoti et al. (2007b) and Tiret & Combes (2008) both recently looked at simulating galaxy merging in MOND. The idea here is that observations of the antennae galaxy (NGC4038/9; Toomre & Toomre 1972) and the Atoms-For-Peace galaxy (NGC 7252) show pairs of galaxies that have collided and thrown out tidal debris in two long arms, but the majority of the two galaxies have recollapsed and are in the process of merging. In the case of NGC 7252, the merger has been completed and the daughter galaxy has settled to a stable configuration.

The way this is presumed to work in standard dynamics is that the dark matter of the two galaxies provides a sort of fluid which the two galaxies use as a reservoir to dump their excess angular momentum and energy via dynamical friction (see Binney & Tremaine 2008). This reservoir is not present in MOND and moreover collision velocities are expected to be higher in MOND (see Angus & McGaugh 2008 and §2.2), so there is extra kinetic energy to get rid of.

Nevertheless, Tiret & Combes (2008) were able to reproduce the morphology of the antennae galaxies in a MOND simulation. Furthermore, they showed that

the formation of the tidal dwarf galaxies mentioned in §1.5.1 is easily possible in MOND.

However, in their simulations, Nipoti et al. (2007b) found that merging timescales in MOND are significantly longer than in standard dynamics and without a dark halo, it is difficult to account for the rapid merging seen in many galaxies. Still, without the complex inclusion of the gaseous component (Springel 2005; Tiret & Combes 2008) of galaxies, which can be a very significant component (Combes 1991; Pfenniger et al. 1994) the physics is insufficiently modelled to draw strong conclusions.

Chapter 2

Clusters of Galaxies

For an excellent introduction to what we know about clusters in a general setting see Diaferio et al. (2008). Clusters of galaxies provide a serious challenge to MOND. The typical accelerations in clusters are $> a_o$, so MOND effects only become important at the edges, meaning gravity theory is unimportant.

Clusters of galaxies are the largest (100-1000kpc scale) virialised systems in the Universe. They consist of hundreds if not thousands of galaxies which make up a small fraction of their total mass in baryons (10-20%) and a hot, ionised, X-ray emitting hot gas component ($T \sim 0.5 - 15keV \sim 10 - 100MK$) which constitutes the lion's share of the baryons (80-90%). It is important to note, however, that these percentages are for the *total* mass in baryons and generally the galaxies dominate the mass on small scales (up to ∼100kpc). This ratio becomes more unbalanced towards hotter, larger clusters ($T > 3keV$) and in fact groups of galaxies ($T < 1.5keV$) that are X-ray bright have their baryon content dominated by the galaxies. Still, in MOND and standard dynamics there remains dark matter at all radii which is more massive than all the baryons by a factor of at least three in total and always more at smaller radii.

That rich clusters contain more mass than meets the eye in MOND goes back to Milgrom's original papers (Milgrom 1983b). At the time, the discrepancy was very much larger than it is today, as it was not then widely appreciated how much baryonic mass resides in the intra-cluster medium (hot gas). Further work on the hot gas (e.g., Sanders 1994, 1999) and with velocity dispersions of galaxies (McGaugh & de Blok 1998) showed that MOND was at least within a factor of a few, but close inspection revealed a persistent discrepancy of a factor of three

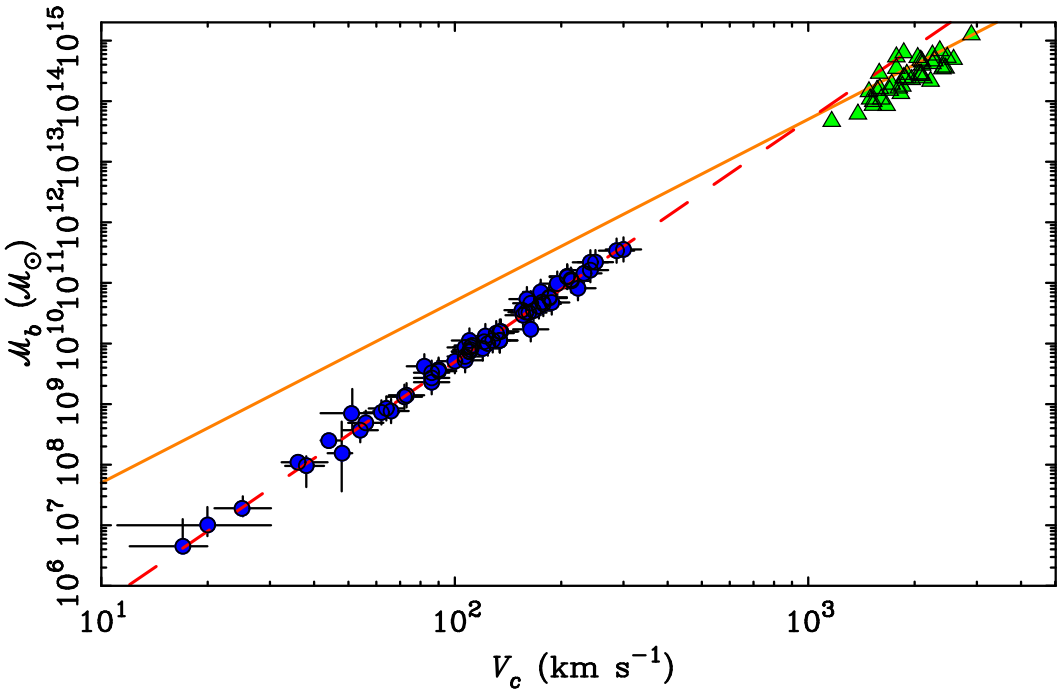

Figure 2.1: Shows baryonic mass against circular velocity. Rotating galaxies (blue circles) are from McGaugh (2005a) and clusters (green triangles) are from Sanders (2003) using the measured temperature to estimate the circular velocity assuming isothermality. The solid orange line is the CDM M-V relation (Steinmetz & Navarro 1999) assuming $M_b = f_b M_{vir}$ with $f_b = 0.17$ (Spergel et al. (2007)) and the dashed red line is the MOND prediction. The spirals lie directly on the MOND prediction, but the clusters are generally 2-3 times in mass below it. The CDM expectation is nicely consistent with clusters, but implies many dark baryons in spirals in addition to the non-baryonic dark matter.

or more in mass (e.g., The & White 1988; Gerbal et al. 1992; Buote & Canizares 1994; Pointecouteau & Silk 2005). Weak gravitational lensing (§2.1;Angus et al. 2007; Takahashi & Chiba 2007; Famaey et al. 2007a) provides a similar result as does strong lensing (Ferreras et al. 2008).

To make matters worse, the distribution of the unseen mass does not trace that of either the galaxies or the hot gas (Aguirre et al. 2001; Sanders 2003; Angus et al. 2008a; Sanders 2007). In Fig 2.1 we plot the baryonic mass of many spiral galaxies and clusters against their circular velocity together with the predictions of MOND and CDM. MOND is missing mass at the cluster scale. CDM suffers an analogous missing baryon problem on the scale of individual galaxies.

The beauty of MOND is that it negates the need for dark matter in galaxies

of all types: dwarfs, spirals and ellipticals. The apparent need for dark matter in clusters doesn't falsify MOND as the need for cold dark matter in a galaxy would, it simply means we don't know all the physics at the cluster scale.

There are at least two approaches to this problem: one approach is to say that MOND as it stands is incorrect and by increasing the acceleration constant a_o by a factor of ten, we could decrease the radius at which MOND effects become important in clusters of galaxies and hence reduce the amount of dark matter in the cluster. This, however, is poorly motivated by fits to rotation curves and obviously the Tully-Fisher relation and is not a serious prospect. There is very little freedom for a_o to vary.

We can however, add mass. The only constraint we have is that it must not affect the dynamics of galaxies (Combes 2004) i.e. the species of dark matter must be unique to clusters of galaxies.

The physics of how the light elements were formed in the early Universe (Big Bang Nucleosynthesis, BBN) strictly limits the amount of baryons in the Universe. They contribute at most 5% to the total mass and energy budget of the Universe. Having said that, at low redshifts, the majority of the baryons are not locked in stars or the cold gas of galaxies, nor in the hot gas of galaxy clusters. Only $\sim$20% of the total baryons are locked up in these species. The rest are presumed to be in a warm-hot intergalactic medium (WHIM; Cen & Ostriker 1999, 2006; Bertone et al. 2008) that has been unambiguously detected (although the exact abundance is unknown) through the absorption of high redshift quasars by highly ionised atomic oxygen (O-VI, O-VII) along the line of sight.

An important point to notice here is that the missing mass in clusters is merely some 5% of the BBN value, so there remains sufficient license to explore baryonic solutions to the cluster problem. To this end, Milgrom (2007a) has suggested the existence of clumps of ultra cold molecular gas (a few Kelvins) in Jupiter mass clumps and with a size similar to that of the Solar System. These clumps have interesting properties because their size means they only provide cloud cover at the 10^{-4} level, which means they are difficult to detect from background quasar absorption and they shouldn't occult X-ray emission. Further, they cannot form stars, since they don't contain a Jeans mass. In addition to this, they might serendipitously resolve the cooling flow problem (Fabian et al. 1994; Dunn & Fabian 2006) i.e. that the cooling time at the centres of clusters is much lower

than a Hubble time and so we should observe the transport of much X-ray emitting hot gas towards the centres (the cooling flow). There is strong evidence for the existence of cooling flows in galaxies and clusters, but not at the level that can transport $10^{13} M_{\odot}$ over a Hubble time. Common solutions to why the centres of the clusters aren't cooling generally rely on some heating mechanism in the centre like from AGN, but these have theoretical problems (Gastaldello et al. 2008). Milgrom's idea is that the cold gas clouds collide and release their vast kinetic energy reservoirs which heats up the gas at the centre of the cluster. The theory of how these cold gas clumps form, or how they survive ablation by the hot gas is currently being developed.

An alternative idea was proposed by Sanders (2003) in a paper where he studied the mass profiles of clusters mainly hotter than T=4keV. This idea was that the 3 known active neutrinos (ν_τ, ν_e and ν_μ) and their anti-particles have masses very near the experimental mass upper limit of 2.2eV measured from the spectrum of electron neutrinos from beta-decay experiments. Basically, the idea of the Mainz/Troitsk experiments are to count the highest energy β-decay electrons of $^3\mathrm{H} \rightarrow {}^3\mathrm{He}^+ + \mathrm{e}^- + \nu_e + 18.57\,\mathrm{keV}$ (the more massive the neutrinos, the lower the cutoff energy of electrons). This current upper limit of 2.2eV for the electron neutrino will be reduced to $\sim$0.3eV by KATRIN (the KArlsruhe TRItium Neutrino experiment) within a few months of taking data in 2009.

Naturally, this only gives us the mass of the electron neutrino, but the three neutrino masses are tied together by the phenomenon known as neutrino flavour oscillation which allows neutrinos to oscillate between the three available flavours while they propagate through space. Specifically, this occurs because the neutrino flavour eigenstates are not the same as the neutrino mass eigenstates. So a neutrino that was produced as an electron neutrino at a given location has a calculable probability to be detected as either a muon or tau neutrino after it has travelled to another location. The first evidence for this quantum mechanical effect came from the discrepancy between the number of electron neutrinos detected from the Sun's core not matching the expected numbers, dubbed as the"solar neutrino problem". In the Standard Model of particle physics the existence of flavour oscillations implies a non-zero neutrino mass, because the amount of mixing between neutrino flavours at a given time depends on the differences in their squared masses.

The differences in the squared masses have been well measured by solar neutrino experiments and in fact the differences in the squared masses are so small ($\sim 0.003eV^2$) that if one neutrino is known to weigh more than ∼0.1eV, the differences are negligible and there is virtually no mass hierarchy. At the upper limit, the neutrinos all weigh 2.2eV which means they can contribute significantly to the energy density of the Universe, which is given by

$$\Omega_\nu = 0.0205 m_\nu. \tag{2.1}$$

Each species contributes 4.5% and there are three active species, so that is 13.5% ($\Omega_\nu = 0.136$) in total. This is a highly significant portion of the crital density of the Universe, $\Omega = 1$, more than half the standard contribution of CDM ($\Omega_{cdm} = 0.22$; Nolta et al. 2008) and would have measureable consequences for the angular power spectrum of the cosmic microwave background (CMB), as will be discussed in §2.5.

This strict relationship between mass and mass density on a cosmological scale makes neutrinos a very appealing candidate for this simple reason that what we see is what we get. Since the neutrino fluid is in thermal equilibrium with the photon bath at early times, the neutrino total number, just like the photon total number stays fixed after the neutrinos freeze out. On the other hand, any detection of massive particles in collider experiments, such as the large hadron collider, will yield nothing more than a particle mass. It will not tell us if they exist cosmologically and it will not tell us their abundances.

Neutrinos have another crucial property in relation to clusters of galaxies. As they are fermions, they naturally obey the Pauli exclusion principle, however, there is a stronger limit on their maximum density than the PEP. In a seminal paper in 1979, Tremaine & Gunn showed that since the neutrino fluid must conserve its phase space density during gravitational collapse (Louiville's theorem), there is a maximum density of each species of neutrino being related to the temperature (velocity dispersion) of the system and the individual neutrino mass as follows

$$\frac{\rho_\nu^{max}}{2.1 \times 10^{-4} M_\odot pc^{-3}} = \left(\frac{T}{1keV}\right)^{1.5} \left(\frac{m_\nu}{2eV}\right)^4. \tag{2.2}$$

The crucial thing to notice here is that the maximum density is proportional to the fourth power of mass, hence why we need the neutrinos to be as massive as

possible to be significant in clusters of galaxies where the dark matter densities are relatively high.

It was claimed by Sanders (2003) that 2eV neutrinos can consistently clump densely enough to account for the majority of the dark matter in rich clusters of galaxies (T > 4keV), however, this was contended by Pointecouteau & Silk (2005) who claimed that the cores of these clusters were unlikely to be consistent with 2eV neutrinos because the densities are above the Tremaine-Gunn limit.

In the following sections, I study a range of galaxy clusters in temperature and measurement technique (weak gravitational lensing and hot gas hydrostatic equilibrium) to grade ordinary active neutrinos and other candidates as the missing mass in MOND clusters.

2.1 The bullet cluster

Another extremely powerful reason to look for a weakly interacting and most probably non-baryonic dark matter solution to the cluster problem in MOND are the observations of the so called "bullet cluster" (Markevitch et al. 2002). The bullet cluster is actually a pair of clusters which have been gravitationally accelerated towards each other against the Hubble flow and have passed directly through each other in the plane of the sky (see Fig 2.2).

Recall that there are 3 components in the clusters: the dark matter, hot gas and galaxies. As the hot gas clouds collide, they trade momentum via ram pressure that slows the gas down like friction. Alternatively, the galaxies present a tiny cross section to each other and do not interact. The dark matter, whether neutrino, cold gas or CDM also has a tiny interaction cross section and the two halos pass directly through each other.

Assuming the galaxies and the dark matter follow each other, there now exist 4 mass centres: the dark matter and galaxies of the larger, main cluster (CM1), the hot gas of the main cluster (XR1), the hot gas of the sub cluster (XR2) and the dark matter and galaxies of the sub cluster (CM2).

The hot gas of the sub cluster has an interesting feature imposed on it because of the passage through the main cluster. The high relative speed between the two clusters has created a bow shock which allows us to measure the speed of the clusters, defined by the angle of the cone. This measurement (around $4500\,\mathrm{km\,s^{-1}}$;

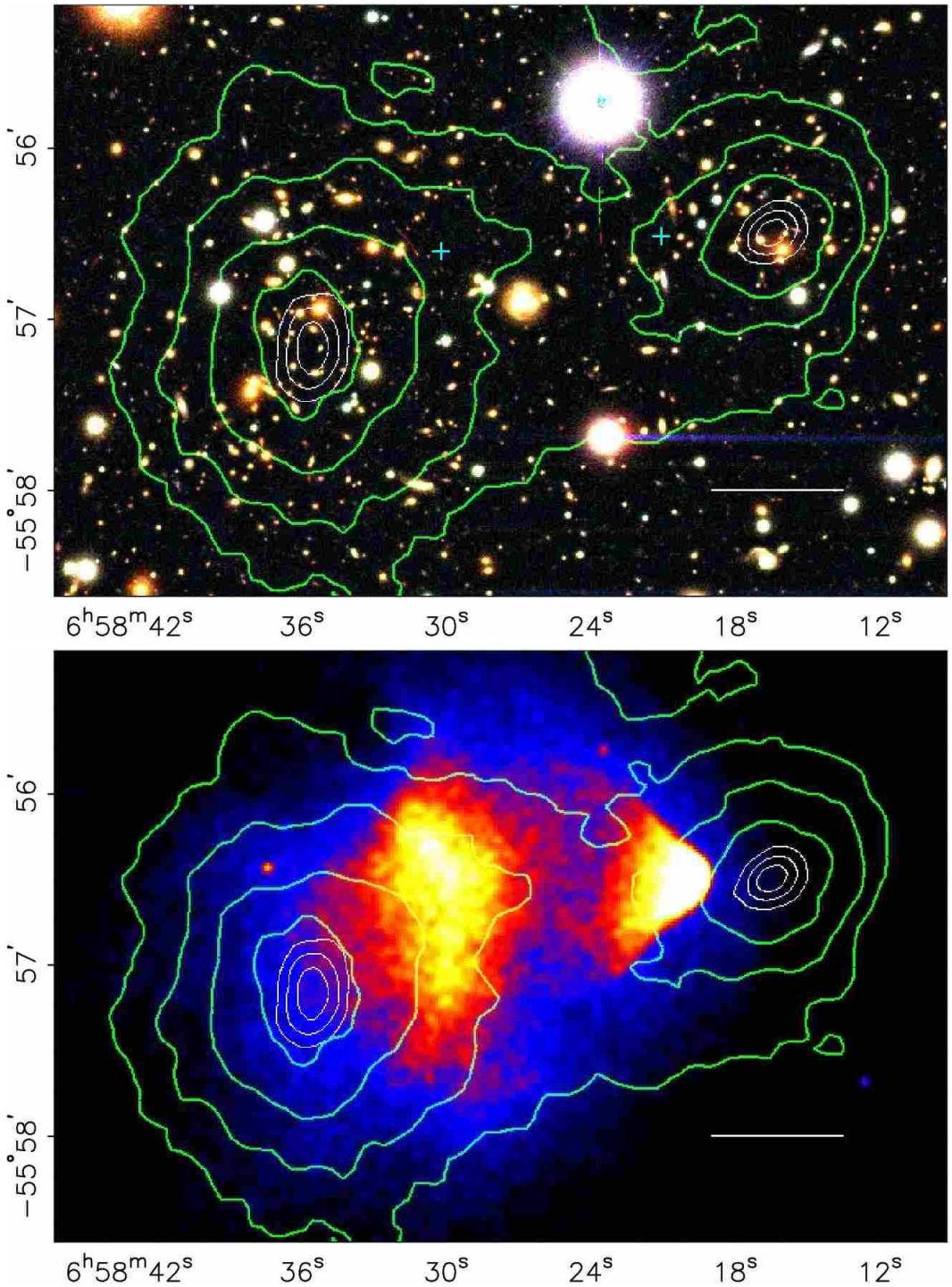

Figure 2.2: (Top panel) The bullet cluster at optical wavelengths. The green contours highlight the total mass surface density, which is well offset from the hot gas to the location of the galaxies and the dark matter. (Bottom panel) The bullet cluster at X-ray wavelengths. The bow shock (since the collision is supersonic) on the hot gas of the sub cluster is evident. The white contours show the error in the position of the brightest cluster galaxy. The surface density is given by $\Sigma = 3.1 \times 10^3 M_{\odot} pc^{-2} \kappa$. The outer contour is κ=0.09 and each contour increases by 0.07. Images courtesy of Douglas Clowe, reproduced from Clowe et al. (2006).

a Mach number of ∼3) is currently slightly contentious and is discussed in some detail in §2.2.

The crucial thing here is that if further modification of gravity were to help solve the cluster problem without the need to invoke dark matter, then any measurements of the strength of gravity in the region surrounding the bullet cluster would highlight the hot gas and not the galaxies because most of the baryonic mass resides in the hot gas, especially for such a hot pair of clusters (the main cluster has a temperature of 14keV and the sub cluster is 6keV).

Fortunately, there is a method to measure the total gravity in the system by the technique of weak gravitational lensing (see Hoekstra & Jain 2008). In parallel, we can get a handle on the galaxy masses from optical observations with the Hubble telescope, which also measures the lensing distortions of the background galaxies at higher redshift for the weak lensing measurement. Furthermore, the projected mass in hot gas can be calculated from its X-ray emission using CHANDRA.

All of these things were done by Clowe et al. (2004b) and then revised in Clowe et al. (2006) with greater precision. Most important is the weak lensing, which is a technique that uses the gravitational distortion and small amplification of background galaxies (far beyond the lens plane) to statistically infer the projected surface density along the line of sight. Basically, if we look at a large sample of galaxies behind the lens plane, we expect the direction of the major axes of ellipticities of the galaxies to be random. However, the small skewing of the light by the gravitational lens creates a prefered direction and magnitude depending on the strength of the lens and obviously the distance from source to lens and observer.

Gravitational lensing of any sort (weak, strong, micro) works exactly the same way in MOND as in GR, the only difference is that the potential, Φ, which describes the lens is different in MOND because it is generated from the matter distribution, ρ through the Modified Poisson equation (Eq 1.8).

For a ray of impact parameter R from the spherical lens, the bending angle θ is given (cf. Zhao et al. 2006) by the following integration along the line of sight

$$\theta(R) = \int_{-\infty}^{+\infty} \frac{2g_{\perp}(R,z)dz}{c^2}, \qquad g_{\perp}(R,z) = g(r)\frac{R}{r}, \tag{2.3}$$

Table 2.1: Best fit parameters of the convergence map. Squared velocities in $(1000\,\mathrm{km\,s^{-1}})^2$ and scale radii, p in kpc.

v^2_{CM1}	v^2_{CM2}	v^2_{XR1}	v^2_{XR2}	p_{CM1}	p_{CM2}	p_{XR1}	p_{XR2}
2.84	1.45	0.38	0.17	227.4	155.4	62.6	33.4
X_{CM1}	Y_{CM1}	X_{XR1}	Y_{XR1}	X_{CM2}	Y_{CM2}	X_{XR2}	Y_{XR2}
-416.7	-173.1	-209.0	1.2	293.0	-2.7	147.5	3.6

where $g_\perp(R,z)$ is the gravity perpendicular to the line of sight, and $g(r)$ is the centripetal gravity at radius $r=\sqrt{R^2+z^2}$.

In Fig 2.2 the concentrations of DM and galaxies and hot gas are overlaid with the convergence, κ, measured by gravitational lensing. In general relativity, the convergence is directly linked to the matter surface density Σ through multiplication by a constant. However in MOND, there is a linear chain linking potential Φ, light bending $\theta(R)$, and convergence κ, but not between convergence and mass surface density.

Nevertheless, thinking in terms of GR, one can see from Fig 2.2 the peaks of the matter distribution highlighted by the green contours are clearly offset towards the location of the galaxies and the dark matter. In fact, so much so that the hot gas barely registers as a perturbation on the map, with only a slight skewing towards the gas of the main cluster.

As mentioned above, Sanders (2003) claimed that the mass profiles of clusters of galaxies might be consistent with 2eV neutrinos, so in Angus et al. (2007) we attempted to test this hypothesis and also make certain that dark matter was definitely necessary at the locations of the galaxies to be consistent with the lensing map.

2.1.1 Modelling the convergence map of the buller cluster

As mentioned above, in GR the convergence map allows us to immediately derive the underlying projected density of matter. However, as shown in Angus et al. (2006), the situation is different in MOND, where *what you see* (in terms of convergence) is *not always what you get* (in terms of density). For that reason, we use a potential-density approach hereafter: we fit the convergence map using a parametric set of potentials, and then use the best-fit potential to derive the corresponding surface density for various choices of the interpolating function μ.

The bullet cluster is 4-centred, CM1, CM2, XR1 and XR2. So, for ease, we chose to model those 4 mass components as 4 spherical potentials: note however that, in non-linear gravity, like MOND, the 4 mass densities corresponding to those spherical potentials will *not* linearly add up, especially when the interpolating function μ is rapidly varying with position inside the system.

We thus write the lens-potential as a superposition of four potentials pinpointed at four centres $\vec{r}_i$:

$$\Phi(\vec{r}) = \sum_{i=1}^{4} v_i^2 \ln \sqrt{1 + \frac{|\vec{r} - \vec{r}_i|^2}{p_i^2}}. \tag{2.4}$$

Each potential is fully described by two parameters, the asymptotic circular velocity v_i and the scale length p_i. In GR these potentials correspond to cored isothermal density profiles.

Using Fig 2.2 which is reproduced from Clowe et al. (2006, hereafter C06) we set up a coordinate system for the bullet cluster. The centres XR1, XR2 and CM2 lie, to a first approximation, along the RA direction, which we chose as our x-axis. Our z-axis is along the line of sight. As suggested by Markevitch et al. (2004) and C06, we chose the four centres of the potential to be exactly in the x-y plane with their (X, Y) coordinates chosen at the four observed peaks.

The parametric convergence map in the $x-y$ plane is simply computed by linear superposition of the individual contributions to the convergence from the four spherical potentials (see Angus et al. 2006), the convergence of each solely depending on its parameters v_i and p_i and the rescaled radius $s_i \equiv p_i^{-1}\sqrt{(x - X_i)^2 + (y - Y_i)^2}$.

The convergence in the x-y plane is given by

$$\kappa(x, y) = \sum_{i=1}^{4} \frac{\pi v_i^2 D_{\rm eff}}{c^2 p_i} \left[(s_i^2 + 1)^{-\frac{1}{2}} + (s_i^2 + 1)^{-\frac{3}{2}} \right]. \tag{2.5}$$

X_i and Y_i are the centres of the four components given in Table 2.1. We then tried to reproduce the observed convergence map (of Fig 2.2) by least-squares fitting the asymptotic velocities v_i and concentration parameters p_i of each of the spherical potentials. To do this we read $n = 233$ points from the $\kappa = 0.16, 0.23, 0.3, 0.37$ contours (always with a constant number of points per contour length) from the convergence map of C06. We tried moving the 2-coordinate centres (X_i and Y_i) for CM1, CM2, XR1 and XR2 within the errors

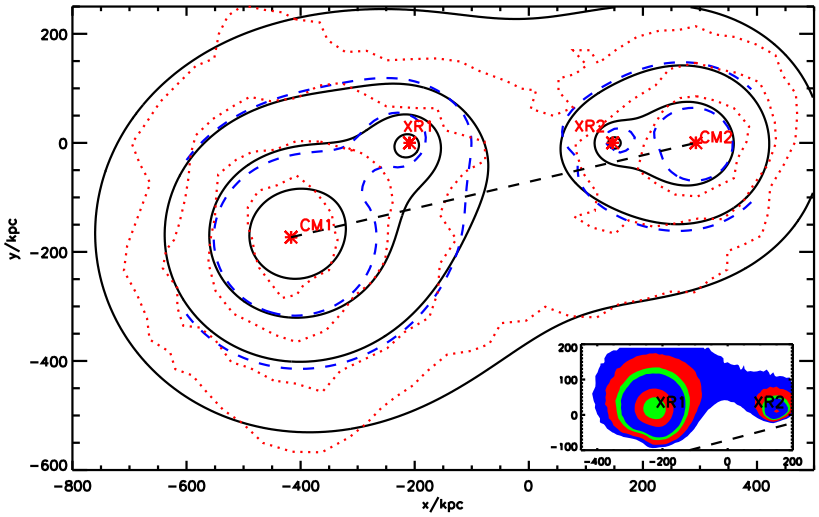

Figure 2.3: Our fitted convergence map (solid black lines) overplotted on the convergence map of C06 (dotted red lines) with x and y axes in kpc. The contours are from the outside 0.16, 0.23, 0.3 and 0.37. The centres of the four potentials we used are the red stars which are labelled. Also overplotted (blue dashed line) are two contours of surface density $[4.8\ \&\ 7.2]\times10^2 M_\odot\ \mathrm{pc}^{-2}$ for the MOND standard μ function; note slight distortions compared to the contours of κ. *Inset:* The surface density of the gas in the bullet cluster predicted by our collisionless matter subtraction method for the standard μ-function. The contour levels are $[30,\ 50,\ 80,\ 100,\ 200,\ 300] M_\odot pc^{-2}$. The origin in RA and dec is $[06^h 58^m 24.38^s$,$-55^o 56'.32]$.

μ	M^{gas}_{XR1}	M^{gas}_{XR2}	M_{CM1}	M_{CM2}	$\overline{\rho CM1}$	$\overline{\rho CM2}$
	r<100/180kpc	r<100/80kpc	r<250kpc	r<250kpc	$r < 100kpc$	$r < 100kpc$
GR	1.05/1.97	0.33/0.27	21.7	17.2	2.63	2.59
standard μ	0.97/1.79	0.29/0.24	9.0	6.78	2.26	2.34
simple μ	0.74/1.33	0.21/0.18	7.13	6.42	1.66	1.76
C06/B06	0.66/2.0	0.58/0.42	20.0/28.0	21.0/23.0		

Table 2.2: Compares the results of C06 and Bradac et al. (2006, hereafter B06) with estimates of projected mass in $[10^{13} M_\odot]$ for gas around the X-ray centres and total mass around the lensing centres in three different gravities (GR, standard and simple μ). B06 used an ellipse with semi-axes of 250 kpc and 150 kpc around XR1, which we compare with a circle of 180 kpc (the same area). The last column predicts the average matter densities in $[10^{-3} M_\odot pc^{-3}]$ within 100kpc of the lensing peaks.

of the brightest cluster galaxy or maximum X-ray luminosity.

The goodness of fit of the model $\kappa_{\mathrm{model},i}$ to observations $\kappa_{\mathrm{obs},i}$ is given by a characteristic variance $\frac{1}{n}\sum_{i=1}^{n}\left(\kappa_{\mathrm{obs},i}-\kappa_{\mathrm{model},i}\right)^2$. Due care was taken to maximise the resemblance to the X-ray gas features with the centres as marked in Fig 2.3. Another constraint was trying to ensure a reasonable mass of X-ray gas to conform with the estimates of C06 and Bradač et al. (2006). The best-fit parameters (listed in Table 2.1) yield the convergence map shown in Fig.2.3 upper panel, with a variance $\sim 0.1 \times 0.07^2$, which is acceptable since 0.07 is both the typical observational error at individual points and the convergence spacing between two neighbouring contours.

2.1.2 Masses of X-ray gas and dark matter in MOND

After achieving a good match to the convergence map, we needed to compute the corresponding mass distribution, which in MOND is not linearly related to the

potential applied.

The average mass density $\overline{\rho}(< r)$ or the total mass (e.g., baryons and neutrinos) of the system enclosed inside any radius r centered on *any position* will thus be estimated from the divergence theorem. If you recall Eq 1.8

$$4\pi G M(r) = \int \nabla \cdot [\mu \nabla \Phi]\, dV = \int \mu \nabla \Phi \cdot dA, \tag{2.6}$$

which gives

$$M_{\rm bary}(r) + M_{\nu}(r) = \int \frac{\partial \Phi(r,\theta,\psi)}{\partial r} \frac{\mu dA}{4\pi G}, \tag{2.7}$$

where the surface area element $dA = r\sin(\theta) d\theta d\psi$ and the interpolating function $\mu(x)$, where $x = \frac{|\nabla\Phi|}{a_0}$. The case $\mu \to 1$ corresponds to General Relativity. We use the simple interpolating function (Eq 1.7) and also the standard (Eq 1.6) for comparison with other works.

Applying Eq 2.7 to our potential model that matches the convergence map allows us to predict the matter volume density in the clusters within certain annuloids, e.g., the values given in Table 2.2. Integrating over the line of sight, we note that the convergence contours are slightly different from that of projected matter contours in non-linear gravities (cf. dashed blue contours of Fig 2.3). However, this non-linear effect appears much milder than suggested in Angus et al. (2006), mainly because gravity is strong (greater than a_o) everywhere across the bullet cluster.

In order to match the observed X-ray gas mass, which is a minor contributor to the lensing map, we use the asymmetry in the calculated surface density to subtract off all the dark matter centred on the galaxies (CM1 and CM2). The key here is to notice the symmetry of the contours around the dashed line joining the centres of the two galaxy clusters (cf. Fig 2.3 upper panel). If we fold the map over the axis of symmetry subtracting the lower part from the upper part we are left with the majority of the gas since it lies significantly above the line. Then we performed a straight forward numerical integration over the areas given in Table 2.2.

The inset panel of Fig 2.3 demonstrates that this technique works well in separating the surface density of gas from the collisionless matter. The values for the gas mass for our three gravities are given in Table 2.2.

Note this technique works less well for the sub cluster (XR2) as it lies quite

close to the axis of symmetry and thus much gas is cancelled out by other gas. For GR only we can directly compare the gas corresponding to the potential and that calculated by our subtraction method. For the main cluster, we find that integration of the surface density gives $2.3 \times 10^{13} M_{\odot}$ within the 180kpc aperture which is 15% more gas than estimated by symmetry. For the sub cluster we find $5.7 \times 10^{12} M_{\odot}$ from integration within the 100kpc aperture of the gas center, 73% more than from symmetry. As such, in MOND we can expect the gas masses to increase by similar amounts and this helps to explain the low gas masses found in the sub cluster (XR2).

The reason our κ-map is skewed towards the gas peaks is a feature of the cored isothermal potentials. Table 2.2 shows we pack too much gas into the central 100kpc of the main cluster compared to that observed only for it to balance by 180kpc. Using a potential that correctly matches the gas density would most likely not skew the map.

A more sophistocated approach to the problem would be to go from density to potential (here we've done the opposite) and input all the observed matter and work backwards to find the DM distribution required to match the convergence map.

Table 2.2 also compares the B06 and C06 projected mass within a 250 kpc circular aperture centred on CM1 and CM2 with our total mass within these apertures for three gravities (GR, simple μ and standard μ). Clearly, these amounts of mass exceed the observed baryons in gas and galaxies over the same apertures, by a factor of 3 even in MOND. While very dense clumps of cold gas or MACHOs are still easily allowed by BBN limits to reside in galaxy clusters without many collisions, we will focus on the possibilities of *fermionic particles* being the dark matter in the lensing peaks.

Following Tremaine & Gunn (1979), we use the densest regions of the dark matter to set limits on the mass of active/sterile neutrinos. A cluster core made of neutrinos of mass $2eV$ would have a maximum density (see Eq 2.30) satisfying $\rho_{\nu}^{\max} = 0.04 M_{\odot} pc^{-3}$ where we adopted the temperature of 14 keV for the main cluster. Comparison with the regions of the highest volume density of matter shown in Fig 2.3 upper panel suggests that the relatively diffuse phase space density in the bullet cluster is still consistent with active $2eV$ neutrinos making up the dark matter component. This prediction is applicable to sterile neutrinos as

well. To be conservative, we avoid extrapolating our predictions to scales smaller than 45 kpc, where the weak lensing data from C06 is limited by smoothing. In B06, the convergence near in the central regions is greatly increased using strong lensing which probes this more efficiently.

Note that while a better fit to the gas mass and the lensing map could be produced by using several ellipsoidal potential components as opposed to the rigid four spheres with fixed centers here, the present model suffices as a demonstration.

2.1.3 Discussion

Here we have shown that the bullet cluster does indeed show undeniable evidence for the need of DM in MONDian clusters of galaxies. At present, the upper limit of the mass of active neutrinos seems consistent with this DM, but since the bullet cluster is very hot, it is not the best test of this species of DM and cooler clusters and groups of galaxies can do better (see §2.3).

We note finally that the work of B06, suggests a higher value for the mass-sheet after breaking the degeneracy will strong lensing. This means the values of κ should all be renormalised up and the implications for 2eV neutrinos have not been rechecked.

Nonetheless, the data still convincingly require a dominant component of collisionless and most probably non-baryonic matter at cluster scales.

A traditional misconception is that the existence of a large quantity of non-baryonic matter would make a modified gravity theory such as MOND *contrived or redundant*. This is *not* the case with active neutrinos, which are too diffuse to either perturb the good MONDian fits to galaxy rotation curves nor explain these curves in GR.

2.2 The collision velocity of the bullet cluster

A pressing question is the apparently high relative velocity between the two clusters that comprise the bullet cluster 1E 0657-56 (C06; B06; Markevitch et al. 2004; Markevitch & Vikhlinin 2007). The relative velocity derived from the gas shockwave is $v_{rel} = 4740^{+710}_{-550}\,\mathrm{km\,s^{-1}}$ (C06). Taken at face value, this is very high, and seems difficult to reconcile with ΛCDM (Hayashi & White 2006). The problem is sufficiently large that it has been used to argue for an additional long

range force in the dark sector (Farrar & Rosen 2007). Here we examine the possibility of such a large velocity in both CDM and MOND.

One critical point that has only very recently been addressed is how the shock velocity (inferred from the bow shock) relates to the pre-collision velocity of the clusters. Naively, one might expect the dissipational collision of the gas clouds to slow the clusters down so that the shock speed would provide a lower limit on the collision speed. Recent hydrodynamical simulations (Springel & Farrar 2007; Milosavljević et al. 2007) suggest the opposite. A combination of effects in the two hydrodynamical simulations show that the shock velocity may be higher than the impact velocity. Basically, the upstream gas of the main cluster is accelerated towards the bullet (the bow shocked gas of the sub cluster) and the bullet is being accelerated towards the DM that it has just been separated from. The results of the two independent hydrodynamical simulations do not seem to be in perfect concordance, and the precise result seems to be rather model dependent. Nevertheless, it seems that the actual relative velocity lies somewhere in the range 3500-4500 $\mathrm{km\,s^{-1}}$.

The difficulties posed by a high collision velocity for CDM have been discussed previously by Hayashi & White (2006) and Farrar & Rosen (2007). And, whereas Springel & Farrar (2007) and Milosavljević et al. (2007) consider the complex hydrodynamic response of the two gas clouds during the ongoing collision, here we investigate the ability of two clusters like those comprising the bullet cluster to accelerate to such a high relative velocity in the case of both CDM and MOND prior to the merger.

Here we compute a simple freefall model for the two clusters in an expanding Universe with realistic mass models, and ask whether the observed collision velocity can be generated within the time available. We take care to match the mass models to the specific observed properties of the system appropriate to each flavour of gravity in order to realistically evaluate the orbit of the clusters prior to their collision.

2.2.1 Modeling the freefall

We wish to address a simple question: given the observed masses of the two clusters, is it possible to account for the measured relative velocity from their gravitational freefall? The expansion of the universe mitigates against large ve-

locities, since the clusters must decouple from the Hubble flow before falling together. Presumably it takes some time to form such massive objects, though this is expected to occur earlier in MOND than in ΛCDM (Sanders 1998, 2001, 2008; McGaugh 1999, 2004; Nusser 2002; Stachniewicz & Kutschera 2005; Knebe & Gibson 2004; Dodelson & Liguori 2006). The clusters are observed at $z = 0.3$, giving at most 9Gyrs for them to accelerate towards each other. This imposes an upper limit to the velocity that can be generated gravitationally. Without doing the calculation, it is not obvious whether the larger masses of the clusters in CDM or the stronger long range force in MOND will induce larger relative velocities.

Since we know the state of the system directly prior to collision, it makes sense to begin our simulations from the final state and work backwards in time towards when the relative velocity was zero. This point, where the clusters have zero relative velocity, is when they turned around from the Hubble flow and began their long journey gravitating towards each other. Working backwards in time leads to potentially counter-intuitive discussions (such as Hubble contraction), which we try to limit.

We must account for the Hubble expansion in a manner representing the universe before $z = 0.3$. The detailed form of the expansion history of the Universe $a(t)$ is not known in the case of MOND, so we take the scale factor of ΛCDM in both models

$$\frac{da(t)}{dt} = H_o \left[\Omega_m a^{-1} + \Omega_\Lambda a^2\right]^{1/2}. \tag{2.8}$$

Where we take $H_o = 72\,\mathrm{km\,s^{-1}} Mpc^{-1}$, Ω_m=0.27 and $\Omega_\Lambda = 0.73$. As will be seen in §2.5 the best fit to the CMB in MOND has virtually the same form, so the expansion history will be identical.

The important aspect is the basic fact that the Universe is expanding and the mutual attraction of the clusters must overcome this before they can plunge together at high velocity.

We implement the scale factor in the simulations through the equation of motion

$$\frac{1}{a(t)}\frac{d}{dt}[a(t)v] = g. \tag{2.9}$$

Computing this numerically, from time step to time step we calculate the ratio

of the scale factor in the previous time step to the current time step (i.e. $\epsilon = a(t_{i-1})/a(t_i)$; we use negative time steps to move backwards in time from the presently known configuration, so $\epsilon > 1$ (higher i means earlier universe). We then have $v(t_i) = v(t_{i-1})\epsilon + g\Delta t$.

The right hand side of Eq 2.9 differs in MOND and CDM not only because the law of gravity is altered, but also because the gravitating masses are higher in CDM.

The initial conditions are the crux of the problem, with at least 4 unknowns. These include the masses of the two clusters, the relative velocity of the clusters, and the distance of separation between the two when they had this relative velocity. The separation is the same in MOND and Newtonian gravity, but the Newtonian mass is higher.

The relative velocity of the two clusters can be measured because, in the last few 100Myrs, the less massive sub cluster has passed through the centre of the more massive main cluster. The ram pressure has imposed a smooth bow shock (Markevitch et al. 2004; Markevitch & Vikhlinin 2007) on the gas of the sub cluster. Since the relative velocity is the foundation of the problem we leave it free and try to estimate it by fixing other variables. In our simulation, we think it sensible to consider the separation of the two clusters (i.e. of the two centres of mass) when they had the calculated relative velocity to be when the leading edge of the sub cluster's gas cloud began to pass through the dense region of gas belonging to the main cluster and separate from the dark matter. It appears that the centre of the sub cluster's gas cloud is preceeded by the nose cone of the bow shock by around 100kpc further in the direction of travel. We take 300kpc to be the radius within which the gas of the main cluster was dense enough to imprint the bow shock. Actually, the gas mass of the main cluster (sub cluster) is only measured out to 180kpc (100kpc) and could not be found further detailed in the literature. However, the uncertainty is large enough that we wished to clarify the impact of different initial separations by always using a range of initial separations of between 350-500kpc. This separation is defined as when the two pre-collision clusters had the relative velocity of v_{rel} related to the shock velocity $4740^{+710}_{-550}\,\mathrm{km\,s^{-1}}$. Now of course, they are on the opposite sides on the sky after having passed through each other and the hot gas has been offset from the DM.

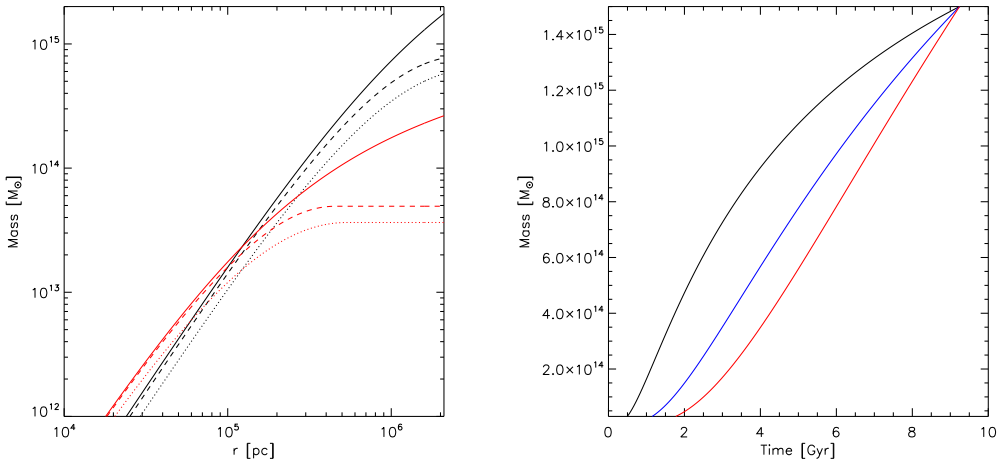

Figure 2.4: (a) The total enclosed masses for the main cluster (black) and sub cluster (red) for CDM (solid), MOND with standard μ (dashed) and simple μ (dotted). (b) The total enclosed masses for the main cluster as a function of time, where 9.3Gyr marks the collision of the two clusters and 0Gyr represents the Big Bang. The three lines correspong to different mass assembly rates α=0.5 (black), 1.0 (blue) and 1.5 (red). The mass loss is halted at $m_{200}/50$.

2.2.2 The collision in CDM

In the CDM framework, it is no problem to generate two clusters in an N-body simulation and calculate all gravitational accelerations exactly. However, in MOND we are dealing with non linear gravity and the tools for such purposes are only now being developed (Nipoti et al. 2007a; Tiret & Combes 2007a). Additionally, since we begin our simulations with the overlap of the two clusters, it is not guaranteed that the clusters preserve their shapes as they separate. Furthermore, it was not possible to simply include accretion history (Wechsler et al. 2002) in the N-body simulations or easily vary the truncation radius of the DM halo as was necessary.

Therefore, a better method was to semi-analytically account for these aspects in a simulation where gravity of one cluster acting on the other is just the mass enclosed by a sphere around the gravitating body's centre of mass with radius equal to the separation of the two cluster's centres of mass. For this procedure, the only two unknowns are the separation, which is initially known and computed each time-step; and the mass enclosed. The enclosed mass depends on the density profile of the two clusters and was fitted by C06 using NFW profiles of the form

$$\rho(r) = \frac{A}{4\pi} m_{200} r^{-1} \left(r + r_{200} c^{-1}\right)^{-2}, A^{-1} = \ln(1+c) - \frac{c}{1+c} \tag{2.10}$$

where c is the concentration. The enclosed mass goes as

$$m(r) = Am_{200}\left[\ln\left(1+\frac{cr}{r_{200}}\right) - 1 + \left(1+\frac{cr}{r_v}\right)^{-1}\right] \tag{2.11}$$

The subscripts like r_{200} refer to the radius at which the dark matter has a density which is 200 times the critical density of the Universe, ρ_c. It is generally accepted that CDM halos are virialised within r_{200}.

For the main cluster C06 gives $m_{200} = 1.5 \times 10^{15} M_\odot$, $r_{200} = 2100kpc$ and concentration c=1.94. For the sub cluster, $m_{200} = 1.5 \times 10^{14} M_\odot$, $r_{200} = 1000kpc$ and c=7.12. We augment the DM with a baryon fraction of 17% (Spergel et al. 2007) which was part of the total mass during freefall. We ran dynamical time steps (negative) such that

$$\Delta t = 10^{-4} \times \sqrt{d[pc]} Myr \tag{2.12}$$

Where d is the separation of the two centres of mass and Δt has a maximum value of 1Myr. Since initially d $\sim$ 400kpc, the starting time steps are $\sim$0.06Myr. The simulations were run until 9Gyr had elapsed.

The mass distributions as functions of radius for the two clusters in CDM and the ones used in the MOND simulations are shown in Fig 2.4(a). A subtle point about the total masses of the two clusters is that we do not expect the mass to remain constant as we go back in time. Presumably they grew from a seed of negligible mass at high redshift. This tends to impede their freefall, reducing the maximum collision velocity to $\sim 2900\,\mathrm{km\,s^{-1}}$ by the estimate of Farrar & Rosen (2007). To include this, without the impedance, we use the procedure of Wechsler et al. (2002) who used the relation

$$M(z) = M(z=0.3)e^{-\alpha(z-0.3)} \tag{2.13}$$

where α obviously encodes the rate of the accretion or assembly of the halo. Typical values used in their work are $0.5 < \alpha < 2.0$. In Fig 2.4(b) we plot the mass enclosed within r_{200} for the two clusters as functions of reshift for α=0.5,1.0 and 1.5. Note we always keep a floor value of cluster mass of $m_{200}/50$ so the halo is never completely disassembled.

Another important point is whether mass integrated out beyond r_{200} should

be included, since the actual virial radius depends on both cosmology and redshift (Bullock et al. 2001). Indeed, the internal gravity of the main cluster has not reached a_o by $r_{200} = 2100kpc$ meaning the MOND dynamical mass has not yet saturated. However, recall that it takes $\sim (r_{200} - d)/v_{rel} = (2100kpc - 400kpc)/3400\,\mathrm{km\,s^{-1}} \sim 500Myr$ for the clusters to separate enough for this extra matter to even begin to manifest itself. The cluster is also losing mass (backwards in time) due to accretion and although it is true that it makes no difference whether the matter is bound to the main cluster to pull the sub cluster towards it, if it is not forming an overdensity it is sensible to assume there is a cancelling mass on the opposite side of the Universe.

Using Eq 2.11 it is straight-forward to include all the enclosed mass out to any radius because the parameters r_{200} and m_{200} do not explicitly force the enclosed mass to truncate at r_{200}, they simply define the shape of the profile in the inner part. Nusser (2007) also investigated the idea of placing a mass overdensity between the two clusters above the typical critical density to show that this can also enhance the relative speed.

2.2.3 The collision in MOND

Recall that in MOND, the basic modification of purely Newtonian dynamics is given by Eq 1.5 and we usually implement one of the common interpolation functions: the "standard" function traditionally used in fitting rotation curves (Eq 1.6) and the "simple" function (Eq 1.7) found by Famaey & Binney (2005) to provide a good fit to the terminal velocity curve of the Galaxy.

A well known problem with implementing the MOND force law in numerical computations is that the original formulation (Eq 1.5) does not conserve momentum. This was corrected with the introduction of a Lagrangian formulation of MOND (Bekenstein & Milgrom 1984; Milgrom 1986) which has the modified Poisson equation (Eq 1.8). This formulation has been shown to obey the necessary conservation laws (Bekenstein & Milgrom 1984; Bekenstein 2006). With some rearrangement, it leads to

$$\mu(x)\mathbf{g} = \mathbf{g_N} + \nabla \times \mathbf{h}, \tag{2.14}$$

which we recognize as Eq 1.5 with the addition of a curl field.

Unfortunately, implementing a numerical formulation of the modified Poisson equation is not a simple one-line change to typical N-body codes: this fails to obey the conservation laws. Instead, one needs an entirely different numerical approach than is commonly employed. Progress has been made along these lines (e.g., Brada & Milgrom 1995, 1999; Ciotti et al. 2006; Nipoti et al. 2007a, 2008; Tiret & Combes 2007a, 2008; see also Nusser 2002; Knebe & Gibson 2004), but we do not seek here a full N-body treatment of complex systems. Rather, we wish to develop and apply a simple tool (Angus & McGaugh 2008) that can provide some physical insight into basic problems. For the specific case of the large collision velocity of the bullet cluster, it suffices to treat the curl field as a small correction to the center of mass motion (Milgrom 1986), which is unimportant here, since we are not interested in mass weighted motions but relative ones.

Recall that the MOND correction to the gravity through the μ function depends on the external gravity (the external field effect §1.4), which here comes from large scale structure. The external field effect (see Milgrom 1983c; Bekenstein 2006) is crudely approximated in Eq 2.15 as a constant of appropriate magnitude (McGaugh 2004). We checked the effect of varying the external field, which is modest. It is not possible to do better without complete knowledge of the mass distribution in the environment of the clusters.

When modeling the bullet cluster in MOND, (§2.1 and Angus et al. 2007) we fitted the convergence map of C06 using spherical potential models for the four mass components. The best fit gives masses for all four components in MOND and standard dynamics. Unfortunately, the map is only sensitive out to 250kpc from the respective centres which neglects an over large portion of the dynamical mass. So, in order to remain consistent with the CDM simulations, we take the NFW profile and calculate what the MOND dynamical masses for the two commonly used interpolating functions (Eq 1.6 & 1.7) are, as shown in Fig 2.4(a). The total Newtonian mass at r_{200} for the main cluster is twice that of the MOND dynamical mass with the standard μ and three times when the simple μ is used.

The mutual gravity imposed upon the sub cluster by the main cluster is

$$\mu\left(\frac{|g_{sub}+g_{ex}|}{a_o}\right) g_{sub} = g_{n,sub} = -GM_{main}(d)/d^2 \tag{2.15}$$

and we simply swap the subscripts around to find the mutual gravity of the sub

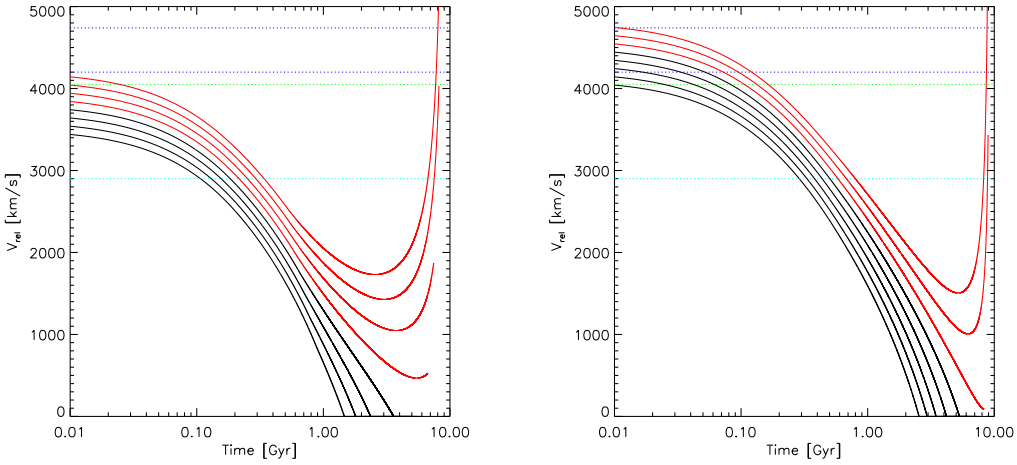

Figure 2.5: Shows the relative velocity of the two clusters plotted against time (a) CDM and (b) MOND. Time=0Gyr is the current (z=0.3) relative velocity of the two clusters with larger times corresponding to higher redshifts. Black lines correspond to relative velocities that are achievable, whereas red lines are not. In (a) we use the simulation (CDM2c) for which α=1.0, d=425kpc and we truncate the halos at r_{200}. The relative velocities used are v_{rel}=3500-4200 km s^{-1} in intervals of 100 km s^{-1}. In (b) we use the simulation (MONDst2) which uses the standard μ function and α=0.5, d=425kpc. The relative velocities used are v_{rel}=4100-4800 km s^{-1} in intervals of 100 km s^{-1}. The 4 dashed lines are the predicted relative velocities according to the mean and 1σ error of the original relative velocity from Markevitch & Vikhlinin (2007) in blue, the simulations of Milosavljević et al. (2007) in green and Springel & Farrar (2007) in turquoise. The high observed collision velocity is more readily obtained in MOND than CDM.

cluster upon the main cluster. Following on from above, d is the distance between the two centres of mass and $M_{main}(d)$ is the enclosed mass within a radius d from the centre of mass of the main cluster. The g_{ex} is the external field limiting the MOND correction which comes from large scale structure and is always assumed orthogonal to the direction of g_{sub}, making the argument of the μ function more easily expressed as $\frac{\left(g_{sub}^2+g_{ex}^2\right)^{1/2}}{a_o}$. The direction and amplitude of g_{ex} is unknown at all times, but we use $g_{ex} = a_o/30$ (Aguirre et al. 2001; McGaugh 2004) which is roughly the external field imposed on the Milky Way by M31 and vice versa (Famaey et al. 2007c; Wu et al. 2007).

2.2.4 N-body collision

Our first attempt at simulating the collision in Newtonian gravity was using a standard N-body tree code. The benefit it gives is that in principal, we can more accurately compute the mutual gravity at the beginning of the simulation when the two clusters overlap. However, this is fraught with difficulties and inconsistencies. The first being that tidal effects undoubtedly stretch the two clusters and 2-body interactions may eject particles from the two halos. Therefore, it makes better sense to begin such a simulation from high redshift where the clus-

ters are greatly separated and tidal effects are negligible and let them freefall in the expanding Universe and when they collide, the tidal effects will be well accounted for. Of course, the problem is that it is not trivial to then sample collision velocities because the separation and time at which the two clusters began their freefall is not simply related. Moreover, the truncation of the two halos and different mass models are not easily varied. Nevertheless, we did attempt a CDM N-body model with truncation at r_{200} for both halos. We found a similar result to that from the semi-analytical models of a relative velocity of $3800\,\mathrm{km\,s^{-1}}$.

2.2.5 Results

The ability of the two clusters that comprise the bullet to bring each other to a halt at a finite time in the past is sensitive to both the flavour of gravity at work and the true relative velocity. For velocities larger than the maximum, the relative velocity never reaches zero and increases sharply at early times (see Fig 2.5). The two clusters do not gravitate strongly enough to generate such high velocities and would have to have had a huge relative velocity towards each other in the early universe in order to overcome the Hubble expansion and fall together with such a high relative velocity at z=0.3. Fig 2.5 shows how the relative velocity of the two clusters varies with time for a large sample of initial (meaning collisional) relative velocities for a CDM and MOND sample simulation. A difference of just $100\,\mathrm{km\,s^{-1}}$ can have a significant impact on the time required to generate such a large velocity and by the same token, the longer the two clusters free-fall, the larger a velocity they can generate. Sadly, there is only a finite time ($\sim$ 9Gyr) since the Big Bang for this to happen.

In Table 2.3 are the key results of the simulations to give a feel for the maximum possible relative velocity. Each velocity is that achieved with an initial separation of 425kpc, where taking 350 or 500kpc induces an increase or decrease of $100\,\mathrm{km\,s^{-1}}$ which we take as the minimum error. The most extreme CDM model is to have no truncation of the DM halos, extending them out to r_1. This extreme allows a maximum relative velocity of $4500\,\mathrm{km\,s^{-1}}$. Then, if we still allow the halos to extend to r_1, but account for some assembly of the halos with $\alpha = 1$ then the relative velocity reduces to $4200\,\mathrm{km\,s^{-1}}$.

More realistically, if we truncate the halos at r_{200} and try four different halo assembly rates such that α = 0.0, 0.5, 1.0 & 1.5 we get respective maximum

Model	Max V_{rel} [$\mathrm{km\,s^{-1}}$]	Truncation Radius	α	Gravity
CDM1a	4500	r_1	0.0	Newtonian
CDM1b	4200	r_1	1.0	Newtonian
CDM2a	4000	r_{200}	0.0	Newtonian
CDM2b	3900	r_{200}	0.5	Newtonian
CDM2c	3800	r_{200}	1.0	Newtonian
CDM2d	3800	r_{200}	1.5	Newtonian
MONDst1	4800	r_{200}	0.0	MOND-standard μ
MONDst2	4500	r_{200}	0.5	MOND-standard μ
MONDsi1	4600	r_{200}	0.0	MOND-simple μ
MONDsi2	4500	r_{200}	0.5	MOND-simple μ

Table 2.3: Shows the parameters used in the different models and gives the maximum attainable relative velocity for each.

relative velocities of 4000, 3900, 3800 and 3800 $\mathrm{km\,s^{-1}}$. These numbers represent the plausible maximum relative velocities in the CDM framework.

For the MOND case we ran simulations with both the simple (Eq 1.7) and standard (Eq 1.6) μ functions. The standard function leads to higher dynamical masses from the NFW profile, but lower MOND correction to the gravity. The standard (simple) function with no accretion and with $\alpha = 0.5$ generate 4800 (4600) and 4600 (4500) $\mathrm{km\,s^{-1}}$ respectively and for comparison, the maximum CDM velocity with those reduced masses is just 2700 (2300) $\mathrm{km\,s^{-1}}$. This is a clear demonstration of the expectation in MOND for larger peculiar velocities. We use the lower assembly parameter $\alpha = 0.5$ because structure is expected to form more swiftly in MOND (Sanders 1998, 2001, 2008).

An important factor is the fitted NFW density profile to the convergence map, in which matter is extrapolated to 2100kpc and 1000kpc for the main and sub cluster respectively. Presumably the significance of the detection of this mass is negligible and the NFW fit has been made assuming if we know the details in the central 250kpc, then we know the density out to r_{200}. The mass sheet degeneracy is broken by constraining the mass at the edges of the fit based on the slope of the density profile in the inner regions - but if the mass profile is wrong then it could lead to the completely wrong measurement for the value of the mass sheet (Clowe et al. 2004a).

All of this means that the density profiles of the two clusters could be moderately different in reality. However, the actual shape of any profile is less important to the relative velocity than simply the normalisation of the total mass. To

this end we have simulated the collision with 10% more and 10% less mass for both clusters (with assembly parameter $\alpha = 1$). The effect is to increase (10% more mass) or decrease (10% less mass) the relative velocity by $200\,\mathrm{km\,s^{-1}}$ from $4800\,\mathrm{km\,s^{-1}}$ for model MONDst1.

Another concern is that the clusters are unlikely to be spherically symmetric (Buote & Canizares 1996) and are presumably elongated in the direction of motion. Again this could lead to an incorrect density profile, whereas ellipticity itself would have little effect on our results.

2.2.6 Discussion

We have constructed specific mass models for the bullet cluster in both CDM and MOND. We integrate backwards from the observed conditions to check whether the large ($\sim 4700\,\mathrm{km\,s^{-1}}$) apparent transverse velocity can be attained in either context. We find that in ΛCDM it is difficult to achieve $v_{rel} > 4500\,\mathrm{km\,s^{-1}}$ under any conditions. Nevertheless, within the range of the uncertainties, the appropriate velocity occurs fairly naturally in MOND. In contrast, ΛCDM models can at most attain $\sim 3800\,\mathrm{km\,s^{-1}}$ and are more comfortable with considerably smaller velocities.

Taken at face value, a collision velocity of $4700\,\mathrm{km\,s^{-1}}$ constitutes a direct contradiction to ΛCDM. Ironically, this cluster, widely advertised as a fatal observation to MOND because of the dark matter discrepancy it shows, seems to pose a comparably serious problem for ΛCDM.

Two critical outstanding issues remain to be clarified. The first is the exact density profiles and virial masses of the two clusters and the second is how the observed shock velocity relates to the actual collision velocity of the two gravitating masses. The recent simulations of Springel & Farrar (2007) and Milosavljević et al. (2007) seem to suggest that, contrary to naive expectations, hydrodynamic effects reduce the relative velocity of the mass with respect to the shock. A combination of effects is responsible, being just barely sufficient to reconcile the data with ΛCDM. Hydrodynamical simulations are notoriously difficult, and indeed these two recent ones do not agree in detail. It would be excellent to see a fully self-consistent simulation including both hydrodynamical effects and a proper mass model and orbital computation like that presented here.

There are a number of puzzling aspects to the hydrodynamical simulations.

First of all, Springel & Farrar (2007) use Hernquist profiles (Hernquist 1990) for the DM distribution in the clusters and not NFW halos. Furthermore, they find that the morphology of the bullet is reproduced only for a remarkably dead head-on collision. If the impact parameter is even 12kpc — a target about the diameter of the Milky Way — quite noticeable morphological differences ensue. This can be avoided if the separation of mass centres happens to be along our line of sight — quite a coincidence in a system already remarkable for having the vector of its collision velocity almost entirely in the plane of the sky. Furthermore, the mass models require significant tweaking from that infered from the convergence map and are unable to reproduce the currently observed, post merger positions of the gas and DM. It appears to us that only the first rather than the last chapter has been written on this subject. Getting this right is of the utmost importance, as the validity of both paradigms rests on the edge of a knife, separated by just a few hundred $\mathrm{km\,s^{-1}}$.

More generally, the frequency of bullet-like clusters may provide an additional test. The probability of high collision velocities drops with dramatic rapidity in ΛCDM at the high velocity tail (Hayashi & White 2006). In contrast, somewhat higher velocities seem natural to MOND. Naively it would seem that high impact velocity systems like the bullet would be part and parcel of what might be expected of a MOND universe. With this in mind, it is quite intriguing that many bullet cluster like systems have been detected (although none quite as unique). The dark ring around Cl0024+17 tentatively observed by Jee et al. (2007), but see also Milgrom & Sanders (2008). The dark core created by the "train wreck" in Abell 520 by Mahdavi et al. (2007), Cl0152+1357 (Jee et al. 2005a), MS1054+0321 (Jee et al. 2005b) and the line of sight merger with $> 3000\,\mathrm{km\,s^{-1}}$ relative velocity observed by Dupke et al. (2007) for Abell 576 may all provide examples and potential tests.

2.3 X-ray analysis of DM in groups and clusters of galaxies

Groups of galaxies are systems generally consisting of a host galaxy and some satellite galaxies considerably less massive. For instance, the Milky Way has several dwarf galaxies orbiting it, but the largest three satellites (at least temporarily) are the two Magellanic clouds and the Fornax dwarf spheroidal; ∼10, 60 and 3000× less massive than the Milky Way. It is a fairly low density environment and the relative velocities of the galaxies are generally quite low (200-400 $\mathrm{km\,s^{-1}}$). This is in contrast to clusters of galaxies which have many large galaxies and the random speeds can be around 1500 $\mathrm{km\,s^{-1}}$. Additionally, the intra-group medium of X-ray emitting hot ionised gas has a temperature of around 0.5-1.5keV whereas clusters are generally much hotter (T>3keV) and denser.

Groups of galaxies were first studied in MOND by Milgrom (1998, 2002) by checking the stellar mass to light ratio required for consistency with the line of sight velocity dispersion of the group galaxies w.r.t. the centre of mass.

$$M \approx \frac{81}{4}\frac{\sigma_{los}^4}{Ga_o}. \tag{2.16}$$

Comparison of this dynamically inferred MOND mass and the luminosity of the galaxies in the groups (the mass-to-light ratio) were around unity which bears the hallmark of no mass discrepancy, however, it could not probe the need for dark matter at smaller radii than these largely separated galaxies (∼500kpc size). Of course, it is possible that this absence of discrepancy is correct in the context of low mass groups with no detected X-ray emission, but in the case of X-ray bright groups and clusters a better gauge of dynamical mass is found using measurements of the properties of the X-ray gas (e.g., The & White 1988; Gerbal et al. 1992; Buote & Canizares 1994; Pointecouteau & Silk 2005) or weak and strong gravitational lensing (Angus et al. 2007; Takahashi & Chiba 2007; Milgrom 2008; Ferreras et al. 2008). The result is that MOND cannot as yet explain the mass discrepancy in X-ray bright groups and clusters of galaxies, especially in their cores, while the gravitational lensing map of the bullet cluster has provided an extremely important constraint on the nature of all the missing mass, i.e. that it must be of a collisionless nature (C06; B06).

It has been conjectured (Sanders 2003, hereafter S03) that the mass discrepancy in galaxy clusters might be resolved by the addition of a component of massive active neutrinos m_ν ∼2eV, very near their maximum experimentally derived limiting mass of 2.2eV. These were indeed shown to be potentially consistent with the majority of clusters with temperature greater than 4 keV by S03, and with the bullet cluster (§2.1; Angus et al. 2007). This hypothesis has the great advantage of naturally reproducing the proportionality of the electron density in the cores of clusters to $T^{3/2}$, as well as global scaling relations (Sanders 2007, hereafter S07). However, in a recent survey, Pointecouteau & Silk (2005, hereafter PS05) studied a large sample of hot clusters (>4keV) and found that the central density of the dark matter was generally greater than allowed by the Tremaine-Gunn limit on neutrino density. This result was not damning, though, since the dynamical mass that could be accounted for by neutrinos under the Tremaine-Gunn limit was generally more than 90%.

This is also apparent from fits to the bullet cluster in §2.1 where the size of the neutrino core is just barely adequate for a fit to the main cluster within the errors, whereas the sub cluster most probably requires a boost to the central density not achieveable by neutrinos, but has not been accurately modelled.

On the other hand, something that has never been addressed in the literature is the application of MOND to X-ray emitting groups and cool clusters in the range $0.5< T <3.0$keV. The closest anyone has come is the study of the large elliptical NGC 720 by Buote & Canizares (1994, 2002) which has T∼0.6keV. They showed that the major axes of the isophotes of the X-ray emission are significantly offset from the major axes of the galaxy and since the galaxy outweighs the gas by more than an order of magnitude, the hot gas should trace the potential of the galaxy assuming the galaxy is not rotating in the plane of the sky. To reconcile this, we need a third, dominant potential which the hot gas is tracing. NGC 720 is currently the only elliptical galaxy for which this misalignment is possibly attributable to dark matter. A program to search for other very isolated, flattened elliptical galaxies that are sufficiently bright in X-rays for this type of study is underway.

2.3.1 Data

We use results obtained for relaxed clusters primarily from two recent studies of X-ray clusters. These systems were chosen to be among the most relaxed known in order to ensure that hydrostatic equilibrium holds most accurately.

We use the published results of Vikhlinin et al. (2006) for 8 of the most massive clusters ($2\,\mathrm{keV} < T < 9\,\mathrm{keV}$). For low-mass clusters (groups) we use results for 16 groups of galaxies (1-2 keV) from the recent work of Gastaldello et al. (2007) and another low-mass cluster (A2589) from Zappacosta et al. (2006). Finally, we include the elliptical galaxy NGC 4125 ($T \sim 0.5$ keV) from Humphrey et al. (2006) to extend our sample of X-ray emitting systems down to the galaxy scale.

The objects in our sample are listed in Table 2.4. We refer the reader to the references for details on the construction of the density, temperature, and Newtonian mass profiles. We note that for the massive systems in the Vikhlinin et al. sample we exclude the central ~ 20 kpc from the analysis. We do this for consistency with their study, even though some of their systems (most notably A2029), do not exhibit substantial morphological irregularities in their cores that would lessen the validity of the approximation of hydrostatic equilibrium.

2.3.2 MOND dynamical mass in groups and clusters

To compute gravitating masses we assume the intracluster medium is represented by a spherical single-phase ideal gas in hydrostatic equilibrium. Although the X-ray isophotes of relaxed clusters are approximately circular with modest ellipticity, the underlying mass distribution is inferred to have substantial ellipiticy (0.4-0.6; Buote & Canizares 1996). Nevertheless, many previous studies have shown that assuming spherical symmetry for relaxed clusters introduces fairly small errors $< 20\%$ which are acceptable for our purposes (e.g., Tsai et al. 1994; Navarro et al. 1995; Buote & Canizares 1996; Evrard et al. 1996; Gavazzi 2005).

We derive the MOND dynamical mass for each system following the approach of Sanders (1999). From the temperature and density profiles of the hot gas, the centripetal gravitational acceleration, g, can be deduced from the equation of hydrostatic equilibrium $dP/dr = d(\rho\sigma^2)/dr = -\rho g(r)$ with $\sigma^2 = kT/wm_p$ which

gives

$$g(r) = \frac{-kT(r)}{\mathrm{w}m_p r}\left[\frac{d\ln\rho_X(r)}{d\ln r} + \frac{d\ln T(r)}{d\ln r}\right], \tag{2.17}$$

where $w = 0.62$ is the mean molecular weight and $wm_p = 5.2\times10^{-58}M_\odot$, the combination $kT(r)$ is in units of keV and the dynamical gravity is $g(r)$. From this, the Newtonian dynamical mass can easily be deduced as $M_n = r^2 g(r)/G$.

Note that since we model clusters as spherical systems, we can ignore the curl field of MOND (see §2.2.3), and since the external field effect from Large Scale Structure (e.g., §2.2) is much smaller than the typical gravitational acceleration in the region of interest, we can simply use the relation of Milgrom (1983c) to derive the MOND dynamical mass:

$$M_m(r) = \frac{r^2}{G} g(r)\mu[g(r)/a_o], \tag{2.18}$$

where $G = 4.42\times10^{-3}\mathrm{pc}(\,\mathrm{km\,s^{-1}})^2 M_\odot^{-1}$ is Newton's gravitational constant. Here the interpolating function $\mu(x)$ is chosen to be Eq 1.7. Taking $\mu = 1$ just reduces to the Newtonian dynamical mass, but the MOND dynamical mass M_m is related to the Newtonian one M_n by

$$M_m(r) = \frac{M_n(r)}{1 + a_o/g(r)}, \tag{2.19}$$

so that in MOND, there is a truncation of the dynamical mass $M_m(r)$ at low accelerations. Here we take the MOND acceleration constant to be $a_o = 3.6\,(\mathrm{kms^{-1}})^2/\mathrm{pc} = 1.2\times10^{-10}\mathrm{ms^{-2}}$ as it is everywhere in the thesis. A subtle point to note is that from Eq (2.19), one can see that at large radii, when $d\ln M_n/d\ln r < 1$ (as is the case for NFW profiles) and $g(r) << a_o$, then the MONDian enclosed dynamical mass begins to drop with radius. This is of course unphysical, and is caused by MOND generically predicting a logarithmic potential at large radii. This makes studies that do not consider the entire dynamical mass profile at all radii worthless when based on a Newtonian NFW profile. In this work, we circumvent this problem by flattening the enclosed MOND mass profile at its maximum value, and numbers in Table 2.4 are quoted at the radius corresponding to this maximum value. Further away, MOND predicts that the potential should not conform to an NFW profile but rather to an isothermal sphere.

For the objects in our sample from Gastaldello et al. (2007); Humphrey et al.

(2006) and Zappacosta et al. (2006), we take the Newtonian dynamical mass profiles used in those studies and simply extract the MOND dynamical mass using Eq (2.19). Those studies produced 20-30 Monte Carlo simulations of Newtonian mass profiles for each object, which were used to produce the errors. For MOND profiles, because the μ-function is not precisely known, any errors on the data are dwarved by the intrinsic errors. Therefore, we take the error on the MOND mass as half the difference between M_m calculated with the simple μ-function (Eq 1.7, which gives a relatively low mass) and M_m with the standard μ-function (Eq 1.6, which gives a relatively high mass). These limits contain the majority of the reasonable MOND profiles and so can be naively taken as 1-σ.

Since we do not have error estimates for the density and temperature profiles of the objects in the Vikhlinin et al. sample, we just use the best-fitting values. However, as the objects are more massive and generally brighter than the lower mass objects, we expect the relative uncertainty on the massive systems to be typically comparable to or less than the lower mass systems. In any case, the systematic errors on the MOND masses calculated by using different μ-functions are large enough to account for any small random errors in the Newtonian mass.

Subtracting the X-ray gas and galaxies

We integrated the hot gas component to find the observed enclosed gas mass, $M_X(r)$ from

$$M_X(r) = \int_0^r 4\pi\rho_X(r)r^2 dr \tag{2.20}$$

where $\rho_X(r)$ is the density of plasma.

Of course, the observable isn't ρ_X, but the emission integral

$$EI = \int n_p n_e dV = \int 0.82 n_e^2 dV \tag{2.21}$$

where n_p and n_e are the number densities of protons and electrons respectively and the integral is an annulus along the line of sight. This can be used to find $\rho_X = \frac{m_p}{w}(n_p n_e)^{1/2}$.

The empirical scheme for the galaxy mass profile employed by S03 and PS05, i.e. $M_*(r)/M_X(r) \approx 0.4(kT/\mathrm{keV})^{-1}$ completely neglects the contribution of galaxies to the cluster mass below 150 kpc where the most massive galaxies reside. Furthermore, for groups this is a poorly motivated scheme and so for

them we only include the mass of the BCG. This is reasonable as the MOND dynamical mass of groups saturates at around 100 kpc and we checked the surrounding 100kpc of the BCG in all systems and found no galaxies contributing more than 5% which is easily contained within the errors on M/L_K.

For the clusters we used both the BCG luminosity and the empirical galaxy density of S03 and PS05. The luminosity of the BCG in the K band from the Gastaldello et al. (2007) sample are taken from their paper, while those from Vikhlinin et al. (2006) are taken from Lin & Mohr (2004) and the 2MASS survey. All are employed using a Hernquist profile (Hernquist 1990). We subtracted this using M/L_K=1 which is standard for these very old stellar populations and a Kroupa IMF (Kroupa 2001); however, if a Salpeter IMF is used, we can expect M/L_K to increase by around 50% (Humphrey 2006). The X-ray studies of groups and clusters (Gastaldello et al. 2007; Zappacosta et al. 2006) typically find M/L_K <1, sometimes << 1 as they try to incorporate an NFW halo. By using M/L_K=1, we are making a conservative estimate of the galaxy contribution.

Subtracting both the X-ray mass and the galaxies from the total MOND dynamical mass leaves the total dark mass (M_{DM}) which is simply the mass of dark matter necessary to reach agreement with the MOND dynamical mass.

2.3.3 Active neutrinos as the MOND dark mass?

At least two of the three active neutrinos (ν_e, ν_τ and ν_μ) have non-zero masses, meaning that they *must* be part of the mass budget of the Universe. Interestingly, in ΛCDM cosmology, it is possible to put stringent limits on the sum of the three neutrino masses, from the angular power spectrum of the Cosmic Microwave Background and from the slope of the matter power spectrum (e.g., Zunckel & Ferreira 2007; Host et al. 2007), essentially because a neutrino component that is too massive would not leave enough room for CDM in the matter budget of the Universe, resulting in the loss of small-scale power for forming structures (discussed in §2.5).

However, these constraints are not necessarily valid in MOND where small scale power arises from the additional gravity of MOND and fits to the angular power spectrum of the CMB must be achieved with dark matter that does not interfere with individual galaxies i.e. hot dark matter.

S03 showed that such 2 eV neutrinos at the limit of detection could indeed

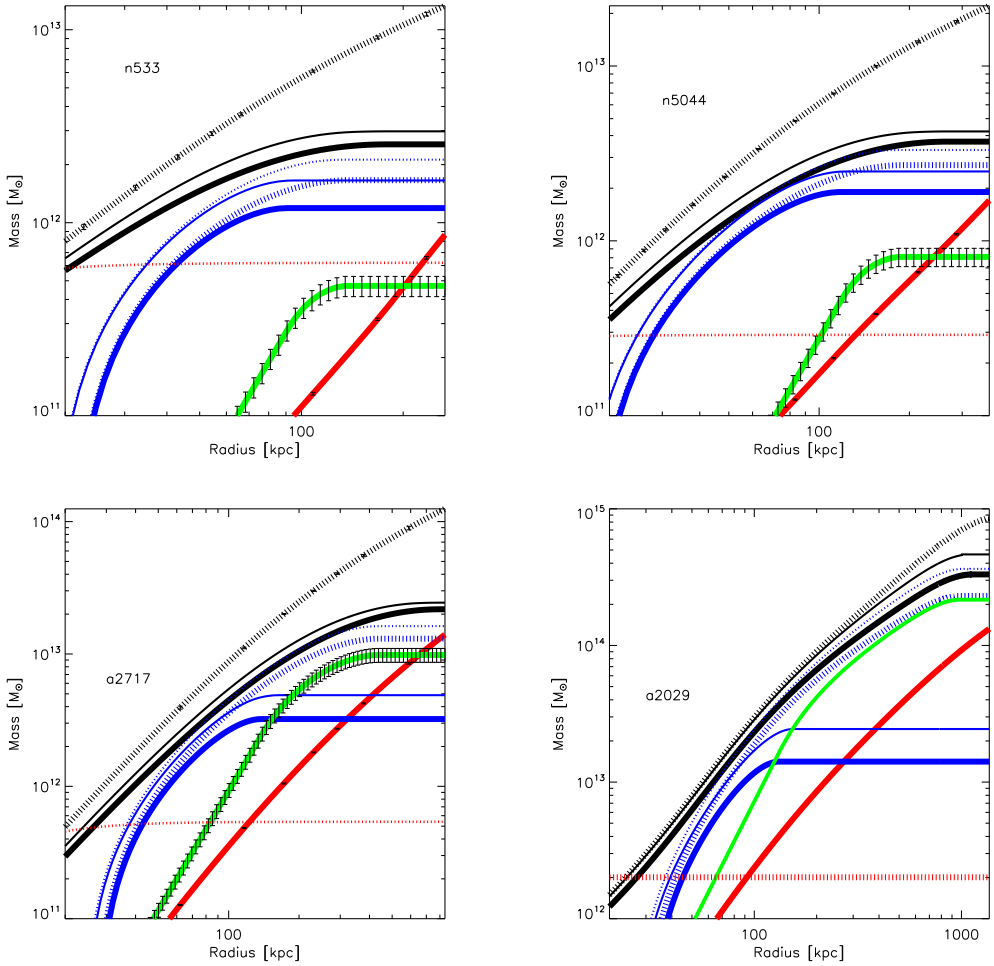

Figure 2.6: Shows the mass profiles of the components of the dynamical mass for 4 representative clusters: N5044 (T=1.0 keV), N533 (T=1.2 keV), A2717 (T=2.2 keV), and A2029 (T=8.5 keV). The total MOND dynamical mass (M_m) is in black with thick-solid linetype and its 1-σ error is the thin-solid black line (there is virtually no error below). The Newtonian dynamical mass is black with a dotted linetype. The solid red line corresponds to the observed mass of X-rays and the dotted red line is the mass of the BCG if M/L_K=1 for which we use a Hernquist profile (Hernquist 1990). The green line is the maximum necessary contribution of neutrinos; by this we mean it is maximal (Eq.2.30) in the centre where the dynamical mass is unexplained, whereas at the outskirts the neutrinos no longer have maximum density, instead they have the density necessary to complete the budget after gas and the residual mass at the centre has been accounted for. The thick solid blue line is the residual mass unexplained by the neutrinos and gas and its 1-σ error is the thin solid blue line. The dotted blue line is the necessary residual mass if we have no significant neutrino density and again the 1-σ error is the thin dotted blue line. Of course there is another error associated with the mass of the neutino, but we have fixed the neutrino mass at 2eV. Obviously a range of blue solid lines are possible between the solid blue and dotted blue depending on neutrino mass. If the neutrino has a mass $<<$2eV then we simply recover the dotted blue line. Clearly, one sees that for low temperature clusters such as N5044, no DM is present at r $>$ 150 kpc. The errors on the different lines are not independent from each other. The firm result here is that no random or systematic errors can ever make the green line (which overestimates the true contribution of 2 eV neutrinos by assuming a fully constant density in the core) reach the thick dotted blue line in the core of clusters, or even anywhere in groups, if the mass of active neutrinos is smaller than its experimental upper bound.

account for the bulk of the dynamical mass in his sample of galaxy clusters of $T > 4\,\mathrm{keV}$ (see his Fig 8). In §2.1 it was shown that such neutrinos could account for the weak lensing map of the bullet cluster (C06; B06). However, looking at the central region of clusters, PS05 showed that neutrinos could not account for the dark matter all the way to the centre because the density reaches values larger than the Tremaine-Gunn limit. However, this residual mass is only a few percent of the dynamical mass explainable by neutrinos or BBN baryons.

Here, we choose as a conservative approach to take the temperature of the neutrino fluid as being equal (due to violent relaxation) to the mean emission weighted temperature of the hot gas. We also assume that they contribute maximally, i.e. that their density is given by the Tremaine-Gunn limit, and constant (which is obviously untrue since the fluid obeys the equation of state of a partially degenerate neutrino gas, discussed later). We thus *overestimate* the true contribution that neutrinos might make. This is of little concern, however, since, as we shall see in the next section, we do not wish to conclude anything beyond the fact that even overestimating the physical contribution of 2 eV neutrinos to the mass budget of the cluster does leave a massive, dense central component of unexplained mass, and contributes nothing to groups which require a dense residual component after subtraction of hot gas and galaxies. We shall estimate the importance of this residual component in clusters and groups, but beyond that we shall also consider the amount of DM needed if neutrinos have a negligible mass and do not contribute at all to the mass budget.

2.3.4 Residual Mass

In Fig 2.6 we plot, for four representative objects, several components of the group or cluster mass distinctly as functions of radius. The total MOND dynamical mass (M_m) is in black with solid linetype, the Newtonian dynamical mass (M_n) is black with a dotted linetype. The red line corresponds to the observed mass of X-rays (M_X) and the dotted red line is the mass of the BCG assuming M/L_K=1 and a Hernquist profile (Hernquist 1990). The green line is the maximum necessary contribution of neutrinos (M_ν). The solid blue line is what we call the residual mass ($M_{m-X-\nu-*}$) unexplained by the neutrinos, galaxies and hot gas, whereas the dotted blue line is the necessary total dark mass ($M_{m-X-*} = M_{DM}$) if we have no significant neutrino density. The various thin lines correspond to the

systematic errors coming from the choice of μ-function. The four representative clusters have respective temperatures 1.0, 1.2, 2.2 and 8.5 keV. Clearly, one sees that for low-temperature groups such as NGC5044, no DM is present at $r >$ 150 kpc.

We conclude that neutrinos might explain the mass discrepancy in the outer parts of the clusters, especially those with high temperatures ($T > 3$ keV), keeping in mind that no dark mass at all is necessary in the outer parts for the cooler clusters. However, to examine the real contribution of massive neutrinos in the outer parts of rich clusters, one should describe the equilibrium distribution expected for the neutrinos, and then examine whether this physically well-motivated profile can fit the data. This is however a non-trivial task in the context of MOND, that requires solution of a Lame-Emden-like equation for polytropic models. Moreover, if the models are made more realistic by not considering purely self-gravitating neutrino spheres but also including a component of baryons, the task becomes even less trivial. This is far beyond the scope of what we want to achieve here, and will be the subject of further studies.

The important result is that even with our overestimate of the neutrino contribution, we found that neutrinos cannot account for the dark mass in the central 150 kpc. Much fuss has been made in the literature about the neutrinos being unable to account for this core of residual mass (PS05; Takahashi & Chiba 2007; Ferreras et al. 2008), which is true. Indeed, every one of the sample clusters has a dominant central core of residual mass. Nevertheless, although all these systems have a residual dark component, it has been neglected as to how serious this extra component is, which the neutrinos cannot account for, and how this varies with temperature and mass of the cluster. Actually, in Fig 2.7(c), which plots the ratio of residual mass (with and without neutrinos) to MOND dynamical mass, we see that for hot clusters, like those studied studied by S03 and PS05, the residual mass (after neutrinos have been added) is a small fraction, with gas and neutrinos being more important globally (even though, as stated above, the contribution of neutrinos is a bit overestimated here). Conversely, for groups like NGC5044, the residual mass is completely dominant and is up to four times more significant than the stellar and gas components and even moreso in the centres. Recall that the neutrinos cannot lay claim to the high densities in the cores due to the Tremaine-Gunn limit (and low temperatures of groups), but at a certain

radius begin to dominate the dynamical mass. Given that our approximation is bound to overestimate the neutrino contribution, this radius is actually the *minimal* radius at which neutrinos might begin to dominate the mass budget of the cluster. This radius r_ν is plotted as a function of temperature in Fig 2.7(a) for 2eV neutrinos.

Of course, if neutrinos are not present, then the residual DM is by far the most dominant component, moreso than the gas and galaxies for all groups and clusters. It is also important to realise that any departures from hydrostatic equilibrium generally cause underestimates of the total mass; i.e., from non-thermal pressure support. This would only exacerbate the problems highlighted in this paper.

In Table 2.4 we list the different mass components in the sample of clusters, and in Fig 2.7(b) we plot the MOND dynamical mass of the clusters against temperature, which is fitted with a curve of the form $M_m \propto T^{2.4}$, close to the MOND prediction (S07) of a relation $M_m \propto T^2$. In order to get a strict $M_m \propto T^2$ the system has to reach the asymptotic MOND regime and the T used should be the asymptotic T, not the emission weighted average (or otherwise) and of course, must be constant. Furthermore, the systems should have the same logarithmic density slope at the measured radius.

We show in Fig 2.7(c) the fraction of residual mass as a function of cluster mass. If neutrinos are not present, then the fraction of residual dark mass is constantly high (between 60% and 80%) because it must account for the largest chunk of the dynamical mass, however, if neutrinos are present then the residual mass becomes less important for heavier clusters. In Fig 2.7(d), one sees that the total dark mass scales with temperature, but that if 2 eV neutrinos are present the residual mass appears to saturate at a temperature of around 3 keV and a mass of $\sim 10^{13} M_\odot$. Interestingly, at the opposite end of the scale, the residual mass is steeply falling towards zero for groups of $T < 2keV$, meaning that the amount of residual mass could in some sense be linked with the energy of X-rays themselves. Below the 0.5 keV threshold we get back to systems like the groups studied by Milgrom (1998, 2002), where no dark mass is needed and X-ray emission is weak.

Brightest Cluster Galaxies

We express the quantity of residual mass in the central parts of the cluster as a MOND dynamical mass-to-light ratio for the BCG, ranging between 1.7 and 20 (see Fig 2.9). This mass-to-light ratio corresponds to an amount of mass that must be present within the radius r_ν. From Fig 2.8(b) we see that the residual mass does indeed scale with the K-band luminosity of the BCG which might be as expected if the BCGs had large M/L_K. However, if this were the case, we should be able to fit the stellar mass profile (with variable normalisation) without a DM profile and it should describe the data well. Unfortunately, the mass profiles of galaxy groups/clusters are not well fit by a de Vaucoulers profile with R_e set to that of the central galaxy but allowing for variable M/L_K. If we did this, we would over predict the interior mass profile. In addition, the barycentres of many clusters do not precisely coincide with the BCG (the bullet cluster for example). This scaling of the residual mass with the luminosity of the BCG could thus rather mean that the heaviest BCGs reside in clusters with more X-ray emitting hot gas, and that large amounts of cold gas clouds are in turn also present (see Milgrom 2007a and §2.3.4).

Transition temperatures

There is an increase in significance of the residual mass component left after the subtraction of hot gas and neutrinos for lower temperature clusters. Furthermore, for groups below 1.5keV, the contribution of neutrinos is negligible compared to the galaxies and hot X-ray gas. Conversely, 2eV neutrinos have the potential to be of great importance in the dynamics of clusters hotter than 3keV, and subsequently are likely to help seed the collapse of these structures from cosmological perturbations (e.g., Sanders 2008).

It is well known that Romanowsky et al. (2003)'s stellar dynamical study using planetary nebulae in purposely X-ray faint elliptical galaxies, generally do not require dark matter in the central parts (which is known as the problem of the dearth of dark matter in elliptical galaxies). The same is true for the sample recently studied by O'Sullivan et al. (2007) which only show non stellar M/L values at large radii, where the acceleration drops below a_o. Consequently, it is not surprising that they have also been shown to be consisent with MOND (Milgrom & Sanders 2003; Angus et al. 2008b; Tiret et al. 2007). In addition,

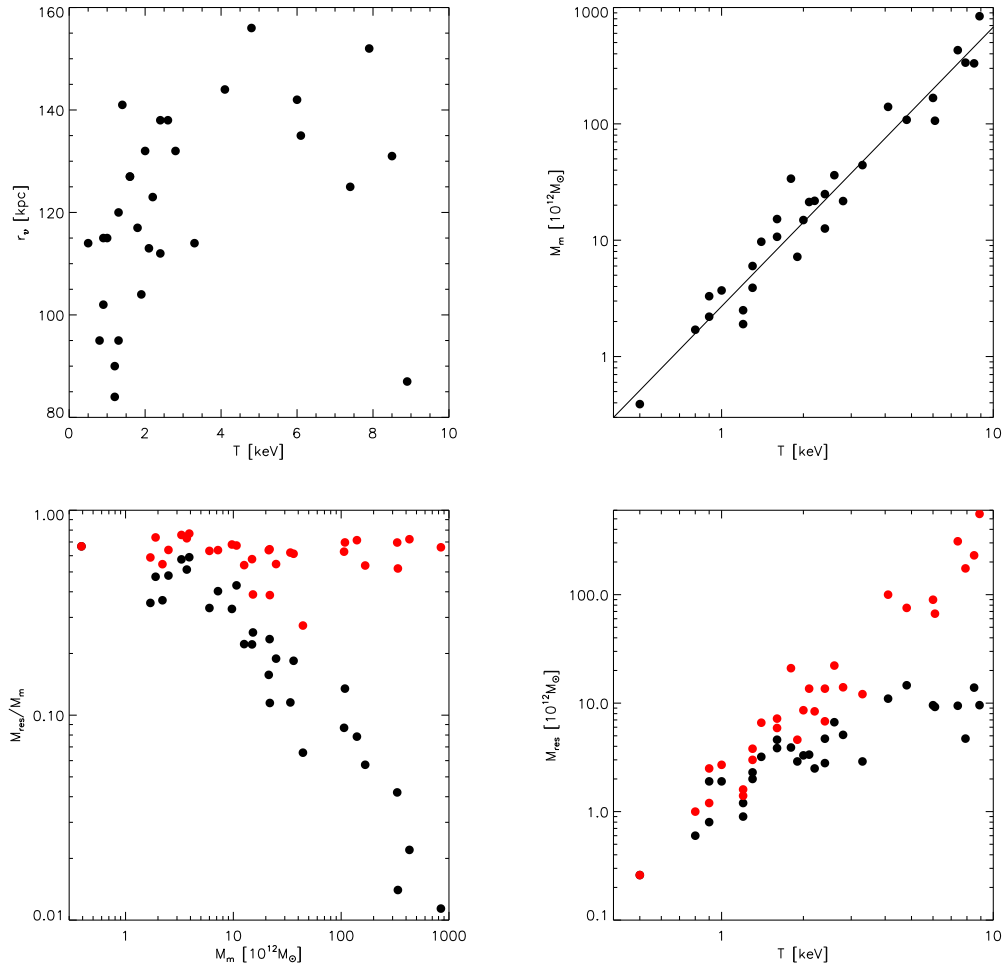

Figure 2.7: The top left figure shows the radius below which neutrinos do not contribute in sufficient density to the MOND hidden mass. The top right figure shows the scaling of the MOND dynamical mass with cluster temperature. The fitted line is $M_m \propto T^{2.4}$. This is higher than the MOND prediction of $M_m \propto T^2$ for the reasons explained in §2.3.4. The bottom left figure shows the fraction of dark mass (red) and of residual mass after neutrinos have been taken into account (black) as a function of the MOND dynamical mass. Clearly the ratio of dark mass stays constantly high (>0.6) if neutrinos are not contributing, but the fraction of residual mass becomes less important for heavier (and hotter) clusters when neutrinos are added. The bottom right figure shows the residual mass discrepancy vs. temperature after subtraction of X-ray gas, the BCG and of the maximum contribution of neutrinos (black) and for the case with no neutrinos (red). In the case of significant neutrino contribution, this discrepancy is a fairly constant value of $\sim 10^{13} M_\odot$ for $T > 3$ keV but drops steadily to zero for $T < 3$ keV. If neutrinos are not present, the dark mass continues to rise with temperature.

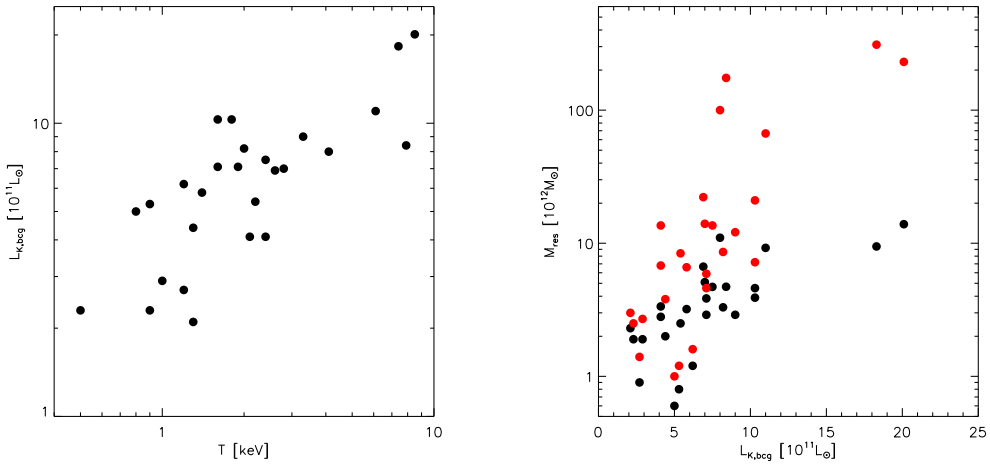

Figure 2.8: The left figure shows the marginal correlation of the K-band luminosity of the BCG with cluster temperature. The right figure shows the residual mass discrepancy with (black) and without (red) neutrinos plotted against the luminosity of the BCG.

the groups of galaxies studied by Milgrom (1998,2002) appear consistent with no dark matter. However, those studies suffer from the well-known degeneracy from slight freedom in the M/L and velocity dispersion anisotropy, which allows a wide range of mass profiles to be consisent with the data.

As will be discussed in the next section, Angus et al. (2008b) used the two cleverly assembled mock galaxy groups of Klypin & Prada (2007) and computed the necessary M/L of the central host galaxy in producing the los velocity dispersions of the stacked satellites. The lower mass host is around $8{\times}10^{10}M_\odot$ using a sensible M/L in the g-band of 1.9-3.3, whereas the higher luminosity host requires $2.8{\times}10^{11}M_\odot$ which can only be achieved with a M/L of 4.2-6.6 whereas the acceptable range is 3-5. So, there exists some evidence that the higher mass elliptical requires a small amount of DM.

We can only be certain that HSB galaxies like those studied by Sanders & Noordermeer (2007) are fully consistent with MOND and no abundance of galactic DM. Below systems of this mass (at least) there is no need for DM in MOND. Studies of very X-ray luminous elliptical galaxies have not generally examined the viablity of alternative gravity theories. A recent exception is the study of the velocity dispersions of globular clusters within the giant elliptical NGC 1399 (Richtler et al. 2008), which has a two-temperature gas of $0.9 - 1.5\ keV$ (Buote

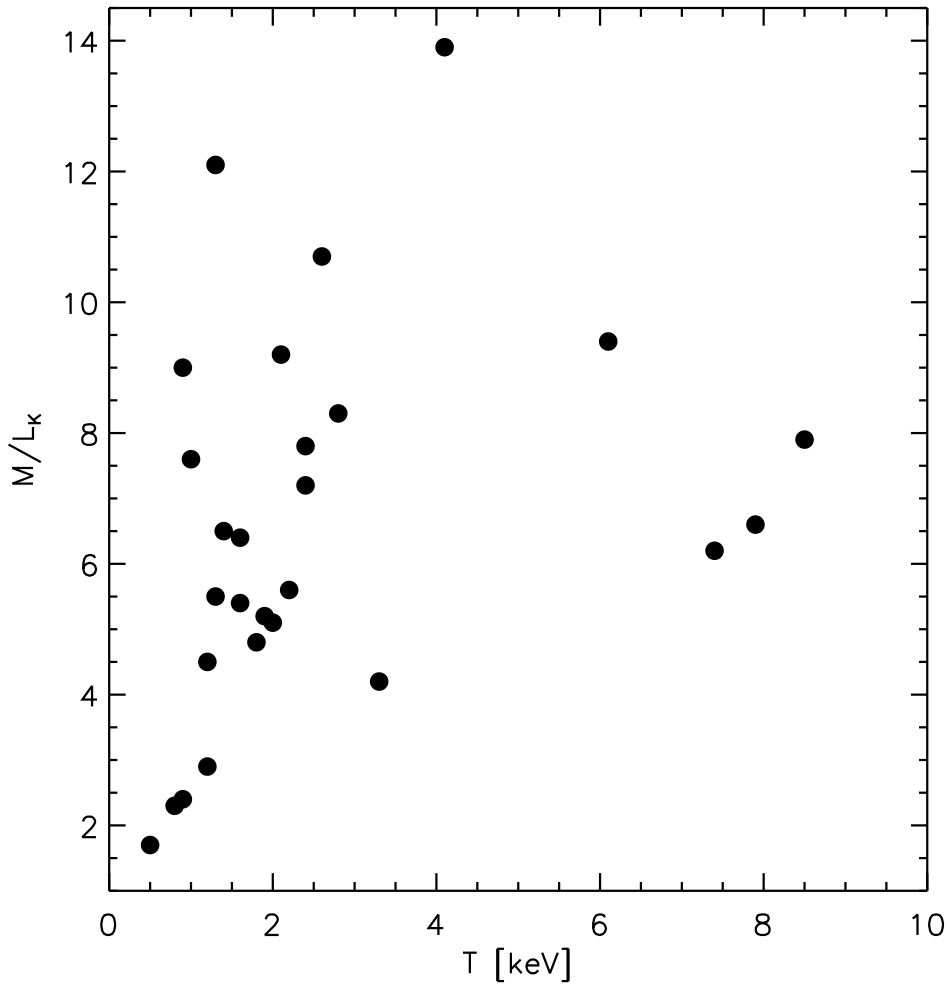

Figure 2.9: Shows the necessary K-band M/L ratio of the BCG to explain the residual mass discrepancy when neutrinos are present. Clearly it dives below temperatures of 1keV towards unity.

et al. 2002), that has revealed some need for DM (although the velocity anisotropy is crucially neglected). Another case is NGC 720, where the observed misalignment of the major axis of the stars and hot gas, along with the elongation of the X-ray isophotes, has been suggested to imply a substantial mass discrepancy (Buote & Canizares 1994; Buote et al. 2002), although there are complicating factors such as rotation and the system is one of a kind). The analysis of the large elliptical galaxy NGC 4125 (included here) with $T = 0.5keV$ shows evidence for a small component of DM with a M/L_K=1.7 making it the only system in our sample that has less DM than luminous matter (note that this mass-to-light ratio in the K-band is obtained after subtracting the hot gas, and cannot be due to this component itself).

The requirement of some DM in MOND at $T = 0.5\ keV$ for NGC 4125 and the hotter groups, but little evidence in the SDSS galaxies or the very HSB galaxies studied by Sanders & Noordermeer (2007) or X-ray dim ellipticals and galaxy groups (Milgrom & Sanders 2003; Milgrom 2002), necessitates a transition temperature below which the fraction of residual mass diminishes in importance and above which it increases in importance, peaks (between 0.5 keV and 2 keV) and then saturates at higher temperatures (unless 2eV neutrinos are present because the residual mass saturates at $10^{13}M_{\odot}$ but the dynamical mass continues to rise). If neutrinos do not contribute significantly, the residual amount of DM would directly scale with temperature. Needing an additional component of DM in clusters with 2eV neutrinos makes them a very poor DM candidate. Why systems cooler than 0.5 keV show virtually no mass discrepancy in MOND must be related to the formation mechanism of such systems, and to the nature of the DM. Let us note that the very presence of DM in MOND seems to be synonymous with the presence of ionised gas and X-ray emission. This might hint at the presence of large quantities of unseen cold gas that could perhaps explain the cluster problem of MOND (Milgrom 2007a).

Cold gas clouds

In the global baryon inventory of the Universe 50% of the baryons produced during Big Bang nucleosynthesis (BBN) are still missing at low redshifts, and assumed to be in the warm-hot intergalactic medium (WHIM, see e.g. Roncarelli et al. 2006). Depending on the actual amount of baryons in the WHIM, there is

Cluster	T	r_{max}	M_Δ	M_X	M_m	M_{DM}	M_ν	r_ν	$M_{m-X-\nu}$	$L_{K,bcg}$	$\Upsilon_{K,bcg}$	Ref
	keV	kpc	$10^{13}M_\odot$	$10^{12}M_\odot$	$10^{12}M_\odot$	$10^{12}M_\odot$	$10^{12}M_\odot$	kpc	$10^{12}M_\odot$	$10^{11}L_\odot$		
(1)	(2)	(3)	(4)	(5)	(6)	(7)	(8)	(9)	(10)	(11)	(12)	(13)
NGC4125	0.5	460	0.6 ± 0.1^c	0.0	0.39	0.26	0.0	114	0.16	2.3	1.7 (1.7)	(d)
NGC5129	0.8	278	0.8 ± 0.1^a	0.8	1.7	1.0	0.3	95	0.6	5.0	2.3 (2.9)	(a)
RGH80	0.9	521	1.9 ± 0.1^d	4.7	2.2	1.2	0.4	102	0.8	5.3	2.4 (3.2)	(a)
NGC4325	0.9	225	1.3 ± 0.2^b	0.7	3.3	2.5	0.7	115	1.9	2.3	9.0 (11.9)	(a)
NGC5044	1.0	369	1.9 ± 0.1^a	1.7	3.7	2.7	0.8	115	1.9	2.9	7.6 (10.4)	(a)
NGC2563	1.2	252	0.9 ± 0.1^b	0.6	1.9	1.4	0.4	84	0.9	2.7	4.5 (6.1)	(a)
NGC533	1.2	265	1.3 ± 0.1^a	0.9	2.5	1.6	0.5	90	1.2	6.2	2.9 (3.6)	(a)
NGC1550	1.3	216	1.4 ± 0.1^b	1.0	3.9	3.0	0.6	95	2.3	2.1	12.1 (15.1)	(a)
MS0116	1.4	405	4.9 ± 1.6^a	2.1	9.7	6.6	3.5	141	3.2	5.8	6.5 (12.4)	(a)
RXJ1159	1.6	708	6.1 ± 3.3^d	7.2	10.7	7.2	2.7	127	4.6	10.3	5.4 (8.0)	(a)
RXJ1159	1.8	700	3.0 ± 0.3^b	15.6	33.8	21.0	17.1	117	3.9	10.3	4.8 (21.4)	(b)
MKW4	1.9	337	3.2 ± 0.1^a	2.5	7.2	4.6	1.6	104	2.9	7.1	5.2 (7.4)	(a)
MKW4	1.6	634	2.8 ± 0.1^a	19.3	15.2	5.9	2.0	127	3.8	7.1	6.4 (9.3)	(b)
ESO552	2.0	484	5.5 ± 0.5^a	4.0	14.9	8.6	5.3	132	3.3	8.2	5.1 (11.5)	(a)
A0262	2.1	650	3.4 ± 0.5^b	14.4	21.3	13.6	10.2	113	3.3	4.1	9.2 (34.2)	(b)
A0262	2.4	276	3.6 ± 0.1^b	2.4	12.6	6.8	4.0	112	2.8	4.1	7.8 (17.6)	(a)
A2717	2.2	840	10.7 ± 0.5^d	14.0	21.8	8.4	5.9	123	2.5	5.4	5.6 (16.5)	(a)
AWM4	2.4	524	7.4 ± 0.6^a	5.8	24.9	13.6	8.9	138	4.7	7.5	7.2 (19.1)	(a)
A1991	2.6	732	12.3 ± 1.7^d	59.8	36.2	22.2	15.5	138	6.6	6.9	10.7 (33.1)	(b)
ESO306	2.8	284	6.0 ± 1.1^b	2.5	21.7	14.0	8.9	132	5.1	7.0	8.3 (21.0)	(a)
A2589	3.3	779	33.0 ± 3.0^c	18.3	44.2	12.1	9.2	114	2.9	9.0	4.2 (14.4)	(c)
A0133	4.1	1007	31.7 ± 3.8^d	94.0	140	100	89.0	144	11.0	8.0	13.9 (125)	(b)
A0383	4.8	944	30.6 ± 3.1^d	227	108	75.5	60.8	156	14.6	...	...	(b)
A0907	6.0	1096	45.6 ± 3.7^d	212	167	89.8	80.2	142	9.5	...	...	(b)
A1795	6.1	1235	60.3 ± 5.2^d	717	106	66.8	57.5	135	9.2	11.0	9.4 (61.7)	(b)
A1413	7.4	1299	75.7 ± 7.6^d	244	430	310	301	125	9.4	18.3	6.2 (171)	(b)
A0478	7.9	1337	76.8 ± 10.1^d	285	336	175	170	152	4.7	8.4	6.6 (209)	(b)
A2029	8.5	1362	80.1 ± 7.4^d	356	331	230	216	131	13.9	20.1	7.9 (116)	(b)
A2390	8.9	1416	107 ± 11^d	588	842	555	546	87	9.5	...	...	(b)

Table 2.4: (1) Designations of the 26 groups and clusters. (2) Mean emission weighted temperature. (3) Radius of last data point. (4) Newtonian dynamical mass at overdensity Δ=1250, 2500, 200 and 500 for the superscripts a, b, c and d respectively. (5) X-ray gas mass at r_{max}, may be larger than required for equilibrium. Error is always less than 1% (6) MOND dynamical mass using the simple μ-function . (7) Residual dark mass required if neutrinos are not present. (8) Contribution of neutrinos to M_m at r_{max}. (9) Minimal radius beyond which neutrinos have high enough density to supply remaining dynamical mass. (10) Residual mass if neutrinos contribute maximally. (11) K-band luminosity of BCG. (12) Necessary M/L_K to account for (10). (13) The reference from which the data is taken. (a) indicates Gastaldello et al. (2007), whereas (b) is Vikhlinin et al. (2006), (c) Zappacosta et al. (2006) and (d) Humphrey et al. (2006). Three clusters overlap between Vikhlinin et al. (2006) and Gastaldello et al. (2007) which we pair in the table and have similar results.

some freedom for the residual mass to be baryonic in MOND. Indeed Fukugita & Peebles (2004) estimate that the observed baryons in clusters only account for 5% of those produced during BBN, while it is clear from our Fig 2.6 that the gas mass is increasing faster than the MOND dynamical mass, and tends to a DM/baryons ratio of about unity at large radii. This means that if only 45% of baryons are present in the WHIM, the remaining 5% would be sufficient to solve the whole problem of missing mass in MOND clusters (even if neutrinos were found by KATRIN in 2009 to have mass much below the present-day experimental limit). One could thus say that, while CDM puts the missing baryons problem in individual galaxies, MOND has put it in galaxy clusters (see McGaugh et al. 2007). It should be highlighted again that DM in MOND only appears in systems with an abundance of ionised gas and X-ray emission (even in the case of galaxies such as NGC 4125). It is then no stretch of the imagination to surmise that these gas rich systems have equal quantities of molecular hydrogen (or other molecules), in e.g. some compact form to satisfy the collisionless criteria imposed by the bullet cluster.

Milgrom (2007d, hereafter M07) has recently proposed that the missing mass in MOND could entirely be "cluster baryonic dark matter" (CBDM), in the form of cold, dense gas clouds. There is an extensive literature discussing searches for cold gas in the cores of galaxy clusters (e.g., Donahue et al. 2006) but what is usually meant there is quite different from what is meant here, since those searches consisted of trying to find the signature of *diffuse* cold molecular gas at a temperature of $\sim$ 30 K. The proposition of M07 rather relies on the work of Pfenniger et al. (1994) and Walker & Wardle (1998), where dense gas clouds with a temperature of only a few Kelvins ($\sim$ 3 K), Solar System size, and of a Jupiter mass, were considered to be possible candidates for both galactic and extragalactic DM. Since the CBDM considered in the context of MOND cannot be present in galaxies, it is however not subject to the galactic constraints on such gas clouds. Note that the total sky cover factor of such clouds in the core of the clusters would be of the order of only 10^{-4}, so that they would only occult a minor fraction of the X-rays emitted by the hot gas (and it would be a rather constant fraction). For the same reason, the chances of a given quasar having light absorbed by them is very small. Still, M07 notes that these clouds could be probed through X-ray flashes generated by individual collisions between them.

Of course, this speculative idea also raises a number of questions, the most serious one being how these clumps form and stabilize, and why they form only in clusters, groups and some ellipticals, but not in individual spiral galaxies at any significant level. As noted above, the fact that missing mass in MOND is always associated with an abundance of ionised gas could be a hint at a formation and stabilization process somehow linked with the presence of hot gas and X-ray emission themselves. Then, there is the issue to know whether the clouds formation would be prior or posterior to the cluster formation. We note that a rather late formation mechanism could help increase the metal abundance, solving the problem of small-scale variations of metallicity in clusters when the clouds are destroyed (Morris & Fabian 2003). M07 also noted that these clouds could alleviate the cooling flow conundrum, because whatever destroys them (e.g. cloud-cloud collisions and dynamical friction between the clouds and the hot gas) is conducive to heating the core gas, and thus preventing it from cooling too quickly. Such a heating source would not be transient and would be quite isotropic, contrary to AGN heating. This highly interesting and innovative scenario to alleviate the cooling flow problem should be the subject of further studies, but is however not the focus of this thesis.

Sterile neutrinos

In addition to the three flavours of active neutrinos, there may be sterile neutrinos of which the particle mass is neither constrained by the CMB or structure formation (e.g., Abazajian et al. 2001), and surely not in a modified gravity scenario. Such sterile neutrinos might be light enough (eV scale, see e.g. Maltoni & Schwetz 2007) not to heavily perturb MOND fits in individual galaxies, but heavy enough to account for the missing mass in groups and clusters. Here, we computed the minimum sterile neutrino mass for a single species using the residual mass densities of NGC 533, NGC 5044, A2717 and A2029 at 20 kpc, assuming the active neutrinos have a negligible mass.

Also assuming the gravity at 20kpc in these system is purely Newtonian which saves any quarrels over interpolating function, we take the enclosed mass for the four plotted clusters (Fig 2.6) and find the density (note $\frac{4\pi}{3}(20\times10^3 pc)^3 \sim 3.35\times 10^{13} pc^3$) for the four clusters to be 0.024, 0.018, 0.015, $0.06 M_\odot pc^{-3}$ respectively. Rearranging Eq 2.30 gives

$$\frac{m_{\nu_s}}{2eV} = \left(\frac{\rho_{\nu_s}^{max}}{7 \times 10^{-5} M_{\odot} pc^{-3}}\right)^{1/4} \left(\frac{T}{1keV}\right)^{-3/8} \tag{2.22}$$

Using the emission weighted temperates from Table 2.4 of 1.2, 1.0, 2.2, 8.5keV we found minimum sterile neutrino masses of 8.0, 8.0, 5.7, 4.8eV. So the existence of an 8 eV sterile neutrino would have the potential to completely solve the cluster problem in MOND. However, further studies should describe the equilibrium distribution expected for such sterile neutrinos, and then examine whether physically well-motivated mass profiles can fit the data. This is presumably why the maximum density is not necessary for the hotter clusters, which is an idea that is further investigated in §2.5.

2.3.5 Discussion

We used high quality data to decompose the mass profiles of 26 X-ray emitting systems in MOND, with temperatures ranging from 0.5 to 9 keV. We confirmed that galaxy groups and clusters in MOND require a huge DM component to account for all the dynamical mass (60-80% of the total dynamical mass at the last observed radius, dropping thereafter). We have shown that, whatever their precise equilibrium distribution, hypothetical 2 eV active neutrinos can never explain a component of residual mass enclosed within the central 100 or 150 kpc. This confirms the result of PS05, but we add an important corollary to this finding, namely that groups with T$\lesssim$ 2 keV cannot be explained by a 2 eV neutrino contribution. Indeed, we have probed far lower masses ($< 10^{13} M_{\odot}$) than PS05, and have shown that this residual mass component, which is present in all known X-ray bright systems hotter than 0.5keV, is the dominant one for groups with T$< 2keV$.

This leads us to believe that, if MOND is correct the active neutrinos are poor candidates for the DM in clusters. To be consistent, we need a form of DM that fits four criteria: 1. It must be collisionless to satisfy the bullet cluster 2. It must not condense significantly in galaxies 3. It must complete the mass budget in clusters 4. It should enable fits to the Cosmic Microwave Background angular power spectrum which is discussed in depth in §2.5.

2.4 Klypin & Prada 2007 and the velocity distribution of the SDSS satellites

Generally, it is forlorn to attack MOND at the galaxy scale because it so outperforms ΛCDM even with zero free parameters; the tidal dwarf galaxies observed by Bournaud et al. (2007) being a great example of this (Gentile et al. 2007; Milgrom 2007b), as manifest in the tight correlation between dark and luminous mass which is inferred under the dark matter paradigm (McGaugh 2005b).

The Sloan Digital Sky Survey (SDSS) brings a new dimension to our ability to test MOND. With such a vast archive of galaxies, and thanks to its piercing magnitude range, Klypin & Prada (2007, hereafter KP07) were able to generate the satellite galaxy line of sight velocity dispersions for a narrow range of host galaxy luminosity. In this small luminosity range, the line of sight (los) velocity dispersions of many satellites were stacked together to essentially create a mock galaxy group with a los velocity dispersion known over a range of projected radii (50-400kpc).

Since there is no evidence for dark matter in small MONDian groups (Milgrom 1998, 2002) one should expect the velocity dispersions calculated from the MOND gravity of the host galaxy in the Jeans equations to coincide with the observed ones. In their recent preprint KP07 claimed that MOND "dramatically fails" to reproduce the falling velocity dispersions. However, their Jeans modelling is based on fairly crude assumptions. Here we re-examine this issue with detailed models.

2.4.1 The Jeans equations in MOND

KP07 chose red galaxies whose geometry is mostly spherical as host galaxies for the satellite distribution. Then, irrespective of the gravitational theory, to calculate the radial velocity dispersions $\sigma_r(r)$ of an equilibrium population in a given spherically symmetric gravitational field, we must solve the Jeans equation (Binney & Tremaine 2008) which basically states how fast the random motions of particles must be to keep a stable configuration under the gravitational force, which is similar to the random motions (pressure) of air molecules in a baloon

balancing the tension in the baloon's surface.

$$\frac{d}{dr}\sigma_r^2(r) + \frac{\gamma(r)}{r}\sigma_r^2(r) = -g(r), \qquad \gamma(r) = \alpha(r) + 2\beta(r) \tag{2.23}$$

where g(r) is the modulus of the internal gravity. The function $\beta(r) = 1 - \sigma_t^2(r)/2\sigma_r^2(r)$ is the anisotropy parameter, where σ_t is the 2-component tangential velocity dispersion and σ_r is the radial velocity dispersion. The function $\alpha(r) = d\ln p(r)/d\ln r$ is the logarithmic gradient of the 3-dimensional number density profile $p(r)$ of satellites. Actually, in the case of satellites, $p(r)$ is rather their probability distribution in configuration space given the few numbers of observed satellites per host galaxy.

KP07 found only 1-2 satellite galaxies per host, hence why they needed to stack many satellites together to reach statistical significance.

We note that the parameter $\alpha(r)$ for the satellite number density is taken to be constant in KP07, but clearly decreases from the observed surface density (Fig 1 of KP07). For this reason, we hereafter consider α and β (and therefore γ) to be functions of r. We take a simple double-power law profile such that the probability density goes like

$$p(r) \propto \left(1 + \frac{r}{r_\alpha}\right)^{\alpha_o} \tag{2.24}$$

where α_o is the asymptotic slope of the probability density and r_α is the break radius of the satellite distribution. It is simple to show that the logarithmic density slope $\alpha(r) = \frac{d\ln p}{d\ln r} = \frac{r}{\rho}\frac{d\rho}{dr}$ is given by

$$\alpha(r) = \alpha_o \frac{r}{r + r_\alpha}. \tag{2.25}$$

Similarly, we can define the velocity anisotropy $\beta(r)$ as

$$\beta(r) = \frac{r - r_\beta}{r + r_\alpha} \tag{2.26}$$

Where r_β is the radius where orbits are isotropic. We use the standard technique of solving first order, linear ODEs and multiply both sides of Eq 2.23 by an integrating factor, $I(r) = e^{\int \gamma(r) r^{-1} dr}$. The left hand side can be simplified to $\frac{d}{dr}[I(r)\sigma_r^2] = -I(r)g(r)$ and from there it can be solved numerically at any given

radius, r_o via the equation

$$\begin{aligned}\sigma_r^2(r_o) &= r_o^{2r_\beta/r_\alpha}(r_o+r_\alpha)^{-\alpha_o-2-2r_\beta/r_\alpha} \\ &\times \int_{r_o}^{\infty} r^{-2r_\beta/r_\alpha}(r+r_\alpha)^{\alpha_o+2+2r_\beta/r_\alpha} g(r)\,dr. \end{aligned} \tag{2.27}$$

For the integration limits we set $\sigma_r(100Mpc) = 0$ which physically must be true.

The MOND equation and the external field effect

When analysing the internal gravity of a system at large radii, as in the case of satellites, a role may be played by the "external field effect" (EFE) linked with the breaking of the Strong Equivalence Principle inherent to any acceleration-based modification of gravity (1.4).

However, for these isolated galaxies (unlike the Milky Way), we have no information on the proximity and masses of nearby massive galaxies. In fact, since these galaxies are stacked together, the individual external field would be different from host to host, therefore, it makes no sense to include a single value for it. If there is indeed an EFE, then to remain consistent with the los dispersions, it must in general be less than $a_o/100$.

Another more theoretical consideration is that the external field strength acting on an isolated galaxy separated by 10s of Mpc from a larger system may be cancelled out by the accelerating expansion of the Universe (dark energy) which effectively smooths out the gravitational potential (curvature due to gravity).

The internal gravity g of an isolated spherical galaxy in MOND is therefore simply determined by

$$g\mu\,(g/a_o) = GMr^{-2} \tag{2.28}$$

where g is the internal gravitational field of the system which we are interested in, and M is the mass of the host galaxy.

2.4.2 Line of sight velocity dispersions

Once Eqs (2.27) and (2.28) are solved, the radial dispersions must be cast into line-of-sight dispersion in order to compare with the SDSS data. The projected number density $\Sigma(R) = 2\int_R^\infty rp(r)\frac{dr}{\sqrt{r^2-R^2}}$ (see Binney & Mamon 1982 is fitted with $r_\alpha = 40kpc$ and $\alpha_o = -3.1$ and is shown in our Fig 2.10 along with the data

Galaxy	Mass [10^{11}M$_\odot$]	M/L_g	α_o	r_α [kpc]	r_β [kpc]
1	0.8	1.9-3.3	-3.1	40	63
2	2.8	4.2-6.6	-3.1	40	63

Table 2.5: Shows the parameters used in the MOND simultaneous fitting of the projected number density of satellite galaxies and los velocity dispersions presented by KP07.

points given by KP07.

This left us with only the galaxy mass, and $\beta(r)$ as free parameters to vary in an attempt to fit the satellite los velocity dispersion of hosts in both magnitude binnings (as described in their Fig 2) by keeping the mass as close to the two representative galaxies given by KP07. The higher we push the galaxy masses, the easier it becomes to fit the los dispersions, however, our M has to be physically consistent with what is expected for the host galaxies i.e. M/L of a few solar units.

The two representative galaxies arise because host galaxies over two ranges of magnitude have their satellite los velocity dispersions binned together and a representative mass for that particular range of magnitudes is chosen. The two ranges are g-band luminosities between 2.4 and $4.2\times10^{10}L_\odot$ for galaxy 1 and between 4.2 and $6.6\times10^{10}L_\odot$ for galaxy 2. KP07 take $M/L_g \sim 2-3$ for galaxy 1 and $M/L_g \sim 3-5$ for galaxy 2. Galaxy 2 actually corresponds to very red galaxies and so there is considerable potential for variability of the chosen mass not just because the binning of galaxies relates to luminosities that vary around their mean by $\sim$25%, but also because of the uncertainty in M/L_g.

In Fig 2.10 we plot the MOND los velocity dispersion for both galaxies along with the data obtained by KP07. The fit parameters are listed in Table 2.5.

We found that the projected number density profile was very constraining to possible fits and if we ignored its shape at small radii as per KP07, we would require lower host galaxy masses. Remaining consistent with the projected number density, we need a mass exactly that quoted by KP07 for galaxy 1 and 40% higher for galaxy 2, which is compatible with the uncertainties linked with the mass-to-light ratios.

Clearly, the fits require substantially radially biased orbits in the outer parts. We use the same $\beta(r)$ for both galaxies, although galaxy 2 (the more massive one) is the more constraining. Both galaxies require $\beta > 0.6$ for radii greater

than 200kpc. The physics of the solutions is as follows: from the Jeans equation (Eq 2.23), to get a high radial dispersion, we need a low absolute value of γ (which from Eq 2.23 must be a negative number in the outskirts where the variation of σ_r is getting nearly constant, cancelling the first term in Eq 2.23). This can be achieved by having a low absolute value of α, but also one tending to get steeper in the outskirts to delay the constancy of σ_r. However, the α needed is too low in absolute value to account for the observed slope. By taking high β, we manage to fit at the same time the slope of $\Sigma(R)$ and the los dispersion. This high radial anisotropy at large radii is nominally what is expected for self-gravitating populations from simulations of elliptical galaxy formation in MOND at radii considerably larger than the half-mass radius of the galaxy (Nipoti et al. 2007a, see their Fig 2). Although it is unclear how valid it is to expand this result to the anisotropy of the satellites test-particle population, we can a priori expect satellites to indeed have such a high radial anisotropy.

An important question is whether the distribution function (DF) corresponding to the model is positive everywhere and stable. A necessary condition is that $\gamma(r) < 0$ everywhere, which is satisfied. When the spatial range of radial orbits is wide, there is a risk of radial-orbit instability (e.g. Aguilar & Merritt 1990). However, this is not a concern here since the regions considered are largely outside the self-gravitating part of the elliptical galaxy, and only satellites taken as test particles are orbiting in this radial range.

2.4.3 Discussion

Building upon the recent preprint of KP07, we found MOND can easily reproduce the observed declining los velocity dispersions for the satellites observed by the SDSS. By solving the Jeans equation in MOND, we have shown that even with the two very constraining datasets consisting of the projected number density profile of satellite galaxies and of their velocity dispersion profile (for a range of host galaxy masses), the data are fully consistent with MOND by simply including an increasing radial anisotropy that requires a single free parameter. These increasing anisotropies are very similar to those found by Nipoti et al. (2007a) from their simulations of dissipationless collapse in MOND. The masses of the host galaxies are reasonable and in accordance with the luminosities of the host galaxies. It is surely possible to obtain even better fits to the projected

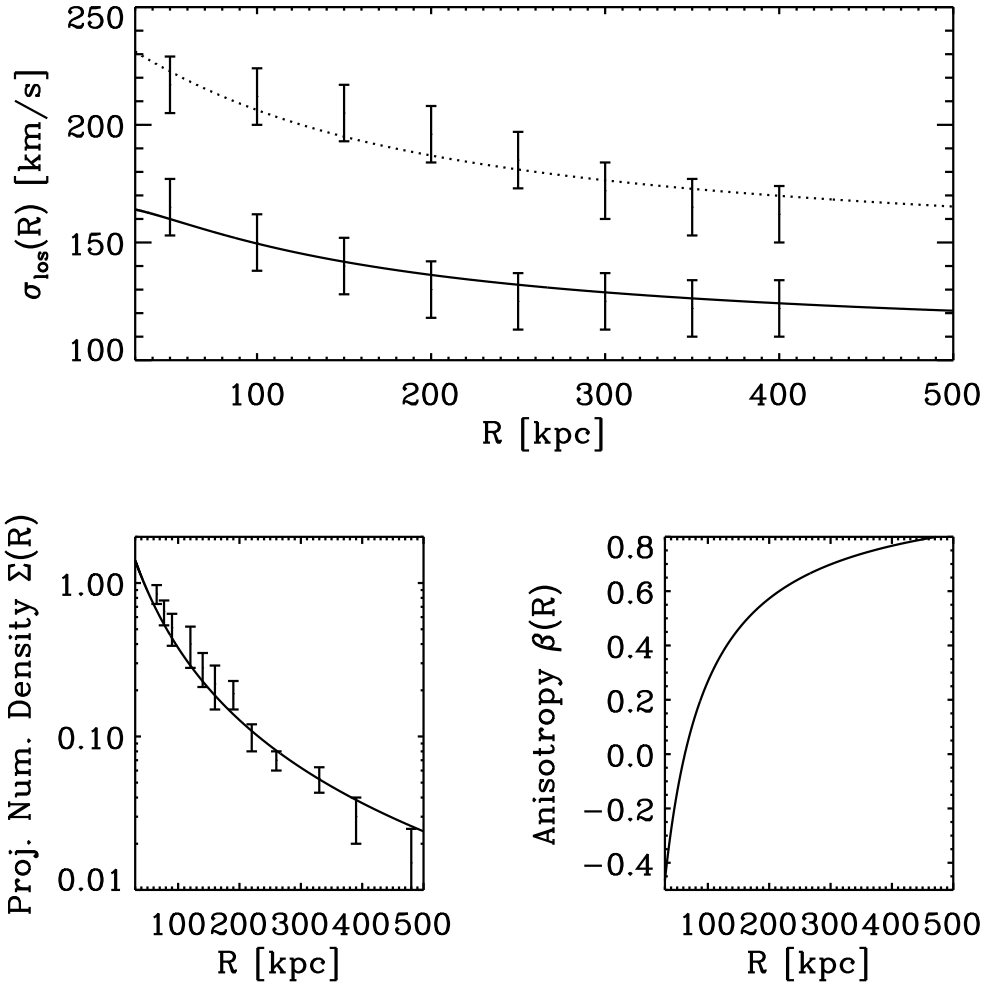

Figure 2.10: *Top panel*: The expected los velocity dispersion profiles in MOND for the two host galaxies along with the observed velocity dispersion profiles with 1σ errors. The solid linetype is for galaxy 1: $M = 8.0 \times 10^{10} M_{\odot}$ for $r_{\alpha} = 40kpc$, $\alpha_o = -3.1$, and $r_{\beta} = 63kpc$. The dashed linetype is for galaxy 2: $M = 2.8 \times 10^{11} M_{\odot}$ and all other parameters are the same as for galaxy 1. *Bottom left*: The surface density profile we used for the fits to the velocity dispersions. The fit involves choosing $r_{\alpha} = 40kpc$ and $\alpha_o = -3.1$ for Eq 2.24 and then integrating along the line of sight. The data points are the observed satellite surface densities from KP07 *Bottom right*: The variation of the velocity anisotropy parameter, β(r) as a function of radius. They transition from more tangentially biased orbits at small radii (<50kpc) and become radially biased with increasing radius.

surface density and los velocity dispersions with more freedom, but the data hardly warrant it.

Finally, we comment that another preprint by Moffat & Toth (2007b) also suffers from an incomplete analysis of MOND which neglected the radial velocity anisotropy and the correct variation of the slope of the tracer density profile, $\alpha(r)$. Moffat & Toth (2007b) claim that the los velocity dispersions are in full agreement with their favoured gravity theory dubbed MOG even though they fit only the los velocity dispersions of the more massive host satellite (galaxy 2, although in fairness this is the more difficult galaxy to use). The goodness of fit looks inferior to the MOND one presented here. Whether their theory can fit the dispersions of the lower mass host with the same set of free parameters remains to be seen. Furthermore their fit requires a host galaxy mass of $6 \times 10^{11} M_{\odot}$ which is more than twice our value and three times that used by KP07 and corresponds to an unlikely g-band mass-to-light ratio of 9-14.

2.5 Sterile neutrinos and the Cosmic Microwave Background

The CMB deserves some introduction at this stage. At very early times, the Universe existed as a homogeneous bath of photons and baryons in causal contact, until quantum fluctuations created small excesses of photons in certain regions and deficits in other places. Then a process called inflation basically magnified the universe many orders of magnitude so that the Universe was too large to be in causal contact, but the quantum fluctuations were frozen in and the elementary particles (protons and electrons) followed the photons. The photons and particles stayed in equilibrium with each other because the Universe was too hot for electrons and protons to bind, so the photons scattered (Thomson scattering) off of the free electrons. The incoming photon's electric and magnetic components accelerated the free electron and cause the electron to radiate which keeps the photons and electrons in equilibrium and chained together.

All this time, the Universe is cooling and eventually it becomes cool enough for the electrons and protons (or nuclei) to combine which makes the Universe transparent to the cosmic radiation since it has nothing to scatter off (no free electrons). This is called last scattering or recombination. This effectively froze

in the state of the radiation at this epoch, but what the radiation was doing at that time, is the interesting part.

Recall that the Universe is expanding, but the dark matter exerts a gravitational force on the baryon-photon fluid. This is like a damped, driven harmonic oscillator with gravity being the driving force and the photon pressure opposing the drive. So, the baryon-photon fluid collapses under gravity and then rarifies (expands) thanks to the photon pressure which builds up under compression. In the short space of time before recombination, different scales (sizes) have undergone different numbers of oscillations and there is naturally a particular scale which has collapsed only once to a maximum (half a period of oscillation) and then the electrons and photons decouple due to recombination.

This collapse and decoupling imprints an anisotropy on the otherwise homogeneous microwave background because the photons now must climb out of the exaggerated potential created by the collapse of the baryon-photon fluid under the gravity of the dark matter (and the baryons). This climbing, costs the photon's energy and they are gravitationally redshifted. This happens on the well measured scale of $\sim 1^o$ and corresponds to the first peak in the angular power spectrum of fluctuations in the temperature of the CMB. Basically one performs a 2-point correlation of many multipole moments, l, of a spherical harmonic expansion to find correlations in the temperates of the CMB photons, since the photons come from all directions on the sky.

The first peak encodes a lot of information, but the second and third peaks are vital for constraining the amount of dark matter and baryons in the Universe at this time. And, although the dark energy component does not influence dynamics at this early stage, we know the Universe is flat (i.e. has a critical density now and in the past) because of the scale of the first peak (its angular size) because the dark energy component has a significant effect on the expansion history of the Universe hence how large the peaks appear to us now.

The second peak is at a smaller angular scale and corresponds to a full oscillation in that the photon-baryon fluid has collapsed and rarefied to a maximum in the time before decoupling. Photons at these scales have the smallest potential well to overcome and hence are the hottest photons or least gravitationally redshifted and are important because they encode the abundance of baryons which repells the collapse under gravity. The third peak is one and a half oscillations

and is of particular importance because it helps identify the dark matter abundance with respect to the baryons. If there is little or no dark matter, then the third peak will be considerably lower than the second which is significantly lower than the first. This is because there is no driving force to collapse the baryons except their own puny self gravity. So the baryonic drag damps the collapse and oscillations get weaker and weaker in amplitude. With the dark matter present the baryons have to work harder to rebound from the initial infall and are driven to recollapse.

Another crucial point is that the fluctuations in the cosmic microwave background are affected differently with hot dark matter compared to cold dark matter especially at the third peak. This is because the third peak is a smaller scale than the first and second, so to drive the recollapse, we need a DM particle that can collapse on such a small scale, which rules out 2eV neutrinos which free-stream out of overdensities at the third peak scale. They simply move too fast to condense. This is another reason why 11eV sterile neutrinos have been ignored, because they were presumed to have insignificant power on small scales. Although the maximum density of a sterile neutrino of 11eV is considerably less than a cold dark matter particle, it still is large enough to drive a high 3rd peak.

Here we take the *ansatz* of McGaugh (2004) that MOND effects are not important for modelling the CMB. A simple argument supporting this is that at a redshift of $z \sim$1080 the angular diameter distance to recombination $D_A = 14Gpc$ and the angular scale, θ, of the first (and largest) peak is 1^o or 0.017rad. So the physical size of the first peak $r = \theta D_A$ is $\sim$240Mpc. Since the average overdensity δ is only 1 part in 10^5 of the critical density $\rho_c(z)$, the typical gravities at a radius r from the centre of one of these overdensities is $g = G\delta M(r)r^{-2} = \frac{4\pi}{3}G\delta\rho_c(z)r$ where $\rho_c(z) = \frac{3H(z)^2}{8\pi G}$ and $H(z)^2 = H_o^2[\Omega_m(1+z)^3 + \Omega_\Lambda$. Compiling all this gives

$$g(r) \sim \frac{1}{2}\delta H_o^2 \left[\Omega_m(1+z)^3 + \Omega_\Lambda\right] r \tag{2.29}$$

At $r = 240Mpc$,

$$g = \frac{1}{2} \cdot 10^{-5} \cdot 7.1 \times 10^{-5} \left[0.27 \cdot 1081^3 + 0.73\right] \cdot 240Mpc \sim 570a_o,$$

where $a_o = 3.6(\,\mathrm{km\,s^{-1}})^2 pc^{-1}$ is the MOND acceleration constant. Typical accelerations so many times greater than a_o are completely unaffected by MOND

gravity and therefore no MOND effects should influence the CMB. However, as z drops, so does $\rho_c(z)$ and thus peculiar accelerations can slide into the MOND regime. Thus, the matter power spectrum can be affected by MOND.

It is often forgotten when looking at MOND cosmology that *no* cold dark matter exists in MOND. Therefore, we must relax many of the constraints that are set by CDM cosmology. The most important and obvious one is that there is now a large gap in the energy-density budget since CDM is not present and it is perfectly reasonable to fill this gap with hot dark matter like neutrinos. The constraints on neutrino masses, for which cosmology is still the most stringent, must be reanalysed in light of MOND. Still, the empirical evidence from supernovae data (Schmidt et al. 1998; Perlmutter et al. 1999) strongly suggest the universes expansion is accelerating owed to the existence of dark energy, Ω_Λ. Furthermore, the baryon budget is strongly constrained by well understood physics to be around $\Omega_b h^2 \sim 0.015 - 0.025$ (Boesgaard & Steigman 1985; Burles et al. 2001; McGaugh 2004), but this still leaves a large amount of latitude in the energy budget for DM.

Any DM, however, must be compatable with clusters of galaxies, the well understood lack of DM in galaxies in MOND and the anisotropies in the angular power spectrum of the CMB. The best candidates for such hot DM are neutrinos.

2.5.1 Active Neutrinos

The three active neutrinos (ν_μ, ν_e and ν_τ) from the standard model of particle physics have been shown to mix between flavours by atmospheric and solar neutrino experiments (Ahmad et al. 2001; Ashie et al. 2004). However, the exact masses of the three active neutrinos are not yet known, only their squared mass differences. Nevertheless, the masses of all three are known to be less than 2.2eV from the Mainz-Troitz experiments (Kraus et al. 2005).

The maximum density that a neutrino species can produce after gravitational collapse is given by the Tremain-Gunn limit (Tremaine & Gunn 1979),

$$\frac{\rho_\nu^{max}}{7 \times 10^{-5} M_\odot pc^{-3}} = \left(\frac{T}{1keV}\right)^{1.5} \left(\frac{m_\nu}{2eV}\right)^4 \tag{2.30}$$

for each of the three species. Thus, the density is greatly dependent on the mass of the neutrinos. However, groups and clusters of galaxies have dark matter

that is much denser than can be produced by the active neutrinos even at the maximum mass of 2.2eV (Angus et al. 2008a). If the dark matter is indeed a neutrino like species, it must be heavier than 8eV (Angus et al. 2008a). There is a further problem with neutrinos at 2.2eV in that the contribution they make to the energy density of the Universe is given by

$$\Omega_\nu = 0.0205 m_\nu, \tag{2.31}$$

meaning that at 2.2eV the three neutrinos make a 13.6% contribution to the energy density of the Universe, but the maximum density is relatively low (see Eq 2.30). Such a huge contribution would be easily detectable in the angular power spectrum of the fluctuations in the CMB as shown for this example in Fig 2.12. Therefore, the active neutrinos are a very poorly motivated candidate.

2.5.2 Sterile Neutrinos and the CMB

As mentioned above, the three active neutrinos are known to have mass. Another oddity arising from this is that the active neutrinos are solely left handedly chiral, whereas all other fermions are ambidextrous. The easiest way to incorporate this into the standard model of particle physics is to introduce a right handed "sterile neutrino". In addition, they are not simply aesthetically pleasing, the introduction of a single sterile neutrino was preferred from analysis of the Miniboone experiment by Giunti & Laveder (2007) (see also Aguilar et al. 2001; Maltoni & Schwetz 2007) with a mass in the range 4eV-18eV to explain the disappearance of electron neutrinos from the beam at low energies.

In the simplest model, if the mixing angle of the sterile neutrino is low enough, then thermalisation in the early Universe can balance the abundance of the sterile and active neutrinos. In this case, the cosmological density is exactly related to their mass, as for the active ones (Eq 2.31).

With the hypothesis that all the DM in MOND comes from a single sterile neutrino, we used the freely available CMB anisotropy code CAMB (Lewis et al. 2000) and incorporated it into a χ^2 minimisation routine comparing with the data from the WMAP5 data release (Dunkley et al. 2008) and the ACBAR 2008 data release (Reichardt et al. 2008). We allowed variation of Ω_b, Ω_{ν_s}, n_s, $dn_s/d\ln k$, τ, H_o and fixed the Universe to be flat meaning $\Omega_\Lambda = 1 - \Omega_b - \Omega_{\nu_s}$.

Obviously, in this MOND inspired model there is no CDM by definition, but since the CDM model works well at producing the CMB anisotropies, we began the search by simply transferring Ω_{cdm} to Ω_{ν_s}. Furthermore, the 3 active neutrinos are taken, for simplicity, to be massless. As discussed later, it is not feasible to have a pair of very massive ($> 0.5eV$) sterile neutrinos because splitting the Ω_{ν_s} between two or more neutrinos reduces the available mass to each neutrino thus detrimentally lowering its Tremaine-Gunn limit ($\rho_\nu^{max} \propto m_\nu^4$) and thus the gravity available to drive the collapse of the baryons prior to recombination on small scales like the third acoustic peak. This is highlighted in Fig 2.12 where the comparison is made between one sterile neutrino and two.

The parameters for the best fit are given in table 1 which also contains the parameters for the WMAP5 fit from Dunkley et al. (2008) and a comparison of the two fits are shown in Fig 2.11. All parameters are consistent with experimental bounds and are not significantly different to the ΛCDM model, which is sensible since the ΛCDM model of the CDM anisotropies is a good one.

The mass of the sterile neutrinos infered from the best fit value of $\Omega_{\nu_s}h^2 = 0.117$ is $m_{\nu_s} \sim 11eV$. This mass range of sterile neutrino has never before been considered in the literature because it is excluded by cosmological data if we assume Newton's law are correct (Dodelson et al. 2006; Seljak et al. 2006) since they cannot influence galaxy rotation curves because they would have a free streaming scale (cf. Sanders 2007) of more than $R_c = 1.3\left(\frac{m_\nu}{1eV}\right)^{-4/3}\left(\frac{V_r}{200\,\mathrm{km\,s^{-1}}}\right)^{1/3} = 50kpc$ in a Milky Way type galaxy, for $V_r = 200\,\mathrm{km\,s^{-1}}$. The total mass this would create within 8kpc is $\sim 5 \times 10^9 M_\odot$ which is about 10% of the total mass and would actually help MOND fits to the Milky Way's rotation curve (Famaey & Binney 2005; Gentile et al. 2008; McGaugh 2008).

In particular, it would have a similar contribution to the energy density as required from cold dark matter fits to the CMB ($\Omega_{\nu_s}h^2 = 0.117$; $\Omega_{cdm}h^2 = 0.108$) and leave the matter power spectrum at large scales ($> 50h^{-1}$Mpc) unaltered. This is shown in Fig 2.13 which compares the observed matter power spectrum with that predicted by the sterile neutrino model here, but with Newtonian instead of MONDian gravity. At scales smaller than $\sim 50h^{-1}$Mpc the computed power spectrum drops many orders of magnitude below the observed one.

Qualitatively, this discrepancy is owed to the fact that structures on these small scales have formed with the assistance of MONDian gravity. For instance,

Parameter	Single ν_s	ΛCDM	Active	Two ν_s
H_o	71.5	72.4	71.5	71.5
$100\Omega_b h^2$	2.4	2.27	2.4	2.4
$\Omega_\nu h^2$	0.117	0.0	0.695	0.117
$\Omega_{cdm} h^2$	0.0	0.108	0.0	0.0
n_s	0.965	0.979	0.856	0.939
No. massless ν	3	3	0	3
No. massive ν	1	0	3	2

Table 2.6: List of parameters used in the figures. The ΛCDM numbers come from Dunkley et al. (2008) but n_s has been scaled from the quoted 0.963 to 0.979 for a better match to the data.

following the argument of Eq 2.29, the redshift by which scales as large as $50h^{-1}$Mpc are deep in the MOND regime (i.e. $g \sim \frac{a_o}{10}$) is roughly

$$z \sim \left[\frac{2g}{\delta H_o^2 \Omega_m r}\right]^{1/3}, \tag{2.32}$$

which for 70Mpc is $z \approx 100$. Certainly many authors (Sanders 2008; Nusser 2002; Knebe & Gibson 2004) have shown that structures can form very quickly in MOND even without CDM and galaxy size objects can be in place as early as $z \approx 10$.

The tools to perform the full matter power spectrum analysis are currently not available for MOND (nor standard dynamics), since they crucially depend on hydrodynamics. Assuming that including the modified dynamics enables a match to the matter power spectrum at all scales, the only conceivable ways of distinguishing between MOND and ΛCDM (if missing satellites, the lack of cusps in DM halos and tidal dwarf galaxies are ignored) is in the complex modelling of galaxy formation, or the unambiguous detection of the hot or cold DM particles.

2.5.3 Discussion

A single massive sterile neutrino appears consistent with the current level of precision in the measurements of the CMB anisotropies. It is also consistent with the matter power spectrum at large scales ($> 50h^{-1}$Mpc) and is able to clump together with densities surpassing the maximum density of the DM in groups and clusters of galaxies where MOND requires dark matter of some form. As discussed

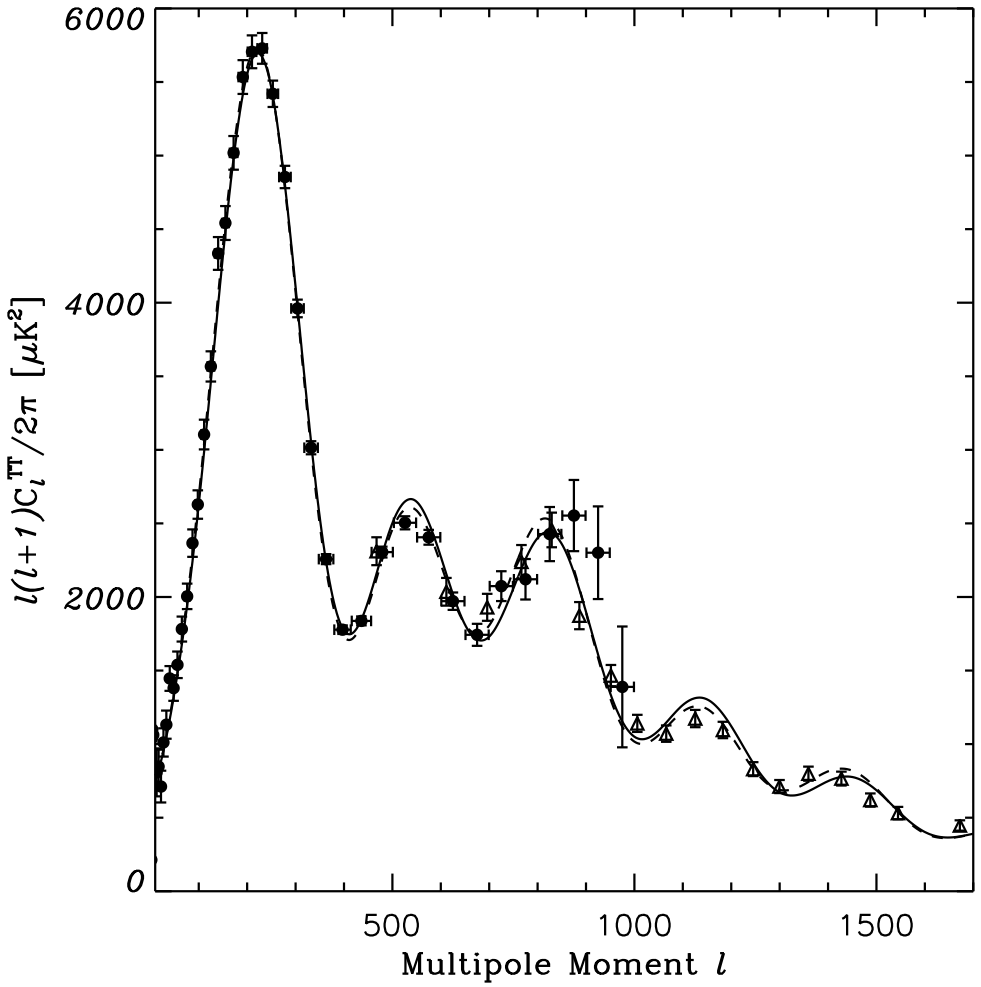

Figure 2.11: Shows the data of the CMB as measured by the WMAP satellite year five data release (filled circles, Dunkley et al. 2008) and the ACBAR 2008 (Reichardt et al. 2008) data release (triangles). The lines are the ΛCDM max likelihood (dashed) and the solid line is the fit with an 11eV sterile neutrino with paramters given in table 1. The n_s for the ΛCDM model has been scaled from the quoted 0.963 in Dunkley et al. (2008) to 0.979 here to better match the data.

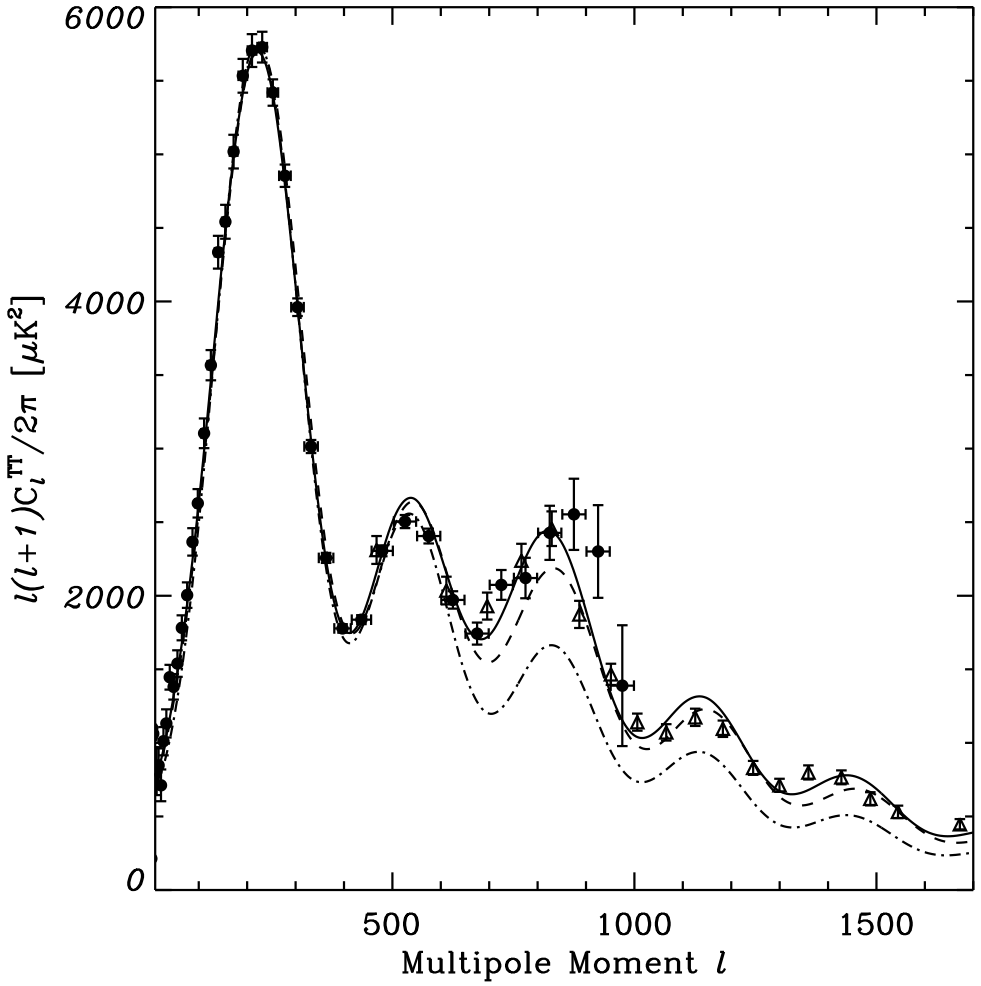

Figure 2.12: As for Fig 2.11 with the solid line again the single sterile neutrino fit with parameters given in table 1, but the dashed line is the fit with 2 sterile neutrinos sharing Ω_{ν_s} and the dotted line is with the maximum active neutrino contribution with $\Omega_\nu = 0.136$ and Ω_Λ compensated for a flat universe. We reduced n_s to 0.856 and 0.939 respectively to match the amplitude of the first acoustic peak, but the second and third peaks are badly matched because there is not enough neutrino DM density on small scales because of the Tremaine-Gunn limit.

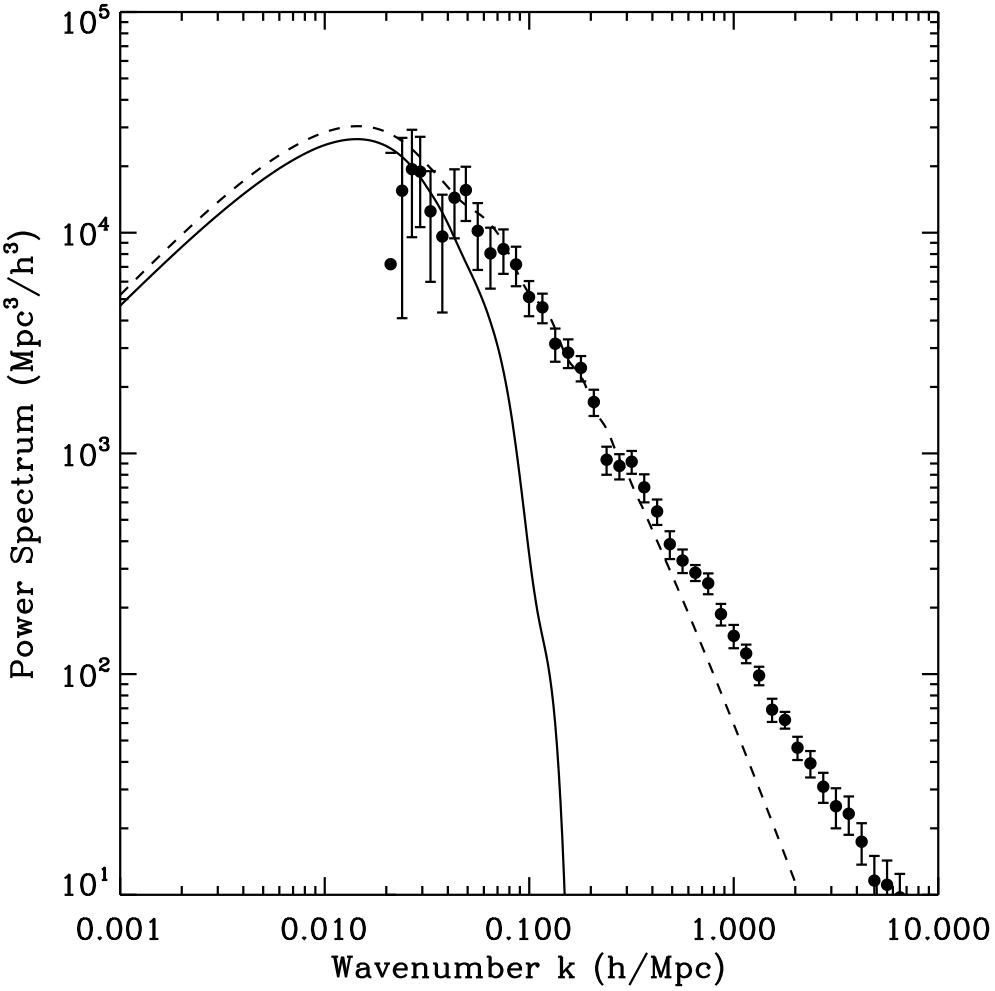

Figure 2.13: The filled circles are the data points from the SDSS (Tegmark et al. 2004), the solid line is the single sterile neutrino model but with Newtonian instead of MONDian gravity. The dashed line is the ΛCDM model.

in Angus et al. (2008a) there appears to be a scale at which MOND begins to poorly describe the dynamics of astrophysical systems. This is highlighted by Romanowsky et al. (2003); Milgrom & Sanders (2003); Angus et al. (2008b); O'Sullivan et al. (2007) which show that no dark matter is necessary to explain the detailed dynamics of relatively low mass groups of galaxies and systems smaller. This is expected for sterile neutrino dark matter because it would have a free streaming length greater significantly larger than a typical galaxy (∼50kpc for the Milky Way. However, just as numerical simulations of clusters of cold dark matter were necessary to show that the CDM halos are a poor match to observed galaxies (de Blok & McGaugh 1998; McGaugh & de Blok 1998; Gnedin & Zhao 2002; Gentile et al. 2004; Gilmore et al. 2007), the equilibrium distribution of the sterile neutrino DM must be checked to be consistent with groups and clusters of galaxies (see Sanders 2007).

On the other hand, the three active neutrinos should probably have masses well below 0.5eV. Otherwise it will become difficult to match the CMB power spectrum because the angular scale of the peaks prefers $\Omega_\nu h^2 = 0.117$ while $\Omega_\nu \propto m_\nu$. Increasing the mass of another neutrino reduces the mass of the sterile neutrino and the amplitude of the third peak of the CMB diminishes due to the rapidly decreasing maximum density ($\rho_\nu^{max} \propto m_\nu^4$).

Certain analyses of neutrino mixing experiments seem to require an additional, sterile neutrino with a mass in the range $4eV < m_{\nu_s} < 18eV$. Here I took the *ansatz* that there is a fourth, sterile neutrino of 11eV mass and that MOND effects are not important at cosmological scales. I showed that its contribution to the dynamics of galaxies would be negligible, but that it could solve all problems MOND has with the dynamics of clusters of galaxies and it can match the angular power spectrum of the CMB. The matter power spectrum needs to be recalculated because MOND gravity is crucial to the formation of these smaller structures and because of the increased dominance of baryons at these scales over DM, hydrodynamics cannot be avoided as in CDM simulations. If experiments can indeed pinpoint the existence of a sterile neutrino with mass ∼11eV this would be a significant advance for the Modified Newtonian Dynamics.

Even if collider experiments detect a CDM candidate with mass of 300GeV, this will give us virtually no information about the cosmological abundance and therefore brings us no closer to solving the dark matter problem. The great thing

about sterile neutrinos is that if we can find the mass from laboratory experiments then this effectively fixes the cosmological abundance AND the contribution the neutrinos can make to clusters of galaxies can be strictly constrained. Henceforth, it would be possible to run structure formation simulations in MOND with all the ingredients.

Chapter 3

Satellites of the Milky Way

3.1 Missing satellites problem

It is possible to run N-body numerical simulations of structure formation in the Universe from the initial density perturbations set by the measurements of the fluctuations in the cosmic microwave background (see §2.5). These simulations track the gravitational growth of structures on all scales, limited only by the number of particles the CPU can handle. With intricate techniques such as variable time-steps for the integration of the equations of motion and different mass scales to resolve high density regions, it is becoming possible to resolve growth down to substructures of galaxies (Diemand et al. 2008).

Although at the moment, the simulations only account for the clustering of dark matter particles (which are $\sim 5\times$ more abundant than the baryons) it is common to assume the baryons follow the dark matter particles and once the dark matter has virialised, the baryons cool and begin to form stars. It is assumed that dark matter halos that are similar in size to the measured halo of the Milky Way form Milky Way size galaxies and those halos the size of galaxy clusters go on to form the hot gas and galaxies of galaxy clusters. This idea was used to estimate the abundance of substructure inside a Milky Way type galaxy, by calculating the number of virialised halos with sizes comparable to the dwarf spheroidal galaxies discussed in this chapter.

It was found independently by Moore et al. (1999a) and Klypin et al. (1999) that there should be more than 500 dwarf galaxies orbiting the Milky Way which is between one and two orders of magnitude more than observed.

In addition to the obvious Magellanic Clouds and the tidally disrupting Sagittarius dwarf (Ibata et al. 1994), the Milky Way (MW) has 8 relatively nearby dwarf spheroidal satellite galaxies: Ursa Minor, Leo I, Leo II, Fornax, Sculptor, Sextans, Draco and Carina. There are also some new dwarfs being found (Zucker et al. 2006; Ryan-Weber et al. 2008) and evidence for additional tidally disrupting dwarfs (Peñarrubia et al. 2005; Belokurov et al. 2006, 2007; Sales et al. 2008). However, these satellites are all very dim and do not explain the deficit of dwarfs that should be more massive than Ursa Minor and Draco.

Furthermore, there has been speculation that Ursa Minor and Draco are formed from the tidal debris of the Magellanic Stream (Lynden-Bell 1983; Metz & Kroupa 2007) and that Leo I, Leo II and Sculptor have similarly formed from debris cast by the tidal break-up of a previously larger Fornax satellite. It also seems likely, the dwarfs were part of two small groups of galaxies that have entered the Milky Way at late times and are on a single passage (D'Onghia 2008) since the Magellanic clouds have escape velocity at their position from the Milky Way (Kallivayalil et al. 2006b,a) and most of the other dwarfs have large velocities. This may reduce the number of actual satellites even further and so is a very difficult problem to solve for the ΛCDM paradigm because the dark matter particles have such low mean free paths (they are so cold) that they can form structure all the way down to the Earth mass level (Diemand et al. 2005; Angus & Zhao 2007).

Therefore, the common explanation is that the star formation efficiency is poor inside these dwarf dark matter halos, caused by the explosion of supernovae or the winds of massive stars feeds back and prevents star formation. This is a hard pill to swallow since it offers no explanation for why the other dwarfs formed and dwarfs like Leo T (Ryan-Weber et al. 2008) have been forming stars all throughout their existence.

A better explanation in MOND might be that dwarf galaxies form from the debris of tidally disrupted progenitor galaxies (Metz & Kroupa 2007). In this case, very little CDM accompanies the stars and gas for the simple reason that the tidal disruption must have torn the gas and the CDM out into streams from which the gas has condensed and formed stars and only a limited amount of CDM can have condensed with it. This is contrary to the standard picture where gas cools and falls onto an already formed CDM halo and then forms stars.

There has been a recent study by Bournaud et al. (2007) of tidal dwarf galaxies formed from the debris of NGC5291. They found a persisting mass discrepancy by measuring the visible galactic masses and comparing with the mass implied by the rotation curves. They proposed the existence of hitherto unheard of disk DM, in the progenitor galaxies, in the form of molecular gas (as opposed to the cold DM of massive particle form). Two simultaneous studies (Milgrom & Sanders 2008; Gentile et al. 2007) in the framework of MOND found the discrepancy was exactly that expected in MOND because the tidal dwarfs are very diffuse and low surface brightness (de Blok & McGaugh 1998) meaning they have low internal accelerations (much less than a_o). In addition, the external acceleration from the large progenitor is also weak (discussed in depth in both papers) allowing a relatively large boost to the internal gravity enabling perfect agreement with the observed rotation curve using just the luminous matter (no need for CDM or molecular disk DM). This is the most remarkable evidence for MOND since the baryonic Tully-Fisher relation was matched in great detail (McGaugh et al. 2000; McGaugh 2005b).

3.2 Dwarf spheroidals of the Milky Way

There are 8 relatively nearby dwarf spheroidal satellite galaxies for which the radial velocities of many hundreds of member stars have been meticulously measured at various projected radii allowing the calculation of the line of sight (los) velocity dispersion as a function of projected radius.[1] If we assume the satellites are spherical and in equilibrium, we can use specific mass models to check the consistency of the luminous matter in replicating the los velocity dispersion profiles through the Jeans equation (Eq 3.3).

It so happens that these small satellites appear to be some of the most heavily cold dark matter (CDM) dominated systems in the Universe and so including only the luminous matter in Jeans analysis underestimates the los velocity dispersions considerably. It is because of the well studied, small spatial scales and large dark matter content that Gilmore et al. (2007) have used the relatively low dark matter density in the cores of dwarf spheroidals to argue for an upper limit on the mass of the DM particles from supersymmetric theories.

[1] There are a few more for which these measurements have not been made.

Previous attempts to check the consistency of the Milky Way's dwarfs with MOND have been limited to single number central velocity dispersions (although see Łokas 2001 which crucially does not include the external field effect). Studies by Gerhard & Spergel (1992) and Milgrom (1995) gave good estimates of the mass-to-light ratios (M/L) for all the dwarfs studied here by considering whether each dwarf was dominated gravitationally by the external field of the Milky Way (MW) or by its own internal gravity. If it was dominated by the external gravity, g_{ex} then the Newtonian M/L was used after renormalisation of Newton's constant, $G_{eff}/G = a_o/g_{ex}$, reducing the M/L in MOND by the same factor. If the external gravity was weak w.r.t. the internal gravity then the dwarf mass was calculated from the relation $M = \frac{81}{4}\frac{\sigma_{los}^4}{Ga_o}$ from which the M/L can be deduced. Nevertheless, proper Jeans modelling with the luminosity profile of the dwarf along with the near exact calculation of the dwarf's internal gravity at all radii by including analysis of the external field effect (see Milgrom 1983c and §1.4) and variation of the velocity anisotropy profile (as used in §2.4) in order to match the observed los velocity dispersions at all radii is far more satisfactory. This also gives tighter limits on the M/L.

3.3 Modeling the los velocity dispersions

The key data for the analysis are the luminosity of the dwarf, its structural profile and the Galactocentric distance. The total luminosities, L_v have been measured only in the V-band and some, especially that of Sextans (Mateo et al. 1995), are very old and we suggest that new K-band images would be more appropriate measures of the stellar mass.

Next we use the King models (concentration c and tidal radius R_t) for the enclosed luminosity profiles, $L_K(r)$, of the dwarfs (mostly taken from Irwin & Hatzidimitriou 1995) that allows us to numerically calculate the luminosity density as a function of radius. Finally, we need the current Galactocentric radius, R_{MW} in order to compute the external gravity from the MW via the flat rotation curve (see McGaugh 2008) $g_{ex} = \frac{(170\,\mathrm{km\,s^{-1}})^2}{R_{MW}}$ where the amplitude of the rotation curve is from the SDSS data compiled by Xue et al. (2008) from the radial velocities of blue horizontal branch stars.

From this we solve for the internal gravity

$$g(r)\mu\left(|g(r)+g_{ex}|/a_o\right) = G(M/L)L_K(r)r^{-2} \tag{3.1}$$

where we use the *simple* μ function (Eq 1.7) and we take $|g(r)+g_{ex}| = \sqrt{g(r)^2+g_{ex}^2}$ which only matters in the small transition region. Then we numerically differentiate the luminosity profile from the King model, $L_K(r)$, to match with the simple function

$$l(r) \propto \left(1+\frac{r}{r_\alpha}\right)^{-\alpha_o} \tag{3.2}$$

which is a luminosity density profile and helps us to analytically define $\alpha(r) = d\ln l(r)/d\ln r = -\alpha_o\frac{r}{r+r_\alpha}$ for solving the Jeans equation for the radial velocity dispersions, σ_r,

$$\frac{d}{dr}\sigma_r^2(r) + \frac{\alpha(r)+2\beta(r)}{r}\sigma_r^2(r) = -g(r) \tag{3.3}$$

and we can cast this into the los with the use of the luminosity density profile, $l(r)$ (see Binney & Mamon 1982) as per §2.4, taking a velocity anisotropy, β of the form

$$\beta(r) = \beta_o - \frac{r}{r_\beta}. \tag{3.4}$$

This and all other fit parameters are given in Table 3.1.

Here we have three free parameters available for matching the observed with the model velocity dispersions. They are the M/L and the two associated with β. M/L adjusts the normalisation, whereas β varies the shape of the los profile. Note that although there are two parameters for the anisotropy, the profile required is virtually the same for 6/8 dwarfs (see Fig 3.3). In any case, Koch et al. (2007) make it clear from their analysis of Leo II that there is compelling evidence for negative (tangential) velocity anisotropy in dwarfs.

By χ^2 fitting the los velocity dispersions of Mateo et al. (2008) for Leo I, Muñoz et al. (2005) for Ursa Minor and Walker et al. (2007) for the remaining 6, with the model MOND velocity dispersions, we were able to best fit the anisotropy profile of all 8 dwarfs and thereby compute the M/L.

The fits are not hugely sensitive to the anisotropy profile. For instance, in Table 3.1 the column of r_β also gives the 1-σ errors on that parameter (found by simply holding M/L and β_o constant and varying r_β. Most dwarfs have very little sensitivity to the rate at which the anisotropy decreases with radius, with the only

exception being Draco. Leo I, Leo II, UMi and Sextans are quite comfortable with constant anistropies, however, none of the dwarfs are consistent with an anisotropy that becomes highly biased towards tangential orbits in small increases of radius.

It is difficult to be quantitative about how we could constrain MOND with any of these velocity anisotropies, since we use a very simple model for this and anisotropy could vary in a non-linear way, or there could be distinct stellar populations with completely different anisotropies. However, if instead of becoming biased towards tangential orbits at large radius, they were in reality biased towards highly radial orbits, there would be a serious problem because no M/L without a dark halo could fit the shape of the profiles. An example of this is given for the Sculptor dwarf in Fig 3.2(b) where the red line shows the fit with a constant $\beta(r) = 0.8$. No scaling with M/L can produce a good fit and it shows how precise knowledge of the velocity anisotropy would be extremely constraining to MOND, whereas no CDM halo can ever be constrained to such detail and thus can never be falsified.

3.3.1 Fits to the measured los velocity dispersions

The fits to the measured los velocity dispersion profiles of all 8 dwarfs are shown in Fig 3.1 and 3.2. The solid line is the best fit and the M/L is given in Table 3.1 along with all other relevant data for each dwarf. The dashed lines are the 1-σ errors in M/L. The reduced $\chi^2/(n - n_{d.f} - 1)$, where n is the number of data points and $n_{d.f}$ is the number of degrees of freedom in the model (always 3), is very reasonable for each dwarf, even though the data are inherently noisy.

A good example of this is the Fornax dwarf (Fig 3.2(a)) in which there are a larger number of data points (15) at large radii (from 500-1000pc) for which the individual errors are relatively small compared to the spread in the data. No straight line (or even one with curvature) through these data points could obtain a low reduced χ^2 and the line of best fit to these data is a very good one.

The velocity anisotropy profiles for each dwarf are plotted in Fig 3.3 against R/R_c and the linetype is given in Table 3.1. It is interesting that, apart from Ursa Minor and Draco, the other 6 dwarfs have very similar velocity anisotropies going from isotropic or slightly radially biased orbits at their centres to more tangentially biased orbits at the edges.

Name	R_{MW} kpc	c	R_t pc	M_v	L_v $10^5 L_\odot$	V_r $\mathrm{km\,s^{-1}}$	r_α pc	α_o	r_β pc	β_o	M/L_v	M/L_N	χ^2_{red}	n	Fig 3.3 linetypes
Carina	101 ± 5	0.51±0.08	581 ± 86	-9.3±0.2	4.4±1.1	8	2000	24	150^{+1050}_{-130}	0.6	$5.6^{+5.2}_{-2.9}$	80	0.72	21	black solid
Draco	93 ± 6	0.72±0.05	1225 ± 80	-9.0±0.3	3.3±1.1	-65	1500	14	500^{+150}_{-85}	0.6	$24.0^{+10.0}_{-7.6}$	270	0.69	6	black dashed
Leo I	257 ± 8	0.39±0.07	1002 ± 50	-12.4±0.2	30±3	178	3700	22	$490^{+\infty}_{-400}$	0.1	$1.35^{+0.95}_{-0.6}$	10	0.42	15	black dotted
Sextans	95.5 ± 3	0.98±0.14	3445 ± 1141	-9.7±0.2	6.3±1.4	75	1200	6	1250^{+8500}_{-600}	0.0	$9.2^{+5.3}_{-3.0}$	102	1.2	20	black dot-dashed
Fornax	138 ± 8	0.72±0.05	2078 ± 177	-13.2±0.2	158±16	-36	3200	14	770^{+1500}_{-450}	0.3	$1.4^{+0.45}_{-0.35}$	11	1.4	43	red solid
Sculptor	87 ± 4	1.12±0.12	1329 ± 107	-11.1±0.2	28±4	95	1200	14	170^{+600}_{-140}	0.5	$3.7^{+2.2}_{-1.4}$	36	0.7	33	red dashed
Leo II	233 ± 15	0.48±0.1	554 ± 68	-9.9±0.3	7.6±3	22	2500	30	$280^{+\infty}_{-255}$	0.56	$1.85^{+2.0}_{-1.1}$	57	1.1	14	red dotted
UMi	76 ± 4	0.64±0.05	1977 ± 104	-10.3±0.4	11.0±4.8	-87	6000	25	$5000^{+\infty}_{-4750}$	0.73	$5.8^{+6.5}_{-3.6}$	440	0.86	23	red dot-dashed

Table 3.1: All distance and magnitude data from Mateo (1998), Galactocentric radial velocities from Wilkinson & Evans (1999) and structural parameters from Irwin & Hatzidimitriou (1995) except Draco's V_r which is from Hargreaves et al. (1996). R_{MW} is actually $R_\odot$, but since satellites have Galactic latitudes such that $90^o < l < 270^o$, this will only underestimate R_{MW}. Recalculated distance (Bellazzini et al. 2002 for both) and structural values of are used for Draco (Odenkirchen et al. 2003) and Ursa Minor (Palma et al. 2003) which lead to new absolute magnitudes. Sextans has an updated distance from Lee et al. (2003) which gives a 20% increased luminosity. Leo I's luminosity and structural parameters come from Smolčić et al. (2007) which makes use of the new distance modulus from Bellazzini et al. (2004). In Angus (2008) we used the luminosity from Sohn et al. (2007), but this increased luminosity comes from extrapolting the surface brightness to large radii based on a ten year old central surface brightness. Luminosity for Leo II corrected for new distance from Bellazzini et al. (2005), as is Sculptor's from Piatek et al. (2006). The solar absolute magnitude is $M_v = 4.8$. W_o parameters for the King model are 1.97, 3.14, 1.51, 4.59, 3.14, 5.29, 1.85, 2.7. The Newtonian M/L come from dividing the dark mass at r_{max} from Walker et al. (2007) by the V-band luminosity (except UMi which comes from Kleyna et al. 2003). n is the number of data points and $n_{d.f}$ is the number of degrees of freedom in the model (always 3).

To be comfortably explained in MOND, these dwarfs should have M/L of around 3 solar units. It is good to see that all four dwarfs associated with the Fornax-Leo-Sculptor stream have normal M/L. This is absolutely necessary because Leo I and Fornax are very massive compared to the rest which means the external gravity of the MW should not disturb them. Furthermore, the two Leo dwarfs are beyond 200kpc meaning even if they had a near pericentre to the MW, they should have returned to equilibrium by now: dynamical times are $\sim \frac{1000pc}{10\,\mathrm{km\,s^{-1}}} = 100Myr$, Orbital periods are $\sim \frac{200kpc}{300\,\mathrm{km\,s^{-1}}} = 700Myr$.

The Carina and Ursa Minor dwarfs have borderline reasonable M/L ($5.6^{+5.2}_{-2.9}$ and $5.8^{+6.5}_{-3.6}$ respectively). When the 1-σ error in M/L is considered along with deviations from spherical symmetry, coupled with other uncertainties in luminosity, distance, structure and possible tidal effects, they may well be safely within the bounds of normal M/L.

Although initially thought to have a large mass discrepancy (Gerhard & Spergel 1992; Milgrom 1995; Łokas 2001; Sánchez-Salcedo & Hernandez 2007, reanalysis of Ursa Minor's structural parameters and distance by Bellazzini et al. (2002) showed it to be more distant and extended, therefore it has a significantly larger luminosity which has reduced the M/L.

Problem cases

There is little doubt that Draco and now Sextans are both concerns for MOND. Their M/L's are uncomfortably high and we seek to find an explanation for this given that the other 6 are more or less compatible. First of all, it is troubling that these two have the noisiest velocity dispersions especially compared to the almost constant velocity dispersions of Fornax, Sculptor, Leo I and even Carina. The dispersions seem to have regions where they are abnormally high and low. In addition there exists a further, extremely cold kinematic substructure in Sextans (Kleyna et al. 2004) which is puzzling and may be the result of a star cluster that has spiralled in under the drag of dynamical friction (see §1.5.2) and has settled to the core of the dwarf and may have heated the dwarf stars in the process.

Ignoring this for the moment, even if we only paid attention to the low values (i.e. with the lower dashed lines in Fig 3.1, the M/L are still unsatisfactory. Draco's luminosity and distance have recently been reviewed by Bellazzini et al. (2002), but Sextans still has a very poorly constrained structure (its tidal radius is

$3445 \pm 1141 pc$) and it would be of great benefit to have its King model parameters and integrated magnitude reanalysed. Still, it is worth bearing in mind that although the M/L are high, they are also poorly constrained and they are only $\sim$2-σ from acceptable values.

The double impact of Galactocentric distance in MOND

For a satellite like any one of the dwarfs studied here, the only influence the Newtonian gravity of the MW exerts is to carve out its orbital path. Any tidal forces are negligible and there is absolutely no difference to the internal gravity. In stark contrast, the MW's MOND gravity has a huge impact on the internal gravity of the low luminosity, nearby dwarfs: Carina, Sextans, Draco and Ursa Minor. As mentioned above, the external field renormalises the effective Newtonian Gravitational constant $G \rightarrow G/\mu(\frac{170^2}{a_o R_{MW}})$ (as long as the external gravity is higher than the internal gravity). As R_{MW} increases, G/μ follows suit reducing all inferred M/L by the same factor. The key thing here is that if new observations increase the distance to a dwarf by 11% (as Lee et al. 2003 has done for Sextans and Bellazzini et al. 2002, 2004, 2005 have done for other dwarfs) not only does the luminosity increase by 21%, which obviously drops any M/L by 17%, but the reduction in the external field effect allows the M/L to drop a further 10% (in that particular case). So, increasing the distance of Sextans by less than 10kpc dropped the M/L from 15 to almost 9.

Sextans: poorly constrained light profile

Sextans has a M/L=$9.2^{+5.3}_{-3.0}$ which is impossible from population synthesis point of view. However, this M/L assumes we know the luminosity of Sextans well. In fact, Sextans is the lowest surface brightness dwarf we study here and it's light profile has not been examined in detail since before Mateo (1998). All of the other dwarfs that have had their luminosity re-evaluated have had it pushed up far beyond the original 1-σ error: UMi, Draco, Carina, Leo I and Leo II. In fact, the first four of those five mentioned saw their luminosities double. When Sextans has its luminosity re-integrated with new photometry, we expect it to rise by at least 50%, but not necessarily by a factor of 3 which would put it in the acceptable zone. This will probably leave it with a similar M/L as Carina and UMi, requiring a modest amount of tidal heating (see next section) to be

consistent with the los velocity dispersions.

At the moment however, it should be noted that although the M/L of Carina and UMi are higher than 3, uncertainties in their los velocity dispersions as well as their luminosity and distance mean they are in agreement within the observational errors. Still, the fact that they are all coherently, higher than preferred compells us to consider why in the next section.

Impulsive tidal heating

The most enticing resolution of the three moderately high M/L dwarfs are that Sextans, Carina and UMi have recently had a close pericentre of the MW and have been slightly tidally heated. The crossing times for stars ($2R/\sigma_{los}$) at the last measured los dispersion radius are 120 (Carina), 300 (Sextans), 150 (Umi) and 110 (Draco) Myr, but recall that relaxation times in MOND are higher than in Newtonian gravity as calculated from galaxy mergers by Nipoti et al. (2007b) and Tiret & Combes (2007b). Using a simple back stepping orbit integrator taking the current Galactocentric radii and radial velocities, with gravity calculated from a flat rotation curve with circular speed of $170\,\mathrm{km\,s^{-1}}$ (see Xue et al. 2008; McGaugh 2008), we found it has been roughly 700 (Carina), 500 (Sextans) and 850 (UMi) Myr since the satellites had their last pericentre.

There is something key to remember here in which MOND differs starkly from Newtonian gravity. A low surface brightness dwarf galaxy has dynamical stability imparted by the MOND enhanced gravity, much like the DM halo provides for Newtonian gravity. If we make the crude but fair assumption, for clarity's sake, that the external field of the MW dominates the internal accelerations of the 3 satellites, then the MOND effect is to renormalise Newton's constant upwards which enhances the internal gravity. So $G \rightarrow G/\mu(g_{ex}/a_o) \sim Ga_o/g_{ex}$.

As the satellites approach the MW this stability is lost due to the rising external field which bleeds the internal gravity of the dwarf. This of course doesn't happen in Newtonian gravity and the dwarfs can withstand tidal forces more easily (the DM halo stays virtually intact until very close to the MW). This makes it far easier to perturb a MOND dwarf. The radii below which tidal effects begin to affect the dwarfs in MOND is $\sim$40kpc as opposed to $<$10kpc for Newtonian gravity with the observed DM halos (see Brada & Milgrom 2000a).

Currently, none of the dwarfs studied here are strictly (within the range of

radii that have measured velocity dispersions), in the non-adiabatic/impulsive regime where the external field varies faster than the dwarf can respond dynamically.

However, they may have just left this region or these effects may be even stronger than expected by Brada & Milgrom 2000a. We slightly repackage Brada & Milgrom's demonstration that tidal effects begin to impose themselves at much larger Galactocentric radii in MOND, by looking at the rate of change of the external field strength during one crossing time at the core radius of each dwarf i.e. $\frac{170^2}{R_{MW}} - \frac{170^2}{R_{MW}-2V_r R_c/\sigma_{los}}$ plotted against M/L for each dwarf in Fig 3.4).

It is not surprising to see those dwarfs with a more rapidly changing external field having higher M/L. This is all a symptom of the lower mass satellites being systematically closer to the MW, intrinsically having less robust luminosities and being more susceptable, as a result, to tides.

Although Sextans, Ursa Minor and Carina are not in the non-adiabatic regime, the magnitude of the external field will have been varying rapidly in the past. It is unknown at present how serious an effect this is, but it needs to be studied with realistic, high resolution MOND simulations (see Nipoti et al. 2007b and Tiret & Combes 2007b) for dwarf galaxies in the external field of the MW, but also for spirals passing through the centres of clusters. This rapidly varying external field we predict is destroying the integrity of spirals in clusters (see Rubin et al. 1999) and also imposes a morphology-position relation in clusters more easily than galaxy harassment (Moore et al. 1999b).

Whether Sextans or any of the others have recently had a close pericentre passage will only be known after accurate proper motions are published. The proper motions of Ursa Minor are known well enough only to say the pericentre lies between 10kpc and 76kpc (Piatek et al. 2005) at 1-σ.

Draco: tidal disruption

If indeed Sextans has a higher luminosity than the currently measured one, or the cold kinematic substructure heated it (through dynamical friction Kleyna et al. 2004), the biggest issue we are left with is Draco with M/L=$24^{+10}_{-7.6}$. Draco is now moving towards the MW at $\sim 65\,\mathrm{km\,s^{-1}}$ which means it is most likely on its first passage of the MW. Ségall et al. (2007) showed that Draco has a symmetric, unperturbed density profile with no evidence for tidal tails - "Draco

has led a quiet existence". This is in line with the fact that it has been on a direct path towards the MW since its creation. However, if its tangential velocity is negligible, its tidal tails may line up along the los.

Since Draco cannot have been tidally heated by a near pericentre passage due to the timescales involved, this leaves us with only one conclusion i.e. that Draco is in the throes of tidal disruption, which is perfectly possible in MOND, but unimaginable in Newtonian gravity. At its apocentre, Draco would have experienced very little external field and thus its low surface density would be enough to maintain its dynamical integrity due to the MOND enhanced gravity. This would make its internal gravity at R=1000pc $\sim \sqrt{3.6 \times 4.4 \times 10^{-3} \times 3 \times 3.3 \times 10^5/1000^2} \sim a_o/30$ (this assumes no external field). However, currently it is at 93kpc and thus the internal gravity is merely $4.4 \times 10^{-3} \times a_o \frac{93 \times 10^3}{170^2} \sim a_o/70$, reduced because of the growing external field.

This loss in binding energy might have recently thrown Draco into the early stages of tidal disruption. Muñoz et al. (2008) have showed with high resolution N-body simulations that even modest tidal disruption near the edges of dwarfs can have a dramatic impact on the observed dynamics. This again must be confirmed by numerical simulations of Draco on a plunging (radial) orbit from a large radius in MOND with a reasonable M/L and velocity dispersion found by solving the Jeans equation (Eq 3.3). Either Draco will begin disrupting at $\sim 100kpc$ and its los velocity dispersions will appear artificially high, or it will have velocity dispersions consistent with the Jeans equation at all radii down to 50kpc or so. At this point, Draco becomes a serious problem for MOND.

Dwarf fly-bys

Is it possible that the dwarfs are co-responsible for their own large dispersions? Draco and Ursa Minor are separated by approximately 20kpc, so the largest external gravity that UMi could inflict on Draco is a mere $Ga_o/g_{ex}(M/L_v)L_{sat}d^{-2} \sim 4.4 \times 10^{-3} \times 10 \times 3 \times 1.1 \times 10^6 \times (20000)^{-2} \sim a_o/10000$. If say the Fornax satellite conspired to collide with Sextans it would have to pass within $d \sim \sqrt{G\frac{a_o}{g_{in}g_{ex}}(M/L_v)L_{sat}} \sim \sqrt{4.4 \times 10^{-3}\frac{400}{a_o} \times 3 \times 1.5 \times 10^7} \sim 4500pc$. That would balance the internal and external accelerations because at 1kpc the internal gravity of Sextans is $a_o/20$. This is at least possible given that they are currently moving away from each other, but highly improbable. Accurate proper

motions would resolve this.

Interloper stars, tidal tails and ellipticity

It was noted by Klimentowski et al. (2007, 2008) and Lokas et al. (2007, 2008) that contaminating field stars and tidal tails along the line of sight can have an adverse effect on the los velocity dispersion. They showed using high resolution N-body simulations as comparisons that the velocity dispersion is boosted by the interloper stars, giving the appearance of a high M/L. The key here is that there is no exact way to distinguish a star along the line of sight of a dwarf as a member star or one that is part of a tidal stream no longer bound or influencing the self gravitation of the dwarf. The relative velocity this star will have with respect to the bulk motion can be considerably high and inflates the deduced velocity dispersion.

We took the los velocity dispersion data from Lokas et al. (2007) for Draco which they had cleaned for interloper stars. This reduced the M/L found using the Walker et al. (2007) sample from 44^{+28}_{-20} to $24^{+10}_{-7.6}$ and could certainly reduce the M/L of the more nearby dwarfs Carina, UMi and Sextans. Since the internal velocity dispersions and only of order $10\,\mathrm{km\,s^{-1}}$ it is often easy to weed out the interloper stars of the Milky Way if the satellite has a large heliocentric velocity like Leo I. However, tidal tails can still be confused as could elongation of the satellite along the line of sight. This needs to be modelled in some detail with N-body simulations to see if this is a strong effect.

Trends with key variables

In Fig 3.4 we plot the M/L against four variables which describe the dwarfs in order to elucidate trends, although we are clearly dealing with large errors and small number statistics. In the top left panel, we plot M/L against Galactocentric distance. There is an obvious division between Fornax and the two Leo dwarfs beyond 130kpc and the other 5 less than 100kpc from the centre of the MW. In addition, there is some evidence for a trend shown in the top right panel for lower surface brightness dwarfs to have higher M/L as well as those with an external field that is varying more rapidly.

However, none of those three independent variables cut a tight correlation with M/L because none of them are the cause of the high M/L, they are merely

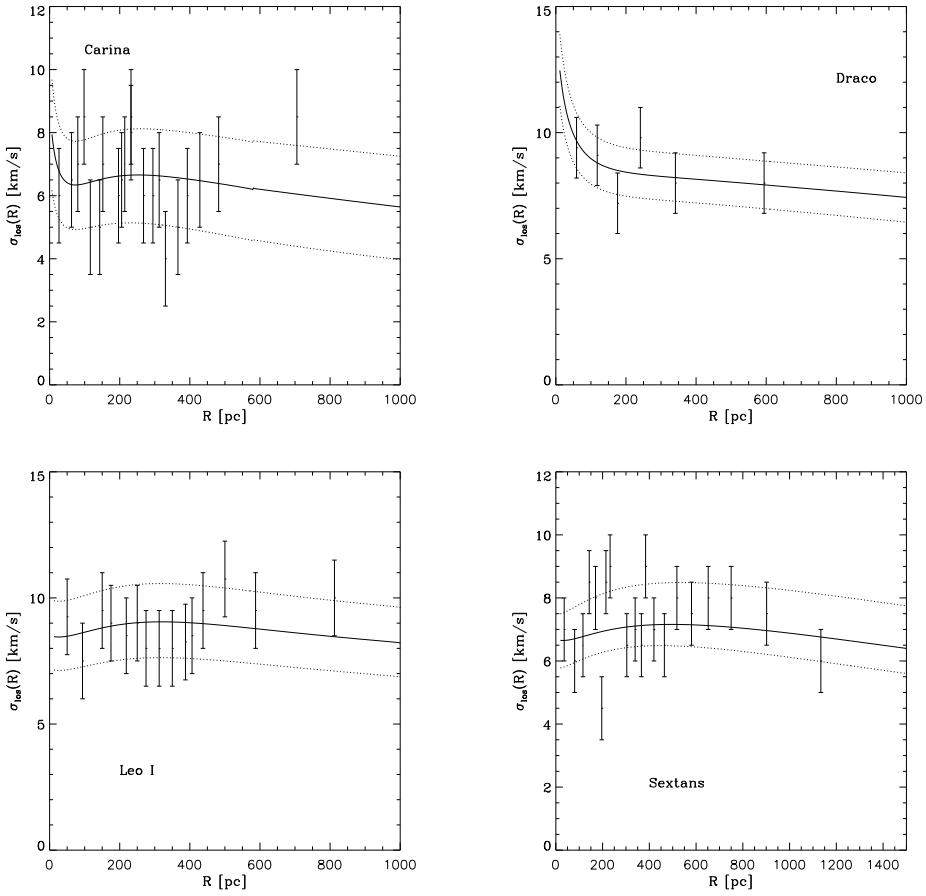

Figure 3.1: Line of sight velocity dispersion profiles, σ_{los}(R), for all 8 dwarfs. Best fit lines have solid line type and the dashed curves correspond to the 1-sigma errors on M/L.

strong indicators. The smaller the Galactocentric radius, the higher the external field and the more energy there is available to perturb the dwarf. The lower the luminosity, the more susceptible the dwarf is to being perturbed by the external field. The radial velocity (bottom left) is a poor indicator because any perturbing of the dwarfs was done near pericentre. This again shows why Galactocentric radius is just an indicator because it simply means the dwarf was more likely to have been at smaller radii but for all we know it may currently be at pericentre (Bellazzini et al. 1996). It is not surprising that Draco with its large M/L has a low Galactocentric radius, surface brightness and large velocity towards the MW as it may well be tidally disrupting.

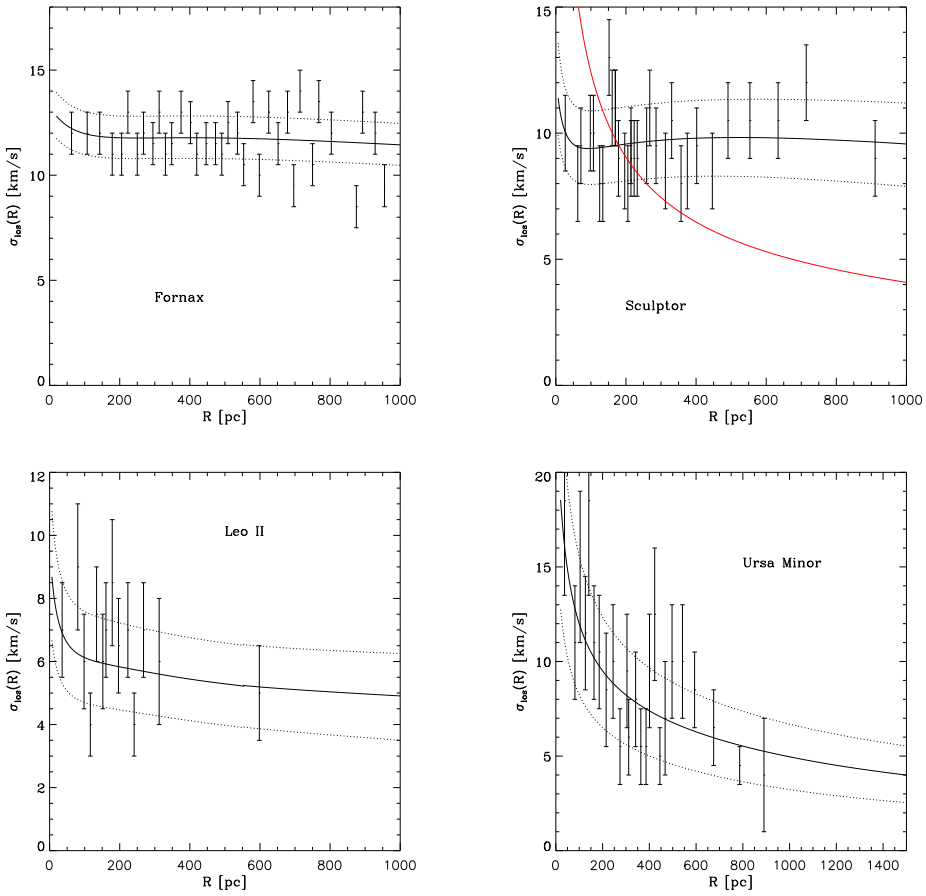

Figure 3.2: As for Fig 3.1. The red line on the Sculptor plot show what the los velocity dispersion would look like if Sculptor had a constant velocity anisotropy $\beta = 0.8$. It is impossible to match with any M/L.

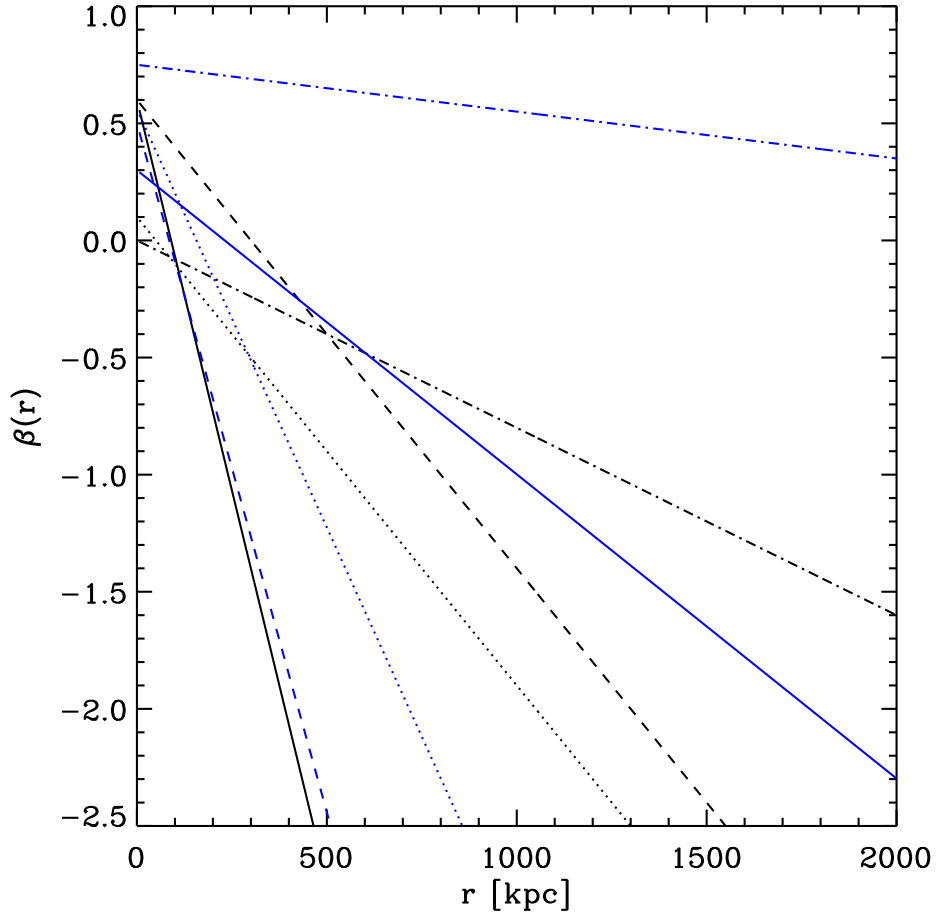

Figure 3.3: Velocity anisotropy profiles, β(r), for all 8 dwarfs. See Table 3.1 for the corresponding linetypes.

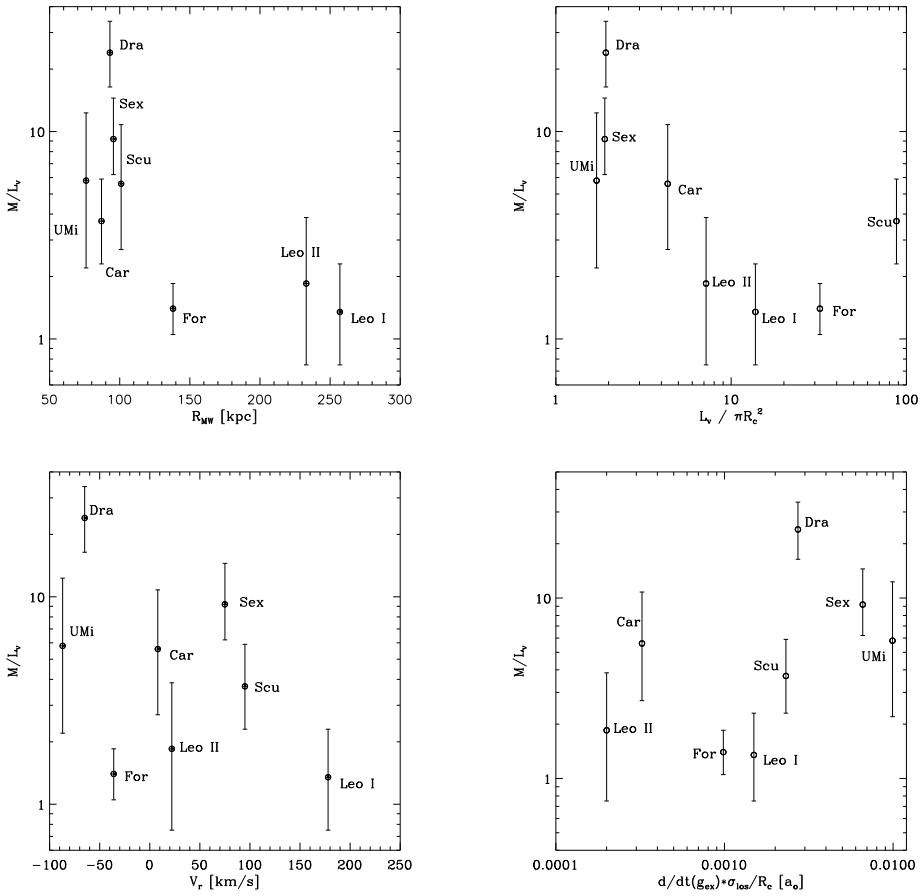

Figure 3.4: Shows M/L against several variables for each dSph. (a) Galactocentric radius, which implies external field strength (b) V band surface density (c) Galactocentric radial velocity (d) Variation of the external field during one dynamical time at the core radius. Note the three dwarfs with large external field variations are Draco, Ursa Minor and Sextans.

3.3.2 Discussion

Here we have studied the los velocity dispersion profiles of 8 of the MW's dwarf satellites in MOND. We have shown that 6 of the dwarfs (Leo I, Leo II, Fornax, Sculptor, Ursa Minor and Carina) have acceptable M/L within their errors. Despite Carina and Ursa Minor having M/Ls of $5.6^{+5.2}_{-2.9}$ and $5.8^{+6.5}_{-3.6}$ respectively, it is pointless to be too concerned about them because they have M/L of 3 within 1-σ and uncertainties in luminosity, ellipticity, structure and equilibrium could easily account for this discrepancy. On the other hand, the remaining 2 (Draco and Sextans) have M/L completely inconsistent with the stellar populations. The possible causes of this have been discussed in depth and 3 testable effects that cause the discrepancies have been suggested.

First of all, the photometry of Sextans is extremely old (more than 13 years; Mateo et al. 1995) and so we suggest K-band images of the dwarf should be acquired to alleviate any doubts on the luminosity of the dwarf and how the light is distributed. However, this is likely to leave Sextans with a M/L similar to Carina, UMi and Sextans (~ 5). To be certain of the effects of non-adiabatic tidal heating of the dwarfs, we need accurate proper motions to make sure Sextans is currently not at pericentre and that Draco is on a highly elongated orbit plunging towards the MW.

If this is the case, then realistic, high resolution simulations (like those of Nipoti et al. 2007a and Tiret & Combes 2008) must be run in order to confirm that the non-adiabatically changing external field effect can indeed make the small boost to the los velocity dispersions in these satellites over the given orbits and timescales and even tidally disrupt Draco. If it turns out that the external field effect is unable to disrupt Draco given its orbital history then it poses a significant problem for MOND.

It is quite remarkable that using only the stellar mass of the dwarfs, we can successfully match the los velocity dispersion profiles with sensible falling anisotropies and get excellent reduced χ^2 for all 8 dwarfs and 6/8 have good M/L. As for Draco, the unknown orbital history is vital to the comprehension of its large M/L and until it is known, we cannot confirm the dwarf galaxies of the MW as a success or failure of MOND.

3.4 Globular clusters of the Milky Way

One promising test of MOND proposed by Baumgardt et al. (2005) employs distant low surface brightness globular clusters of the Milky Way. Globular clusters (GCs) are not generally inferred to have their own dark matter. This is consistent with MOND insofar as GCs are dense enough that they are in the Newtonian rather than MOND regime. However, systems that are remote enough and low in density should show some mass discrepancy. This is not expected in the dark matter (DM) picture in which GCs apparently form as baryonic star clusters free of DM. Baumgardt et al. (2005) identified some candidates for this test. A larger sample is desirable because the unknown orbital history of each globular cluster is a potential source of confusion, with tidal effects. Here we estimate the central escape velocity of Galactic GCs in MOND in order to identify further potential candidates.

The central escape velocity of a gravitating system is an important property which sets limits on the system's ability to retain stars and gas and is simply defined as the speed required to transport a star (or test mass) from one position in the potential well, $\Phi(r)$, to infinity where the potential and velocity are zero. It is well defined in Newtonian gravity, but requires substantially more thought in MOND. The effective logarithmic potential of MOND makes the notion of escape from an isolated object ill-defined. In practice, there is no such thing as an isolated object, and the escape velocity is set by the external field effect (EFE, §1.4).

The EFE arises when the MOND gravity from a neighbouring object dampens the usual MOND correction to a system's internal gravity. Whether this is an important effect depends on the magnitude of the external field with respect to the internal gravity and the acceleration constant of MOND, a_o. The EFE sets the maximum possible size of bound objects; it can even dominate the internal dynamics of diffuse systems (Milgrom 1983c; Sanders & McGaugh 2002; McGaugh 2004; Famaey et al. 2007b; Wu et al. 2007), leading to very different results than might naively be expected for isolated objects.

An obvious class of system subject to the EFE are globular clusters (GCs). These agglomerations of old stars appear to be free of dark matter, as expected for dense systems in MOND (Milgrom & Sanders 2003). They are embedded in the tidal field of the Galaxy, and the transition from internal to external field

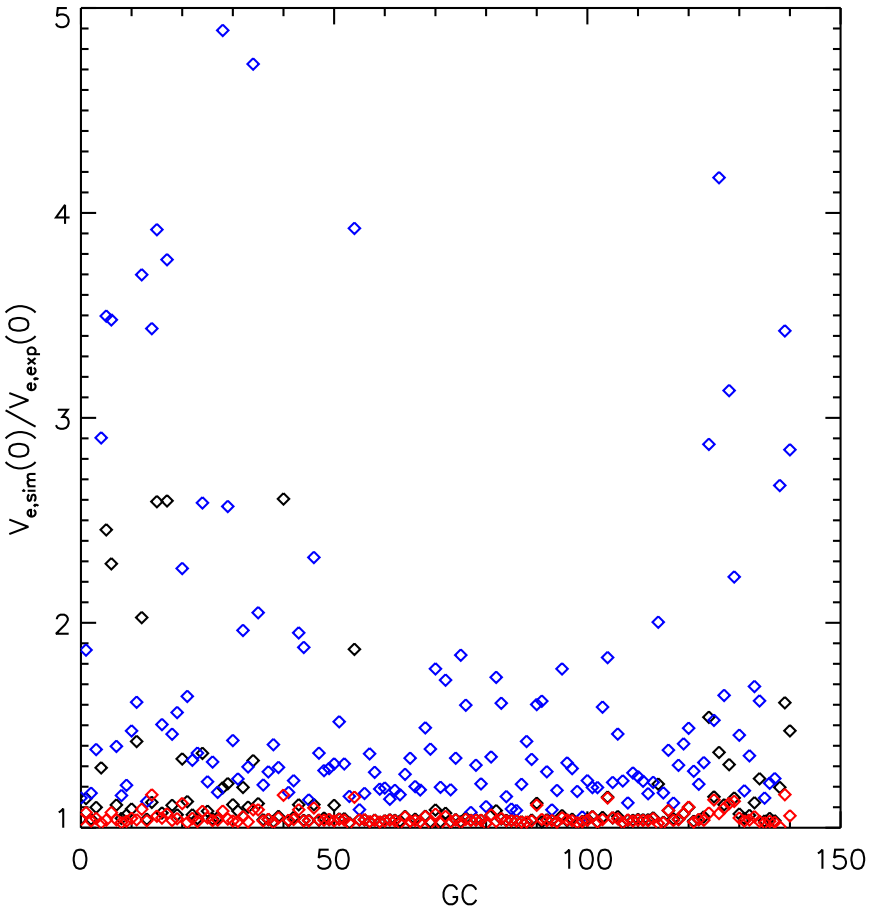

Figure 3.5: Comparison of the simulated escape velocities with the theoretical values of Gnedin et al. (2002, hereafter G02) in three situations for all 141 GCs. The red points are the simulations run with Newtonian gravity and are almost entirely exactly unity as expected. The black points are for MOND and most are overlapping with the red points because there has been little enhancement to the escape velocity when the EFE is considered. The blue points are for MOND with no external field. This case should have infinite escape velocity, but the 3kpc radius cut-off imposes an artificial limit. Nevertheless, the distinction between the isolated and EFE cases is obvious, so the 3 kpc criterion suffices for our purposes.

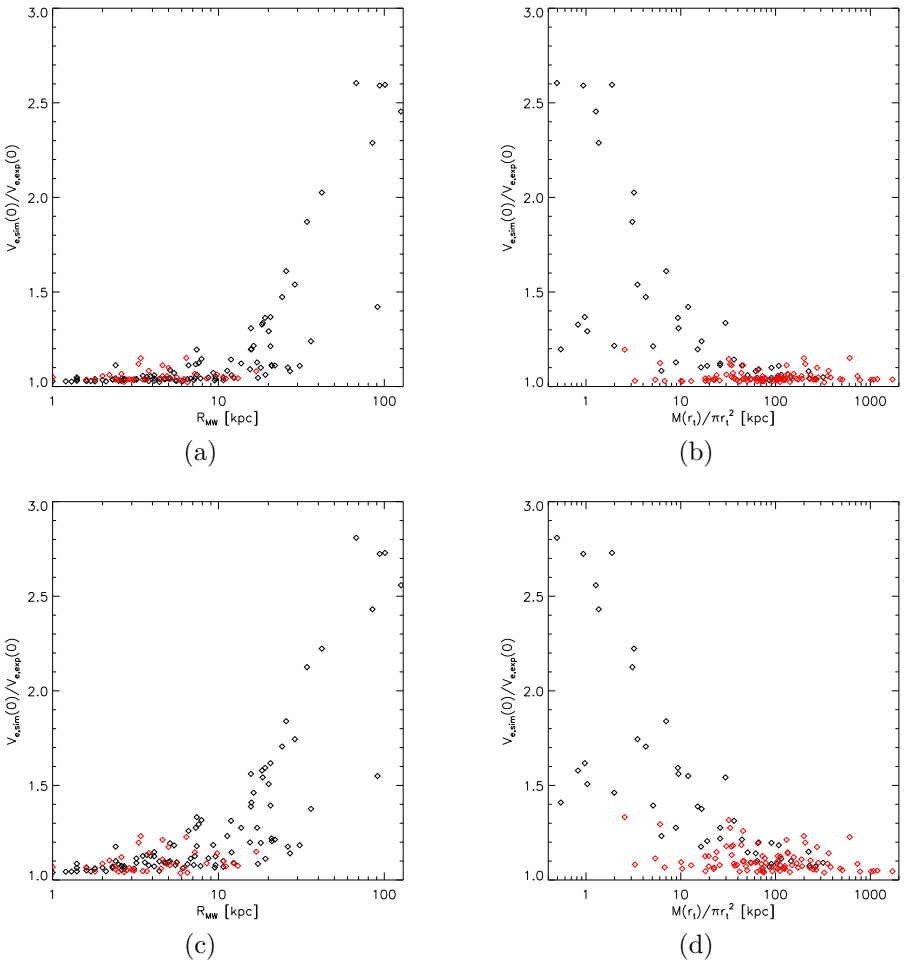

Figure 3.6: Shows the ratio of our simulated MOND escape speeds to the theoretical Newtonian escape speed given by G02 as functions of GC Galactocentric radius (left) and mean surface density (right) for both standard (top) and simple (bottom) μ functions. In all four plots there are symbols of two colours: in the plots for Galactocentric radius, the GCs with mean surface density above the MOND transition value ($126 M_{\odot} pc^{-2}$) are red and those below are black. For the mean surface density plots, those GCs orbiting beyond 10kpc are black and those below are red. As a guide, red means there shouldn't be an appreciable MOND effect.

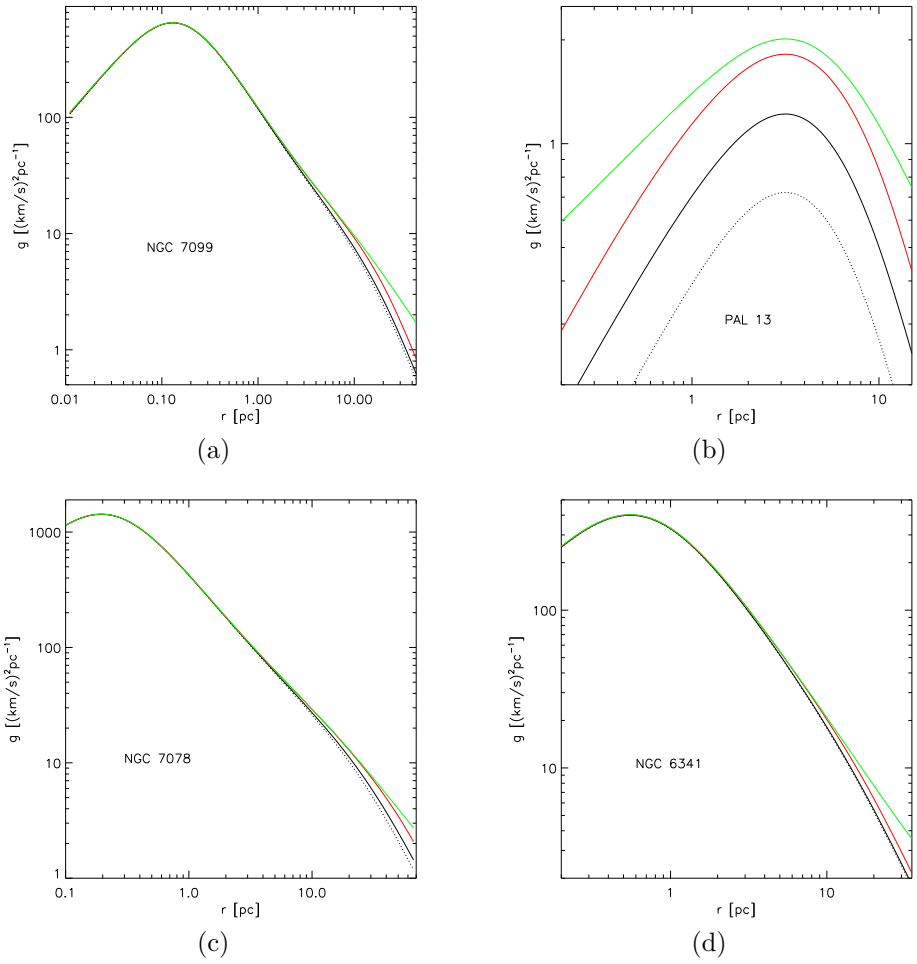

Figure 3.7: Shows gravity versus radius for Newtonian (black dashed), MOND with anti-parallel EFE (red), MOND with parallel EFE (black) and MOND with no EFE (green). (a) NGC7099 shows virtually no deviation from Newtonian gravity due to strong EFE. When the EFE is anti-parallel, the small reduction in $\mathbf{g} + \mathbf{g_{ex}}$ renormalises G as discussed in §3.4.4, but gravity still declines in a Keplerian fashion ($\propto r^{-2}$). (b) Pal 13 shows a moderate increase in gravity depending on azimuth relative to the external field. However, since the internal gravity is everywhere dominated by the strength of g_{ex} the gravity is simply renormalised with a scaled Newton's constant $G \rightarrow G/\mu(\frac{\mathbf{g}+\mathbf{g_{ex}}}{a_o})$. (c) NGC 7078 and (d) NGC 6341 show virtually no deviation from Newtonian gravity, so with the exception of Pal 13, we expect these GCs to demonstrate the same dynamical behaviour in MOND as in Newtonian gravity.

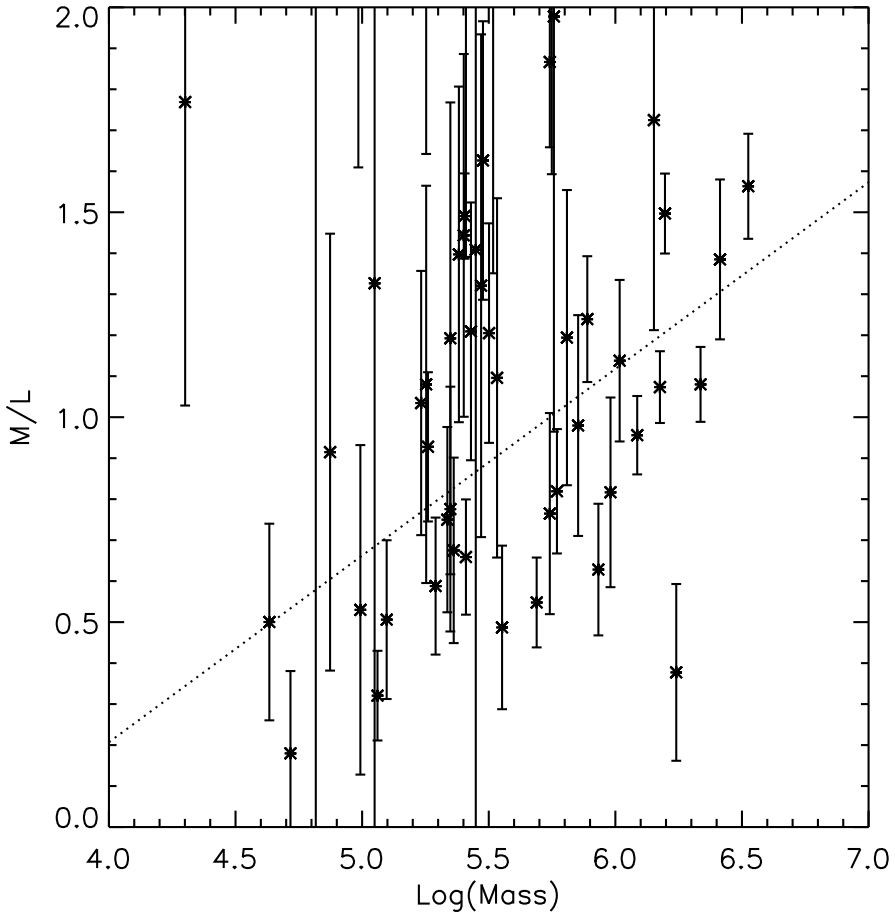

Figure 3.8: Shows the slight scaling of the M/L of GCs with GC mass. The data was compiled by taking the observed velocity dispersions from Pryor & Meylan (1993) for 60 GCs and rescaling the M/L of G02 so that their model velocity dispersions matched those of Pryor & Meylan (1993). The line is the best fit to the data, weighting each point with its uncertainty in central velocity dispersion.

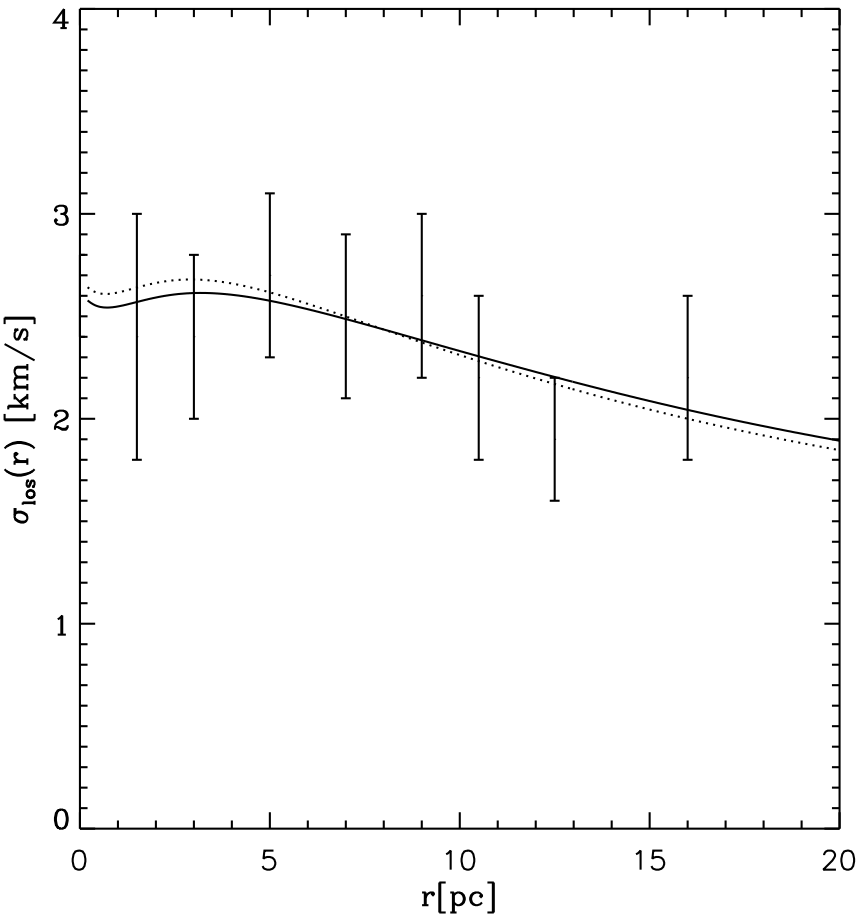

Figure 3.9: Fit to the los velocity dispersion data for NGC 288 obtained by Scarpa et al. (2007). The MOND fit (solid black) uses M/L=1.7 and the Newtonian fit (dashed black) uses M/L=2.0. Both are projected into the los with the fitted light profile from the King model and both use a slowly varying anisotropy of $\beta(r) = 0.2 - 1.1\frac{r}{r+10pc}$ as per §2.4. Clearly, using GCs with such proximity to the Galaxy makes it extremely difficult to distinguish between MOND and Newtonian gravity.

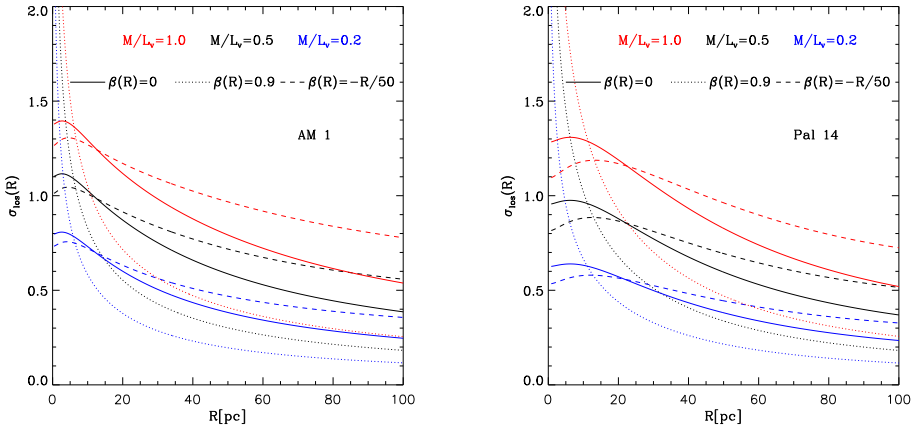

Figure 3.10: Shows the first order predictions of the los velocity dispersions for the distant LSB GCs AM 1 and Pal 14. The red, black and blue lines correspond to M/L of 1.0, 0.5 and 0.2 respectively in the V-band and the solid, dotted and dashed lines correspond to isotropy, radial anisotropy, and anisotropy that decreases with radius. The blue dotted line corresponding to M/L=0.2 and highly radial orbits is the lower limit of what we might expect in MOND.

domination may potentially provide interesting tests of MOND (Baumgardt et al. 2005; Scarpa et al. 2003, 2007).

The density profiles of GCs are usually fitted with King models $M_K(r)$ with a total mass M_{gc}, tidal radius R_t, and core radius R_c. The latter two define the concentration parameter $c = \log_{10}(R_t/R_c)$.

We seek here not to exactly compute the central escape velocity in MOND for all GCs of the MW, but rather estimate the central escape velocity in a rapid way for a large number of GCs which enables us to compare the result with the Newtonian escape velocity and hence identify interesting GCs that can distinguish bewtween MOND and Newtonian gravity if observed in detail. The necessary data come from Gnedin et al. (2002) in which 141 GCs of the Milky Way have their structural parameters tabulated. There is a difficulty in distinguishing between MOND and Newtonian gravity due to the unknown mass-to-light ratios of GCs. Gnedin et al. (2002, hereafter G02) chose M/L=3 for all GCs, but many authors suggest a lower value should be adopted (e.g., Harris 1996). Further, Hilker (2006) showed a significant drop in M/L for lower mass systems, a result which we confirm here and this degeneracy is discussed later.

3.4.1 The external field effect

We implement two possible versions of the interpolation function: the *standard* (Eq 1.6) and the *simple* (Eq 1.7) functions.

We do not wish to ignore the EFE, so we expand Eq 1.5 to explicitly include the external field $\mathbf{g_{ex}}$ as well as the internal field $\mathbf{g}$ which gives

$$(\mathbf{g}+\mathbf{g_{ex}})\mu\left(\frac{|\mathbf{g}+\mathbf{g_{ex}}|}{a_o}\right) = -g_{Nex} - GM_K(r)\frac{\mathbf{r}}{r^3} \tag{3.5}$$

as our starting point. This leads to the important equation

$$\mathbf{g}\mu\left(\frac{|\mathbf{g}+\mathbf{g_{ex}}|}{a_o}\right) + \mathbf{g_{ex}}\left[\mu\left(\frac{|\mathbf{g}+\mathbf{g_{ex}}|}{a_o}\right) - \mu\left(\frac{g_{ex}}{a_o}\right)\right] = -GM_K(r)\frac{\mathbf{r}}{r^3} \tag{3.6}$$

by noting that the object embedded in the external field obeys $\mu(g_{ex}/a_o)g_{ex} = g_{Nex}$ (with scalar $g = |\mathbf{g}|$). The external field dominates the argument if $g_{ex} \gg g$ leading to a simple rescaling of the gravitational constant $G \rightarrow G/\mu(g_{ex})$. An external field limits the escape velocity of stars from a system because the potential does not increase indefinitely as for an isolated system in MOND, $\Phi \propto \ln(r)$. Indeed, in the limit of strong external field domination, one would expect to see a Keplerian decline in velocity but with a mass excess given by the rescaled gravitational constant (Milgrom 1995). This occurs in the outskirts of all systems and allows stars to escape. For example, the Milky Way might have an escape of only $\sim 550\,\mathrm{km\,s^{-1}}$ thanks to the proximity of M31 (Famaey et al. 2007b). In the case of globular clusters, which are known to lose stars (e.g., Combes et al. 1999; Leon et al. 2000), the external acceleration g_{ex} is provided by the Milky Way, just as for the dwarf spheroidals in §3.2.

3.4.2 Orbit integration in MOND

Our method was to simulate the orbit of a single star on a radial orbit from the centre of a GC while the GC is orbiting the Milky Way (MW). To do this in MOND, we needed two important pieces of information; the mass distribution throughout the GC and the distance of the GC from the centre of the MW (see §2.2.3 for a similar problem involving the collision of the bullet cluster).

For the mass distributions we took the 141 GCs tabulated by G02[2] and gen-

[2]http://www.astro.lsa.umich.edu/~ognedin/gc/vesc.dat

erated the enclosed mass as a function of radius defined by their King model fits. This allowed us to compute the Newtonian gravity, $g_N(r) = -GM_K(r)/r^2$ as a function of radius. The distance from the Galactic centre gives us the external gravity of the Milky Way via the rotation curve, $g_{ex} = V(R_{MW})^2/R_{MW}$, where $V(R_{MW}) = 170\,\mathrm{km\,s^{-1}}$ as per §3.2. This allowed calculation of g from Eq 3.6.

A simple orbit

All we know is the instantaneous external field due to the GCs current position. We would prefer to simulate the change of the external field as the GC orbits the Galaxy. However, without accurate proper motions, the best we can do is place the GC on a circular orbit at its given Galactocentric radius. Since an orbital period of a star in a GC is of the order 0.1-1Myr and a GC's orbit around the Milky Way is usually >200Myr, this is a tolerable if imperfect assumption. This is not as important an effect as one might think. The only reason any orbit is invoked is to remove the effect of preferred directions created by not including the curl field.

We create the effect of a circular Galactic orbit by modulating the direction of the external field while the GC is freefalling with g_{ex}. The modulation was implemented by taking the angular period of the GC on a circular orbit defined as $\omega = \sqrt{g_{ex}/R_{MW}}$ and $\mathbf{g_{ex}} = g_{ex}\exp(\mathbf{i}\omega\mathbf{t})$. From here we can solve the full MOND equation including the external field (Eq 3.6) to find the internal gravity acting on a single star on a radial orbit inside the GC and follow that orbit to conclude whether it remains bound or escapes. In this framework, $|\mathbf{g} + \mathbf{g_{ex}}|$ (from Eq 3.6) $=\sqrt{[g + g_{ex}cos(\omega t)]^2 + [g_{ex}sin(\omega t)]^2}$. The real gravity experienced by the star w.r.t. the GC's centre of mass is $\mathbf{g}$. Since the GC is freefalling, the external gravity only acts on the star in an indirect manner through the μ-function. Though we include the EFE, we ignore the curl field shown by Angus et al. (2006) to be quite small in cases of high symmetry. In addition, Wu et al. (2007) showed the inclusion of the curl field in calculating the escape speed from the Milky Way was unwarranted by comparison with the work of Famaey et al. (2007b). Nevertheless, we emphasise that our work is a first approximation, and the curl-field might be important in some cases.

Adaptive time steps

We calculate the velocity and position using the standard method of orbit integration $\mathbf{v_{i+1}} = \mathbf{v_i} + \mathbf{g}(\mathbf{r})\Delta t$ and $\mathbf{r_{i+1}} = \mathbf{r_i} + \mathbf{v_i}\Delta t$. We use time steps such that Δt [yrs] = r [pc]. We began our simulations with the stars at 0.02pc where the dynamical time is at most 0.02pc/200 km s^{-1}=100yrs and our time steps are 0.02yrs. By 100pc our time steps are 100yrs and the dynamical time is 10Myrs. Using such a basic orbit integrator is not ideal, but since the computational requirements are not excessive, this set up is more than adequate to preserve numerical accuracy.

Definition of escape speed

Now that we are capable of following a star's orbit in a GC, the crux of the problem becomes defining escape speed numerically in finite time. We use a simple criterion such that if the star completes a full orbit (i.e. turns twice) it is bound. On the other hand, if it is unbound, it never returns. Rather than follow every escaping star to infinity, we impose a large but finite cutoff radius of 3kpc. If a star reaches 3kpc it has escaped. This is much larger than the scale of the host GC (typically tens of pc, so is extremely generous). If a star ever wandered this far from its host, it would easily be scattered by other stars or star clusters and would effectively be lost, even in MOND. The choice of 3kpc is obviously arbitrary, but we found very little variation of escape speed with different cut off radii. For instance we took a sample GC with a >40% increase in central escape speed (Rup 106) in MOND compared to Newtonian gravity and tested the escape speed for a range of truncations. We found that there was a smooth decrease in escape speed from 13.5 to 13.4 km s^{-1} by changing the truncation radius from 3kpc to 400pc. By 100pc it was still 13.1 km s^{-1}. This variation of 0.1 km s^{-1} is easily within the intrinsic uncertainties.

In Fig 3.5 we plot the ratio of the escape velocity from our simulations to the theoretically expected Newtonian value from G02 in three situations for all 141 GCs. First we determine the Newtonian escape velocity by our method; this returns the correct value in agreement with G02. We then compute the MOND escape velocity for both the simple and standard interpolation functions with the EFE imposed by the Milky Way at the location of each GC. In the majority of cases this is not perceptibly different from the Newtonian case, but some GCs show an effect in excess of 10%. We also check the case of MOND with no EFE.

In this case the escape velocity is formally infinite, but our 3kpc criterion returns a finite value. The EFE and no-EFE cases are nevertheless easy to distinguish.

Naturally, this method only calculates whether a single velocity is larger or smaller than the central escape speed. We use the bisection method of root finding to identify the escape speed down to a level of $\pm 0.1\,\mathrm{km\,s^{-1}}$. Resolving any lower not only takes much longer, but is unwarranted by errors in total mass and density profile.

Note that the direction of the star's orbit should not affect the escape speed. We checked this again for the GC Rup 106, and found that testing all angles resulted in less than a $\pm 0.05\,\mathrm{km\,s^{-1}}$ variation. This is also a check that the curl field is unimportant, at least for GCs on circular orbits in an axis-symmetric potential.

3.4.3 Escape velocity trends with R_{MW} and Σ

The further a GC is from the MW (R_{MW}) and the lower its surface brightness (Σ) is, the lower the external and internal gravities are respectively. It is when both these requirements are satisfied that we can expect MOND effects. Otherwise, GCs should behave as Newtonian systems with no apparent need for dark matter.

The modification of the force law at an acceleration scale a_o is equivalent to that at a transition surface density (Milgrom 1989),

$$\Sigma_{\rm t} = a_o/2\pi G \sim 126 M_\odot pc^{-2}. \tag{3.7}$$

High surface brightnesses generally imply strong gravity and hence no MOND effects. GCs with pericentres that cause them to cross the disk are unlikely to differ between CDM and MOND. Not only is the external gravity of the MW too strong to permit MOND effects, but the GCs must be very dense to withstand disk shocking and tidal stresses over a Hubble time.

At the other end of the scale, isolated low surface brightness objects were predicted by Milgrom's original papers (Milgrom 1983a, 1988; de Blok & McGaugh 1998) to be a critical test of MOND because they should appear extremely DM dominated. Much more satisfactorily, MOND imparts dynamical stability to such LSB disks ($\Sigma < \Sigma_{\rm t}$) leading to the Freeman limit in the surface brightness distribution (Milgrom 1989; McGaugh 1996).

GCs capable of testing MOND must therefore satisfy two criteria:
1. They must orbit in a region of low external field ($g_{ex} \lesssim a_o$).
2. They must have surface densities approaching or lower than the transition value ($\Sigma \lesssim \Sigma_{\rm t}$).
Most GCs have mean surface densities ($M_{GC}/\pi R_t^2$) far in excess of the limit in Eq 3.7, making MOND only significant beyond the tidal radius. However, as we show in Fig 3.6, which plots the ratio of the MONDian escape speed to the Newtonian one as functions of both Galactocentric radius and mean surface density, there is a trend for GCs with low surface densities and large galactocentric radii to have an enhanced central escape velocity. The trends with R_{MW} and Σ are the same for both interpolation functions. There is a moderate increase of escape velocity in some GCs with $R_{MW} < 10$kpc and $\Sigma > \Sigma_{\rm t}$ for the simple function that is not seen with the standard function. This occurs because the standard function tends towards the Newtonian regime (μ=1) more sharply than the simple function (Famaey et al. 2007c), which gives a stronger MOND effect around a_o.

Good test candidates

In Table 3.2 we list the properties of the 19 GCs with central escape speeds increased by more than 40% (20%) for simple (standard) μ. A property of MOND in these systems is that we should see stars orbiting beyond the classical tidal radius, because they can still be bound to the parent GC at larger radii than in Newtonian gravity. Examples of this kind of behaviour is made obvious by measurements of the satellite galaxies of the Milky Way (see Irwin & Hatzidimitriou 1995; Walker et al. 2007).

We predict the 5 GCs (AM1, Eridanus, Pal 3, Pal 4, and Pal 14) with a MONDian escape speed > 140% (120%) larger than the Newtonian value could have interesting properties, but these GCs are between 67-130kpc from the Sun making them challenging observational targets. It is also worth keeping in mind that with the advent of the SDSS it is possible to identify low luminosity and distant GCs (see Koposov et al. 2007), therefore the number of good test GCs for MOND may increase further.

3.4.4 Implications for internal structure and line of sight velocity dispersions

Studies of GCs in the Galaxy by Scarpa et al. (2003, 2006) have claimed that GCs display odd behaviour in a Newtonian sense because their velocity dispersion profiles become constant at the largest measured radii. This is expected in pressure supported systems in MOND such as elliptical galaxies (Milgrom & Sanders 2003) which become isothermal at large radii. However, ellipticals in the field are not subject to strong external fields ($g_{ex} \sim a_o/30$) whereas GCs of the MW are mostly exposed to strong external fields of order a_o.

Scarpa et al. studied NGC 7078, NGC 7099 and Pal 13 in some detail. We have mass models for these GCs from the King models of G02. NGC 7099 has a mean surface density $\sim 39 M_{\odot} pc^{-2}$, however, its los velocity dispersion profile is only studied in sufficient detail out to 16pc (whereas R_t=44.3pc) within which the mean surface density is $\sim 249 M_{\odot} pc^{-2}$. Furthermore, NGC 7099 is a mere 7.1kpc from the Galactic centre meaning the EFE is strong ($g_{ex} \sim 2a_o$). Both these factors culminate in the expectation that NGC 7099 should show no MOND behaviour.

This is shown in Fig 3.7a which plots gravity (Newtonian, MOND no EFE, MOND with parallel EFE and MOND with anti-parallel EFE) against radius from the centre of the GC. The MOND with no EFE and Newtonian curves are the limits of what can be expected in MOND with EFE. In the central 2pc, the internal gravity is very large (of order $100a_o$) and far greater than the external field. Conversely, beyond 20pc the internal gravity is much lower than the external gravity. Recall that we can approximate Eq 3.6 as $g = \frac{G}{\mu(|\mathbf{g}+\mathbf{g_{ex}}|)} M_K(r) r^{-2}$, which is simply Newtonian gravity with a renormalised gravitational constant such that $G \rightarrow G/\mu(|\mathbf{g}+\mathbf{g_{ex}}|)$ (μ being less than unity). Therefore, the direction of the EFE has some small bearing on the gravity because when the internal gravity is opposing the external gravity (i.e. the side of the GC nearest the Galaxy centre) then since it is the vector addition of the two components which enters the μ function. The sum of these two gravities is lower than if they are in the opposite direction which means $\mu(|\mathbf{g}+\mathbf{g_{ex}}|)$ is lower making the gravity slightly stronger.

We see this effect in Fig 3.7a where the MOND with anti-parallel EFE curve feels a stronger correction than the opposite side of the GC. The velocity disper-

sion profile of NGC7099 therefore should decay as $\sigma \propto r^{-1}$ beyond 10pc where the external field dominates.

Pal 13 has a very low surface density ($\sim 7 M_{\odot} pc^{-2}$). At 25.6kpc from the Galactic centre it is everywhere dominated by the EFE ($g_{ex} \sim 0.4 a_o$). Consequently, the gravity is merely that of Newtonian gravity with a renormalised gravitational constant as discussed above. When the external gravity opposes the internal gravity, just as for NGC 7099, the gravitational constant is renormalised to a slightly higher value than when they are parallel. This effect is far more prominent for Pal 13 than for NGC 7099 because Pal 13 has a low surface density and feels a weak external field. This would act like tidal gravity and would stretch the GC. Tidal streams would preferentially be leaked opposed to the MW and not towards it because gravity is stronger on the near side, so stars with a certain energy could be bound at one side of the GC, but not at the opposite.

This effect should make GCs like Pal 13 non spherical and we would expect these elongations to line up with the external field.

In a recent preprint, Scarpa et al. (2007) showed similar flat dispersion curves for another three GCs, namely NGC 7078, NGC 6341 and NGC 6171. The flat dispersions must simply be a result of the velocity anisotropy since they orbit near the bulge and thus are not good tests of MOND. In fact, we tried fitting the velocity dispersion of NGC 7078 using the method of §3.2 and it was not possible to simultaneously fit the curve below and above 30pc, most probably meaning that the dispersions of the stars beyond 30pc from the centre are inflated tidally, or it has a complex velocity anisotropy.

A recent preprint by Moffat & Toth (2007a) makes a claim that MOND is inconsistent with these GCs of Scarpa et al., however, since these GCs are all in the Newtonian regime due to the strong external field, it makes no sense to talk about MOND having a problem, it is also a problem for Newtonian dynamics which for these strengths of gravity MOND has identical predictions. It is only for more distant GCs that additional, non-trivial tidal effects in MOND due to varying external field strengths can influence the dynamics (see Brada & Milgrom 1999, 2000b).

Mass-to-Light ratio variation

It was pointed out by Hilker (2006) that the M/L of GCs are correlated with mass. He showed that lower mass GCs had a tendency to require lower M/L to be consistent with their central velocity dispersions. For the ∼60 GCs which had their central velocity dispersions measured by Pryor & Meylan (1993) we calculate the rescaling of the M/L and error required for the M/L of G02 to agree with those measured by Pryor & Meylan (1993). We assume the Newtonian limit that $\sigma^2 \propto M/L$, so $\frac{\sigma_g^2}{\sigma_{pm}^2} \propto \frac{3}{M/L_{pm}}$. In Fig 3.8 we show the slight correlation of M/L with GC mass and we note that the mean M/L of the sample is 1.

Unfortunately, this affects our ability to distinguish between MOND and Newtonian gravity because the best test cases are LSB GCs at great distances. However, these GCs are $\sim 10^4 M_\odot$ and as such are very consistent with M/L of 0.5. Therefore, a GC found with a large los velocity dispersion for its luminosity may be interpreted in two ways, either as a high M/L in Newtonian dynamics or low M/L in MOND as long as the M/L in both cases stays between comfortable limits (i.e. 0.5-3). The cleanest test would be to find a distant LSB GC with a much higher Newtonain M/L (say >10) which is inconsistent with the current picture of GCs in Newtonian gravity. If this GC, when studied in MOND, was found to have a M/L of order unity, then it could be strong evidence for MOND. On the other hand, if such a GC was found to have a moderately low M/L in Newtonian gravity (say ∼0.5), then a MOND M/L of <0.1 is not appealing, but this is insufficient and both los velocity dispersions must be measured as well as accurate analysis of the stellar populaions to estimate the M/L.

The difficulty of finding good tests is exemplified by Fig 3.9 which shows the fitted velocity dispersion to the data of NGC 288 (obtained by Scarpa et al. 2007) in MOND and Newtonian gravity. NGC 288 is at a Galactocentric radius of 11.9kpc, where MOND effects might only manifest themselves weakly. We fit the los velocity dispersions in MOND found by solving the Jeans equation in MOND, accounting for the external field effect and projecting the radial velocity dispersions into the line of sight with the same methods as employed in §3.2. The fit is quite good in both MOND (solid black line) and in Newtonian gravity (dashed). Indeed, there is virtually no distinction, except that in MOND we use M/L=1.7 and in Newtonian gravity we use M/L=2.0. Clearly this cannot distinguish between the two. The external gravity at 11.9kpc is still too large to

allow for a significant correction due to MOND. More distant GCs or satellite galaxies must be used.

3.4.5 Application to AM 1 and Pal 14

AM 1 and Pal 14 are a pair of very low surface brightness GCs which were predicted by Baumgardt et al. (2005) to be critical tests of MOND, a fact which we confirm here by showing them both to have central escape speeds more than 2.5× higher than the Newtonian prediction. Recently, Jordi et al. (2007) speculated that Pal 14 had a curiously low line of sight (los) velocity dispersion and this was discussed by Moffat & Toth (2007a) as being problematic for MOND, but exactly as expected for their preferred modified gravity theory MOG. It is indeed true that if a sample of distant LSB GCs were shown to have very low velocity dispersions in Newtonian gravity, corresponding to small fractions of a solar mass to light ratio (M/L), the MOND M/L would be even smaller.

The data generally merit an analysis that accounts for anisotropy, β. We present here predictions of the MOND los velocity dispersion profile for 3 different anisotropy profiles and 3 M/L for both Pal 14 and AM 1 (Fig 3.10). We use the updated structural parameters and luminosities meticulously derived by Hilker (2006). An important point to keep in mind is that observing los velocity dispersions to this accuracy ($0.2\,\mathrm{km\,s^{-1}}$) is extremely difficult and also very sensitive to elongations and tidal tails along the line of sight (Hilker 2006), as well as to global rotation of the GC.

3.4.6 Discussion

We have constructed a simple orbit integrator for MOND assuming no curl field, taking care to properly incorporate the external field effect. We have applied it to investigate the escape velocity of stars from globular clusters which are themselves orbiting within the Milky Way. We have used the King models of the 141 Milky Way GCs tabulated by G02 to construct MOND mass models. The external field imposed on each cluster by the Milky Way has been computed by using the cluster Galactocentric distances and the MOND Milky Way model of McGaugh (2008).

In contrast to the naive expectation of an infinite escape velocity for isolated

GC	R_{MW} [kpc]	$\Sigma\left[\frac{M_\odot}{pc^2}\right]$	g_{ex}/a_o	$V_{e,sim}$ [$\mathrm{km\,s^{-1}}$]	$V_{e,exp}$ [$\mathrm{km\,s^{-1}}$]	$\frac{V_{e,sim}}{Ve,exp}$
(1)	(2)	(3)	(4)	(5)	(6)	(7)
Pal 1	20.1	1.0	0.54	5.1 (4.39)	3.4	1.51 (1.29)
AM 1	126.1	1.3	0.07	10.7 (10.31)	4.2	2.56 (2.45)
Eridanus	84.8	1.4	0.11	11.2 (10.53)	4.6	2.43 (2.29)
NGC 2419	91.0	12.0	0.10	43.1 (39.51)	27.8	1.55 (1.42)
Pyxis	42.0	3.2	0.23	10.7 (9.72)	4.8	2.22 (2.03)
Pal 3	93.8	0.9	0.10	12.0 (11.40)	4.4	2.72 (2.59)
Pal 4	101.0	1.9	0.09	13.4 (12.72)	4.9	2.73 (2.60)
Rup 106	18.5	29.6	0.60	15.3 (13.23)	9.9	1.54 (1.34)
NGC 5053	19.1	9.3	0.57	14.2 (12.13)	8.9	1.59 (1.36)
NGC 5466	16.3	2.0	0.70	13.9 (11.55)	9.5	1.46 (1.22)
Pal 5	18.3	0.8	0.61	5.1 (4.25)	3.2	1.58 (1.33)
Pal 14	67.7	0.5	0.14	7.0 (6.51)	2.5	2.81 (2.60)
Pal 15	34.2	3.1	0.29	9.1 (8.04)	4.3	2.13 (1.87)
Terzan 7	28.9	3.5	0.35	9.9 (8.77)	5.7	1.74 (1.54)
Arp 2	20.6	1.0	0.53	6.1 (5.20)	3.8	1.62 (1.37)
Terzan 8	15.7	9.5	0.73	8.1 (6.80)	5.2	1.56 (1.31)
Pal 12	15.8	0.5	0.73	7.8 (6.58)	5.5	1.41 (1.20)
Pal 13	25.6	7.0	0.41	6.4 (5.64)	3.5	1.84 (1.61)
NGC 7492	24.2	4.3	0.43	11.3 (9.72)	6.6	1.71 (1.47)

Table 3.2: (1) The designations of the GCs. (2) The Galactocentric radius of the GC. (3) The mean surface density of the GC within the tidal radius. (4) The external field at the position of the GC. (5) The central escape speed of the GC in MOND for the simple and (standard) μ functions. (6) The Newtonian central escape speed. (7) The ratio of MOND to Newtonian escape speed for the simple and (standard) μ functions.

MONDian systems, we find that the escape velocity from globular clusters is only marginally enhanced over the purely Newtonian case. This is both due to the gravitational field of the Milky Way, which does lay claim to stars with sufficient velocity to become unbound from the cluster, and the high surface densities of most of the GCs.

We highlight 5 GCs with large increases in escape speed in MOND and another 14 with significant increases. Furthermore, for very low surface brightness GCs (like Pal 13), the direction of the external field with respect to the internal gravity exerts a significant tidal force on the GC possibly inducing elongations and polarised streams.

In the last section we give the MOND prediction to the los velocity dispersion of the extremly LSB GCs AM 1 and Pal 14, for a selection of M/L and velocity anisotropies. When high quality data becomes available for these two GCs, we can exactly fit the M/L with tight errors. Crucially, we advocate here amassing the velocity dispersions of a large sample of GCs that can test MOND as well as data for newly discovered distant dwarf galaxies (Ryan-Weber et al. 2008) to complement the dwarf spheroidals.

Chapter 4

Conclusion

There are many reasons to seek new theories of gravity. The cosmological constant for which no physical basis is ascribed. The lack of any good cold dark matter candidates. The conflict between observations and predictions of the ΛCDM model. Still, many new theories continue to pay for the sins of the father by not addressing the question of the absolute regularity in galaxies as observed in the Tully-Fisher relation (§1.3) and the existence of a critical acceleration scale given by Milgrom's constant $a_o \approx 10^{-10} ms^{-2}$ which is related to the cosmological constant, Λ, by $a_o \approx c\sqrt{\Lambda/3}$.

It was the goal of this thesis to identify new tests for MOND away from spiral galaxies which it models so well. In §3 a special code was designed to identify distant, low surface brightness globular clusters that will make strong tests of MOND and predictions for the awaited measurements were given. The modelling relies on the external field effect, which is a symptom of MOND's non linear gravity.

Next, the brand new data on the line of sight velocity dispersions for eight dwarf galaxies of the Milky Way was taken and modelled in MOND by solving the Jeans equation for variable velocity anisotropy and accurate light profiles for the dwarfs. As for the globular clusters, the external gravity of the Milky Way provides an additional constraint on the internal dynamics, nevertheless, the agreement with the data was excellent. Two problem cases with high (non-stellar) mass-to-light ratios were highlighted: Sextans and Draco. Sextans has an extremely old and poorly constrained luminosity and structure and is not expected to remain a problem when new data becomes available. Draco's mass-

to-light ratio suggests it might be tidally disrupting and numerical simulations of Draco on an orbit of the Milky Way are planned.

MOND is known to have a problem with clusters of galaxies, which was emphasised by §2.1 in which the bullet cluster was modelled in MOND. The bullet cluster was shown to give direct empirical proof of dark matter in clusters of galaxies from the weak lensing reconstruction, which was confirmed in more detail for a large temperature range of groups and clusters of galaxies in §2.3. There it was shown that ordinary massive neutrinos near the experimental upper limit of 2.2eV are unable to be the dark matter of MOND galaxy clusters from measurements of the temperature and density profiles of the hot X-ray emitting gas.

The analysis of the SDSS groups of galaxies discussed in §2.4 in which the claim that MOND fails to reproduce the line of sight velocity dispersions of groups of galaxies by 10σ by Klypin & Prada (2007) was shown to be entirely consistent with MOND by invoking a varying velocity anisotropy, as was used for the dwarf galaxies. This analysis showed that these small groups of galaxies were consistent with no dark matter, whereas groups of galaxies above a temperature of around $0.5keV$ began to show evidence for dark matter. This suggested a type of dark matter which free streams out of galaxies, but can condense in high density in clusters of galaxies, like the ordinary neutrinos except heavier – at least 8eV to clump densely enough.

Unusual neutrino physics has been detected by many experiments and suggests the existence of sterile neutrinos which are right handed counterparts to the left handed active neutrinos. Using an online package which computes the detailed physics that models the generation of the cosmic microwave background, it was shown that a single 11eV sterile neutrino was capable of generating enough driving force to produce the high third peak observed by the WMAP satellite. The fit is as good as the ΛCDM fit, with fewer free parameters.

This leaves MOND at a very interesting position where it can begin to compete at the same weight division as ΛCDM because it has all the ingredients which allow investigations into the formation of galaxies. The expansion history of the Universe is known, the ingredients of the energy-density are known and the tools for simulations are being rapidly developed. The true test of MOND now is to see how effectively it can form cosmic structure and how good the correspondence with large galaxy surveys is.

Bibliography

Abazajian, K., Fuller, G. M., & Patel, M. 2001, Phys. Rev. D, 64, 023501

Aguilar, A., Auerbach, L. B., Burman, R. L., et al. 2001, Phys. Rev. D, 64, 112007

Aguilar, L. A. & Merritt, D. 1990, ApJ, 354, 33

Aguirre, A., Schaye, J., & Quataert, E. 2001, ApJ, 561, 550

Ahmad, Q. R., Allen, R. C., Andersen, T. C., et al. 2001, Physical Review Letters, 87, 071301

Angus, G. W. 2008, MNRAS, 387, 1481

Angus, G. W., Famaey, B., & Buote, D. A. 2008a, MNRAS, 387, 1470

Angus, G. W., Famaey, B., Tiret, O., Combes, F., & Zhao, H. S. 2008b, MNRAS, 383, L1

Angus, G. W., Famaey, B., & Zhao, H. S. 2006, MNRAS, 371, 138

Angus, G. W. & McGaugh, S. S. 2008, MNRAS, 383, 417

Angus, G. W., Shan, H. Y., Zhao, H. S., & Famaey, B. 2007, ApJ, 654, L13

Angus, G. W. & Zhao, H. 2007, MNRAS, 375, 1146

Ashie, Y., Hosaka, J., Ishihara, K., et al. 2004, Physical Review Letters, 93, 101801

Baer, H., Belyaev, A., & Summy, H. 2008, ArXiv e-prints, 802

Baumgardt, H., Grebel, E. K., & Kroupa, P. 2005, MNRAS, 359, L1

Bekenstein, J. 2006, Contemporary Physics, 47, 387

Bekenstein, J. & Milgrom, M. 1984, ApJ, 286, 7

Bekenstein, J. D. & Sagi, E. 2008, ArXiv e-prints, 802

Bellazzini, M., Ferraro, F. R., Origlia, L., et al. 2002, AJ, 124, 3222

Bellazzini, M., Fusi Pecci, F., & Ferraro, F. R. 1996, MNRAS, 278, 947

Bellazzini, M., Gennari, N., & Ferraro, F. R. 2005, MNRAS, 360, 185

Bellazzini, M., Gennari, N., Ferraro, F. R., & Sollima, A. 2004, MNRAS, 354, 708

Belokurov, V., Evans, N. W., Irwin, M. J., et al. 2007, ApJ, 658, 337

Belokurov, V., Zucker, D. B., Evans, N. W., et al. 2006, ApJ, 642, L137

Bertone, S., Schaye, J., & Dolag, K. 2008, Space Science Reviews, 134, 295

Binney, J. 2004, in IAU Symposium, Vol. 220, Dark Matter in Galaxies, ed. S. Ryder, D. Pisano, M. Walker, & K. Freeman, 3–+

Binney, J. & Mamon, G. A. 1982, MNRAS, 200, 361

Binney, J. & Tremaine, S. 2008, Galactic Dynamics: Second Edition (Galactic Dynamics: Second Edition, by James Binney and Scott Tremaine. ISBN 978-0-691-13026-2 (HB). Published by Princeton University Press, Princeton, NJ USA, 2008.)

Boesgaard, A. M. & Steigman, G. 1985, ARAA, 23, 319

Bond, J. R. & Efstathiou, G. 1984, ApJ, 285, L45

Bonnell, I. A., Bate, M. R., Clarke, C. J., & Pringle, J. E. 2001, MNRAS, 323, 785

Bonnell, I. A., Bate, M. R., & Zinnecker, H. 1998, MNRAS, 298, 93

Bournaud, F., Duc, P.-A., Brinks, E., et al. 2007, Science, 316, 1166

Brada, R. & Milgrom, M. 1995, MNRAS, 276, 453

Brada, R. & Milgrom, M. 1999, ApJ, 512, L17

Brada, R. & Milgrom, M. 2000a, ApJ, 541, 556

Brada, R. & Milgrom, M. 2000b, ApJ, 531, L21

Bradač, M., Clowe, D., Gonzalez, A. H., et al. 2006, ApJ, 652, 937

Bullock, J. S., Dekel, A., Kolatt, T. S., Primack, J. R., & Somerville, R. S. 2001, ApJ, 550, 21

Buote, D. A. & Canizares, C. R. 1994, ApJ, 427, 86

Buote, D. A. & Canizares, C. R. 1996, ApJ, 468, 184

Buote, D. A., Jeltema, T. E., Canizares, C. R., & Garmire, G. P. 2002, ApJ, 577, 183

Burles, S., Nollett, K. M., & Turner, M. S. 2001, ApJ, 552, L1

Carroll, S. M. 2006, Nature, 440, 1132

CDMS Collaboration. 2008, ArXiv e-prints, 802

Cen, R. & Ostriker, J. P. 1999, ApJ, 514, 1

Cen, R. & Ostriker, J. P. 2006, ApJ, 650, 560

Chernin, A. D., Karachentsev, I. D., Teerikorpi, P., et al. 2007, ArXiv e-prints, 706

Ciotti, L. & Binney, J. 2004, MNRAS, 351, 285

Ciotti, L., Londrillo, P., & Nipoti, C. 2006, ApJ, 640, 741

Clowe, D., Bradač, M., Gonzalez, A. H., et al. 2006, ApJ, 648, L109

Clowe, D., De Lucia, G., & King, L. 2004a, MNRAS, 350, 1038

Clowe, D., Gonzalez, A., & Markevitch, M. 2004b, ApJ, 604, 596

Cole, S., Aragon-Salamanca, A., Frenk, C. S., Navarro, J. F., & Zepf, S. E. 1994, MNRAS, 271, 781

Colless, M., Dalton, G., Maddox, S., et al. 2001, MNRAS, 328, 1039

Combes, F. 1991, ARAA, 29, 195

Combes, F. 2004, in IAU Symposium, Vol. 220, Dark Matter in Galaxies, ed. S. Ryder, D. Pisano, M. Walker, & K. Freeman, 219–+

Combes, F., Leon, S., & Meylan, G. 1999, A & A, 352, 149

de Blok, W. J. G. & McGaugh, S. S. 1998, ApJ, 508, 132

Diaferio, A. 2008, ArXiv e-prints, 802

Diaferio, A., Schindler, S., & Dolag, K. 2008, Space Science Reviews, 134, 7

Diemand, J., Kuhlen, M., Madau, P., et al. 2008, ArXiv e-prints, 805

Diemand, J., Moore, B., & Stadel, J. 2005, Nature, 433, 389

Dodelson, S. & Liguori, M. 2006, Physical Review Letters, 97, 231301

Dodelson, S., Melchiorri, A., & Slosar, A. 2006, Physical Review Letters, 97, 041301

Donahue, M., Horner, D. J., Cavagnolo, K. W., & Voit, G. M. 2006, ApJ, 643, 730

D'Onghia, E. 2008, ArXiv e-prints, 802

Dunkley, J., Komatsu, E., Nolta, M. R., et al. 2008, ArXiv e-prints, 803

Dunn, R. J. H. & Fabian, A. C. 2006, MNRAS, 373, 959

Dupke, R. A., Mirabal, N., Bregman, J. N., & Evrard, A. E. 2007, ApJ, 668, 781

Eisenstein, D. J., Zehavi, I., Hogg, D. W., et al. 2005, ApJ, 633, 560

Evrard, A. E., Metzler, C. A., & Navarro, J. F. 1996, ApJ, 469, 494

Fabian, A. C., Johnstone, R. M., & Daines, S. J. 1994, MNRAS, 271, 737

Famaey, B., Angus, G. W., Gentile, G., Shan, H. Y., & Zhao, H. S. 2007a, ArXiv e-prints, 706

Famaey, B. & Binney, J. 2005, MNRAS, 363, 603

Famaey, B., Bruneton, J.-P., & Zhao, H. 2007b, MNRAS, 377, L79

Famaey, B., Gentile, G., Bruneton, J.-P., & Zhao, H. 2007c, Phys. Rev. D, 75, 063002

Farrar, G. R. & Rosen, R. A. 2007, Physical Review Letters, 98, 171302

Ferreras, I., Sakellariadou, M., & Yusaf, M. F. 2008, Physical Review Letters, 100, 031302

Fukugita, M. & Peebles, P. J. E. 2004, ApJ, 616, 643

Gastaldello, F., Buote, D. A., Brighenti, F., & Mathews, W. G. 2008, ApJ, 673, L17

Gastaldello, F., Buote, D. A., Humphrey, P. J., et al. 2007, ApJ, 669, 158

Gavazzi, R. 2005, A & A, 443, 793

Gentile, G., Famaey, B., Combes, F., et al. 2007, A & A, 472, L25

Gentile, G., Salucci, P., Klein, U., Vergani, D., & Kalberla, P. 2004, MNRAS, 351, 903

Gentile, G., Zhao, H. S., & Famaey, B. 2008, MNRAS, 385, L68

Gerbal, D., Durret, F., Lachieze-Rey, M., & Lima-Neto, G. 1992, A & A, 262, 395

Gerhard, O. E. & Spergel, D. N. 1992, ApJ, 397, 38

Gilmore, G., Wilkinson, M., Kleyna, J., et al. 2007, Nuclear Physics B Proceedings Supplements, 173, 15

Giunti, C. & Laveder, M. 2007, ArXiv e-prints, 707

Gnedin, O. Y. & Zhao, H. 2002, MNRAS, 333, 299

Gnedin, O. Y., Zhao, H., Pringle, J. E., et al. 2002, ApJ, 568, L23

Granett, B. R., Neyrinck, M. C., & Szapudi, I. 2008, ArXiv e-prints, 805

Hargreaves, J. C., Gilmore, G., Irwin, M. J., & Carter, D. 1996, MNRAS, 282, 305

Harris, W. E. 1996, AJ, 112, 1487

Hayashi, E. & White, S. D. M. 2006, MNRAS, 370, L38

Hernquist, L. 1990, ApJ, 356, 359

Hilker, M. 2006, A & A, 448, 171

Hoekstra, H. & Jain, B. 2008, ArXiv e-prints, 805

Host, O., Lahav, O., Abdalla, F. B., & Eitel, K. 2007, Phys. Rev. D, 76, 113005

Humphrey, P. J., Buote, D. A., Gastaldello, F., et al. 2006, ApJ, 646, 899

Ibata, R. A., Gilmore, G., & Irwin, M. J. 1994, Nature, 370, 194

Irwin, M. & Hatzidimitriou, D. 1995, MNRAS, 277, 1354

Jee, M. J., Ford, H. C., Illingworth, G. D., et al. 2007, ApJ, 661, 728

Jee, M. J., White, R. L., Benítez, N., et al. 2005a, ApJ, 618, 46

Jee, M. J., White, R. L., Ford, H. C., et al. 2005b, ApJ, 634, 813

Jordi, K., Grebel, E. K., Hilker, M., Baumgardt, H., & Kroupa, P. 2007, in American Astronomical Society Meeting Abstracts, Vol. 211, American Astronomical Society Meeting Abstracts, 58

Kallivayalil, N., van der Marel, R. P., & Alcock, C. 2006a, ApJ, 652, 1213

Kallivayalil, N., van der Marel, R. P., Alcock, C., et al. 2006b, ApJ, 638, 772

Kennicutt, Jr., R. C. 1998, ApJ, 498, 541

Kleyna, J. T., Wilkinson, M. I., Evans, N. W., & Gilmore, G. 2004, MNRAS, 354, L66

Kleyna, J. T., Wilkinson, M. I., Gilmore, G., & Evans, N. W. 2003, ApJ, 588, L21

Klimentowski, J., Lokas, E. L., Kazantzidis, S., et al. 2008, ArXiv e-prints, 803

Klimentowski, J., Łokas, E. L., Kazantzidis, S., et al. 2007, MNRAS, 378, 353

Klypin, A., Kravtsov, A. V., Valenzuela, O., & Prada, F. 1999, ApJ, 522, 82

Klypin, A. & Prada, F. 2007, ArXiv e-prints, 706

Knebe, A. & Gibson, B. K. 2004, MNRAS, 347, 1055

Koch, A., Kleyna, J. T., Wilkinson, M. I., et al. 2007, AJ, 134, 566

Koposov, S., de Jong, J. T. A., Belokurov, V., et al. 2007, ApJ, 669, 337

Kraus, C., Bornschein, B., Bornschein, L., et al. 2005, European Physical Journal C, 40, 447

Kroupa, P. 2001, MNRAS, 322, 231

Lee, M. G., Park, H. S., Park, J.-H., et al. 2003, AJ, 126, 2840

Leon, S., Meylan, G., & Combes, F. 2000, A & A, 359, 907

Lewis, A., Challinor, A., & Lasenby, A. 2000, Astrophys. J., 538, 473

Lin, Y.-T. & Mohr, J. J. 2004, ApJ, 617, 879

Łokas, E. L. 2001, MNRAS, 327, L21

Lokas, E. L., Klimentowski, J., Kazantzidis, S., & Mayer, L. 2008, ArXiv e-prints, 804

Lokas, E. L., Klimentowski, J., & Wojtak, R. 2007, ArXiv e-prints, 712

Lynden-Bell, D. 1983, in IAU Symposium, Vol. 100, Internal Kinematics and Dynamics of Galaxies, ed. E. Athanassoula, 89–91

Mahdavi, A., Hoekstra, H., Babul, A., Balam, D. D., & Capak, P. L. 2007, ApJ, 668, 806

Maltoni, M. & Schwetz, T. 2007, Phys. Rev. D, 76, 093005

Markevitch, M., Gonzalez, A. H., Clowe, D., et al. 2004, ApJ, 606, 819

Markevitch, M., Gonzalez, A. H., David, L., et al. 2002, ApJ, 567, L27

Markevitch, M. & Vikhlinin, A. 2007, Physics Reports, 443, 1

Mateo, M., Fischer, P., & Krzeminski, W. 1995, AJ, 110, 2166

Mateo, M., Olszewski, E. W., & Walker, M. G. 2008, ApJ, 675, 201

Mateo, M. L. 1998, ARAA, 36, 435

McGaugh, S. 2008, ArXiv e-prints, 804

McGaugh, S. S. 1996, MNRAS, 280, 337

McGaugh, S. S. 1999, ApJ, 523, L99

McGaugh, S. S. 2004, ApJ, 611, 26

McGaugh, S. S. 2005a, Physical Review Letters, 95, 171302

McGaugh, S. S. 2005b, ApJ, 632, 859

McGaugh, S. S. & de Blok, W. J. G. 1998, ApJ, 499, 66

McGaugh, S. S., de Blok, W. J. G., Schombert, J. M., Kuzio de Naray, R., & Kim, J. H. 2007, ApJ, 659, 149

McGaugh, S. S., Schombert, J. M., Bothun, G. D., & de Blok, W. J. G. 2000, ApJ, 533, L99

Metz, M. & Kroupa, P. 2007, MNRAS, 376, 387

Milgrom, M. 1983a, ApJ, 270, 371

Milgrom, M. 1983b, ApJ, 270, 384

Milgrom, M. 1983c, ApJ, 270, 365

Milgrom, M. 1986, ApJ, 302, 617

Milgrom, M. 1988, ApJ, 333, 689

Milgrom, M. 1989, ApJ, 338, 121

Milgrom, M. 1995, ApJ, 455, 439

Milgrom, M. 1998, ApJ, 496, L89+

Milgrom, M. 2002, ApJ, 577, L75

Milgrom, M. 2007a, ArXiv e-prints, 712

Milgrom, M. 2007b, ApJ, 667, L45

Milgrom, M. 2008, ArXiv e-prints, 801

Milgrom, M. & Sanders, R. H. 2003, ApJ, 599, L25

Milgrom, M. & Sanders, R. H. 2008, ApJ, 678, 131

Milosavljević, M., Koda, J., Nagai, D., Nakar, E., & Shapiro, P. R. 2007, ApJ, 661, L131

Moffat, J. W. & Toth, V. T. 2007a, ArXiv e-prints, 708

Moffat, J. W. & Toth, V. T. 2007b, ArXiv e-prints, 708

Moore, B., Ghigna, S., Governato, F., et al. 1999a, ApJ, 524, L19

Moore, B., Lake, G., Quinn, T., & Stadel, J. 1999b, MNRAS, 304, 465

Morris, R. G. & Fabian, A. C. 2003, MNRAS, 338, 824

Muñoz, R. R., Frinchaboy, P. M., Majewski, S. R., et al. 2005, ApJ, 631, L137

Muñoz, R. R., Majewski, S. R., & Johnston, K. V. 2008, ApJ, 679, 346

Navarro, J. F., Frenk, C. S., & White, S. D. M. 1995, MNRAS, 275, 720

Nipoti, C., Ciotti, L., Binney, J., & Londrillo, P. 2008, MNRAS, 472

Nipoti, C., Londrillo, P., & Ciotti, L. 2007a, ApJ, 660, 256

Nipoti, C., Londrillo, P., & Ciotti, L. 2007b, MNRAS, 381, L104

Nolta, M. R., Dunkley, J., Hill, R. S., et al. 2008, ArXiv e-prints, 803

Nusser, A. 2002, MNRAS, 331, 909

Nusser, A. 2007, ArXiv e-prints, 710

Odenkirchen, M., Grebel, E. K., Dehnen, W., et al. 2003, AJ, 126, 2385

O'Sullivan, E., Sanderson, A. J. R., & Ponman, T. J. 2007, MNRAS, 380, 1409

Palma, C., Majewski, S. R., Siegel, M. H., et al. 2003, AJ, 125, 1352

Peñarrubia, J., Martínez-Delgado, D., Rix, H. W., et al. 2005, ApJ, 626, 128

Peebles, P. J. & Ratra, B. 2003, Reviews of Modern Physics, 75, 559

Percival, W. J., Cole, S., Eisenstein, D. J., et al. 2007, MNRAS, 381, 1053

Perlmutter, S., Aldering, G., Goldhaber, G., et al. 1999, ApJ, 517, 565

Pfenniger, D., Combes, F., & Martinet, L. 1994, A & A, 285, 79

Piatek, S., Pryor, C., Bristow, P., et al. 2005, AJ, 130, 95

Piatek, S., Pryor, C., Bristow, P., et al. 2006, AJ, 131, 1445

Pointecouteau, E. & Silk, J. 2005, MNRAS, 364, 654

Primack, J. R. 2007, Nuclear Physics B Proceedings Supplements, 173, 1

Pryor, C. & Meylan, G. 1993, in Astronomical Society of the Pacific Conference Series, Vol. 50, Structure and Dynamics of Globular Clusters, ed. S. G. Djorgovski & G. Meylan, 357–+

Reichardt, C. L., Ade, P. A. R., Bock, J. J., et al. 2008, High resolution CMB power spectrum from the complete ACBAR data set

Richtler, T., Schuberth, Y., Hilker, M., et al. 2008, A & A, 478, L23

Romanowsky, A. J., Douglas, N. G., Arnaboldi, M., et al. 2003, Science, 301, 1696

Roncarelli, M., Moscardini, L., Tozzi, P., et al. 2006, MNRAS, 368, 74

Rubin, V. C., Thonnard, N., & Ford, Jr., W. K. 1978, ApJ, 225, L107

Rubin, V. C., Waterman, A. H., & Kenney, J. D. P. 1999, AJ, 118, 236

Ryan-Weber, E. V., Begum, A., Oosterloo, T., et al. 2008, MNRAS, 384, 535

Sales, L. V., Helmi, A., Starkenburg, E., et al. 2008, ArXiv e-prints, 805

Sánchez-Salcedo, F. J. & Hernandez, X. 2007, ApJ, 667, 878

Sánchez-Salcedo, F. J., Reyes-Iturbide, J., & Hernandez, X. 2006, MNRAS, 370, 1829

Sanders, R. H. 1994, A & A, 284, L31

Sanders, R. H. 1998, MNRAS, 296, 1009

Sanders, R. H. 1999, ApJ, 512, L23

Sanders, R. H. 2001, ApJ, 560, 1

Sanders, R. H. 2003, MNRAS, 342, 901

Sanders, R. H. 2007, MNRAS, 380, 331

Sanders, R. H. 2008, MNRAS, 386, 1588

Sanders, R. H. & McGaugh, S. S. 2002, ARAA, 40, 263

Sanders, R. H. & Noordermeer, E. 2007, MNRAS, 379, 702

Sanders, R. H. & Verheijen, M. A. W. 1998, ApJ, 503, 97

Scarpa, R., Marconi, G., & Gilmozzi, R. 2003, A & A, 405, L15

Scarpa, R., Marconi, G., & Gilmozzi, R. 2006, in American Institute of Physics Conference Series, Vol. 822, First Crisis in Cosmology Conference, ed. E. J. Lerner & J. B. Almeida, 102–104

Scarpa, R., Marconi, G., Gilmozzi, R., & Carraro, G. 2007, A & A, 462, L9

Schmidt, B. P., Suntzeff, N. B., Phillips, M. M., et al. 1998, ApJ, 507, 46

Ségall, M., Ibata, R. A., Irwin, M. J., Martin, N. F., & Chapman, S. 2007, MNRAS, 375, 831

Seljak, U., Makarov, A., McDonald, P., & Trac, H. 2006, Physical Review Letters, 97, 191303

Smolčić, V., Zucker, D. B., Bell, E. F., et al. 2007, AJ, 134, 1901

Sohn, S. T., Majewski, S. R., Muñoz, R. R., et al. 2007, ApJ, 663, 960

Somerville, R. S. & Primack, J. R. 1999, MNRAS, 310, 1087

Spergel, D. N., Bean, R., Doré, O., et al. 2007, ApJ, 170, 377

Springel, V. 2005, MNRAS, 364, 1105

Springel, V. & Farrar, G. R. 2007, MNRAS, 380, 911

Stachniewicz, S. & Kutschera, M. 2005, MNRAS, 362, 89

Steinmetz, M. & Navarro, J. F. 1999, ApJ, 513, 555

Takahashi, R. & Chiba, T. 2007, ApJ, 671, 45

Tegmark, M., Blanton, M. R., Strauss, M. A., et al. 2004, ApJ, 606, 702

The, L. S. & White, S. D. M. 1988, AJ, 95, 1642

Tiret, O. & Combes, F. 2007a, A & A, 464, 517

Tiret, O. & Combes, F. 2007b, ArXiv e-prints, 712

Tiret, O. & Combes, F. 2008, ArXiv e-prints, 803

Tiret, O., Combes, F., Angus, G. W., Famaey, B., & Zhao, H. S. 2007, A & A, 476, L1

Toomre, A. & Toomre, J. 1972, ApJ, 178, 623

Tremaine, S. & Gunn, J. E. 1979, Physical Review Letters, 42, 407

Tsai, J. C., Katz, N., & Bertschinger, E. 1994, ApJ, 423, 553

Vikhlinin, A., Kravtsov, A., Forman, W., et al. 2006, ApJ, 640, 691

Walker, M. & Wardle, M. 1998, ApJ, 498, L125+

Walker, M. G., Mateo, M., Olszewski, E. W., et al. 2007, ApJ, 667, L53

Walter, F., Brinks, E., de Blok, E., et al. 2005, in Bulletin of the American Astronomical Society, Vol. 37, Bulletin of the American Astronomical Society, 1258–+

Wechsler, R. H., Bullock, J. S., Primack, J. R., Kravtsov, A. V., & Dekel, A. 2002, ApJ, 568, 52

Weinberg, S. 1993, The first three minutes : a modern view of the origin of the universe (New York : Basic Books, c1993. Updated ed.)

White, S. D. M. & Rees, M. J. 1978, MNRAS, 183, 341

Wilkinson, M. I. & Evans, N. W. 1999, MNRAS, 310, 645

Wu, X., Zhao, H., Famaey, B., et al. 2007, ApJ, 665, L101

Xue, X. ., Rix, H. ., Zhao, G., et al. 2008, ArXiv e-prints, 801

Zappacosta, L., Buote, D. A., Gastaldello, F., et al. 2006, ApJ, 650, 777

Zhao, H., Bacon, D. J., Taylor, A. N., & Horne, K. 2006, MNRAS, 368, 171

Zucker, D. B., Belokurov, V., Evans, N. W., et al. 2006, ApJ, 650, L41

Zunckel, C. & Ferreira, P. G. 2007, Journal of Cosmology and Astro-Particle Physics, 8, 4